ORBITAL MOTION IN UNIFORMLY ROTATING SECOND DEGREE AND ORDER GRAVITY FIELDS

by

Weiduo Hu

A dissertation submitted in partial fulfillment
of the requirements for the degree of
Doctor of Philosophy
(Aerospace Engineering)
in The University of Michigan
2002

Doctoral Committee:

Assistant Professor Daniel J. Scheeres, Chair
Professor Pierre T. Kabamba
Associate Professor Arthur D. Kuo
Professor N. Harris McClamroch

UMI Number: 3057964

UMI Microform 3057964

ProQuest Information and Learning Company
300 North Zeeb Road
P.O. Box 1346
Ann Arbor, MI 48106-1346

To all those who helped me.

ACKNOWLEDGEMENTS

I am appreciated very much to my advisor Prof. Scheeres, who gives me the opportunity to do the new and challenging research which I am interested. Throughout the research of dissertation, he not only gives me directions, but also takes part in much of detailed work. And I can not forget that he always patiently corrects my errors in my papers and dissertation. These thanks are extended to my doctoral committee: Prof. McClamroch, Prof. Kabamba and Prof. Kuo.

Special thanks are given to my family for their encouragement and support.

I also give thanks to my friend Margaret, Prof. Ping Lu and other friends and Professors.

The work described in this dissertation was funded by the TMOD Technology Program with a grant from the Jet Propulsion Laboratory, California Institute of Technology which is under contract with the National Aeronautics and Space Administration.

TABLE OF CONTENTS

LIST OF FIGURES

Figure

LIST OF TABLES

Table

List of Symbols

a	semi-major axis
e	eccentricity
i	inclination
Ω	longitude of ascending node
ω	argument of periapsis
f	true anomaly
M	mean anomaly
n	mean motion rate
E	eccentric anomaly
μ	gravitational parameter
ω_T	central body uniformly rotation rate
I_{xx}, I_{yy}, I_{zz}	moment of inertia with axes x,y,z
U_2	gravity potential of 2nd degree and order
S/C	spacecraft
STM	State Transition Matrix
KAM theory	Kolmogorov-Arnold-Moser theory
3-D	three dimension
RTBP	Restricted Three Body Problem
URSDOGF	Uniformly Rotating Second Degree and Order Gravity Field
FFT	Fast Fourier Transformation
M:N resonance	ω_T/n is a ratio of two integers

LIST OF APPENDICES

Appendix

CHAPTER I

INTRODUCTION

This dissertation studies spacecraft orbital motion about a rotating 2nd degree and order gravity field, with its main application to orbital motion about an asteroid. These dynamical systems are non-integrable in general. Our goal is to understand how the dynamics of this system changes as a function of the central body's rotation rate and mass distribution. To carry out this analysis we use three different approaches: averaging, resonance analysis, and periodic orbit computation. By using these analyses, we can better understand the whole character of a spacecraft's motion around an asteroid, which is much different from the character of spacecraft motion around the Earth, or other planets in Solar system.

1.1 Application and Background

Space missions to send a spacecraft to orbit about an asteroid or comet have been carried out and are currently being prepared or proposed [2],[14],[41],[17]. Orbits around an asteroid or a comet are considerably different from the Keplerian orbits in the two-body problem. This is due to two reasons: the irregular shape of an asteroid, and the rotation of the asteroid. These two effects are coupled and can cause the spacecraft orbit to experience large energy and angular momentum changes within

short time periods [38], occurrences that are not seen for spacecraft motion around planetary bodies. Due to these effects the study of spacecraft motion about asteroidal bodies is new and challenging.

For the general two body problem, if we assume the spacecraft is a point mass, its position vector in inertial coordinates satisfies the equation of motion,

$$\ddot{\mathbf{r}}_\mathbf{i} = \mathbf{F}, \tag{1.1}$$

where $\mathbf{r}_\mathbf{i}, \mathbf{F}$ are the position and acceleration vectors. The ideal case occurs when there is no perturbation, $\mathbf{F} = -\mu \mathbf{r}_\mathbf{i}/r_i^3$, meaning that the attracting body is a point mass (or a sphere with uniform mass distribution), with its principle moments of inertia equal, $I_{xx} = I_{yy} = I_{zz}$. Then the spacecraft orbit is a classical Keplerian orbit and its semi-major axis a, eccentricity e, inclination i, longitude of ascending node Ω, argument of periapsis ω are all constant. These elements are well-defined in many text books such as [4]. Also, see Appendix C.1.

When the attracting body is an oblate body rotating about its axis of symmetry (such as a planet), the spacecraft orbit is perturbed from its ideal Keplerian orbits, but its acceleration $\mathbf{F}$ has no relation with the main body's rotation. Since the shape of an oblate body is symmetric about its rotation axis, the relation between their moments of inertia is $I_{xx} = I_{yy} < I_{zz}$. Spacecraft motion around an oblate body has been widely studied since the 1960's [11],[25],[7]. This is the well-known J_2 (i.e. C_{20} only) perturbation problem. Normally, for spacecraft motion around an oblate body, the orbit's semi-major axis a, eccentricity e, and inclination i are constant on average, but its longitude of ascending node Ω and argument of periapsis ω have secular variations. Some of these results are used to design satellite orbits for specific applications, such as Sun-synchronous orbits.

For spacecraft motion around an asteroid whose moments of inertia are, in general, different from each other, $I_{xx} < I_{yy} < I_{zz}$, the acceleration $\mathbf{F}$ has a close relationship with the asteroid's rotation, making the study of motion around an asteroid completely different from the case of motion around an oblate body. Not only will Ω and ω change, but i, and even a and e may also change drastically over time. For some cases these changes are rapid, making the spacecraft motion unpredictable to some degree, this unpredictability is an instance of chaotic motion, which exists in many dynamic systems [33],[8],[12]. Here we define "chaotic" motion as sensitive dependence on initial conditions.

Thus, the problem of spacecraft motion around an asteroid is not only a practical engineering problem, but also a theoretical problem in dynamical systems as well.

There are some approches that can be used to model the acceleration $\mathbf{F}$. One is to model the asteroid as an ellipsoid [35], and calculate its gravity potential and derivatives whose first order partial derivatives are the acceleration $\mathbf{F}$. The second method represents the gravity force potential using a polyhedron model [44]. The third method is to use the spherical harmonics expansion of the gravity potential. Scheeres [36],[37],[39] calculated and analyzed spacecraft motions for a number of specific asteroids. In these studies, the polyhedron and spherical harmonics expansion gravity models are used.

In this dissertation we focus on the general problem of spacecraft motion around asteroids by modeling the asteroid perturbation potential with the two most significant gravity coefficients, C_{20} and C_{22}. The model is simple, but can describe the main character of spacecraft motion about an asteroid. One of these characteristics is that the spacecraft motion is also affected by the central body's rotation. Since our gravity field is rotating with the asteroid, some aspects of our problem have

Central body-shape	Sphere	Oblate	Irregular
Moments of interia	$I_{xx} = I_{yy} = I_{zz}$	$I_{xx} = I_{yy} < I_{zz}$	$I_{xx} < I_{yy} < I_{zz}$
Gravity coefficients	$C_{20} = C_{22} = 0$	$C_{20} < 0, C_{22} = 0$	$C_{20} < 0, C_{22} > 0$
Relation to ω_T	No	No	Yes
Motion constants	a, e, i, Ω, ω	$\bar{a}, \bar{e}, \bar{i}$	No

Table 1.1: The summary of application and background

similarities to the three body problem, which is discussed comprehensively in [42] and has been studied for the last one hundred years.

Table 1.1 gives a summary of the discussion in this section.

1.2 Thesis Organization

In Chapter II, we first review some basic notations and equations which will be used in this dissertation. Then we propose a definition for size-shape stabililty and present two facts which are related to the orbital stability of spacecraft motion around an asteroid. Finally, we give a preliminarily analysis of some basic questions concerning our problem using a numerical study. These questions will subsequently be discussed in the rest of the dissertation.

In Chapter III, we use averaging methods to remove the rapidly changing variables and keep the slowly changing variables that describe an orbit's secular motion. We study the averaged motion for three cases: when the central body does not rotate, rotates slowly, and rotates rapidly. For the slow rotation cases, we derive the averaged Lagrange planetary equations for this system and use them, in conjunction with the Jacobi integral, to give a complete description of orbital motion. We show that,

under the averaging assumptions, i.e., with the size-shape stability condition, the problem is completely integrable and can be reduced to quadratures. For the case of no rotation these quadratures can be expressed in terms of elliptic functions and integrals. For the rapid rotation case, motion can be reduced to the well-known oblate body perturbation problem. One application of the secular motion analysis is to discuss the condition of periodic orbits, for example the 1:2 periodic family discussed in Section 5.5.3. One conference [20] and two journal papers [40],[20] have been published from this chapter.

In Chapter IV, we analyze the short-period motion which is closely related to resonance. The study of resonace can answer some of the size-shape stability problems which are proposed in Section 2.3.3. Resonance in our system exists because of the longitudinal dependent tesseral C_{22}, and due to commensurability between orbital mean motion n and the asteroid rotation ω_T. Specifically, we use elliptic expansions to derive the Fourier expansions of semi-major axis $a(t)$ and eccentricity $e(t)$ for nominal orbits in our system, i.e., the frequencies, amplitudes and phase angles of the Fourier expansion of $a(t), e(t)$ are estimated. With the Fourier expansions, we can explain the dynamics of the semi-major axis for near circular orbits. Additionally, by averging along near resonant orbits, we can explain why $a(t)$ and $e(t)$ sometimes experience large changes over short time spans. Together with the resonant integral analysis [38], we can estimate a stability index for our size-shape stability analysis, proposed in Chapter II. Additionally, the Fourier expansion of $a(t)$ and $e(t)$ can be used to analyze the periodic orbits in Chapter V, for example the 1:2 periodic family in Section 5.5.3. Some numerical analyses and verifications are also given.

Chapter V studies periodic orbits around asteroids. First, we analyze the four equilibrium points in the rotating 2nd degree and order gravity field. Two of them are

always unstable, the other two can be stable or unstable, their stability determined by the central body rotation rate ω_T, the two gravity coefficients, C_{20} and C_{22}, and the asteroid's mass. Next we compute families of periodic orbits. In our searching procedure, we remove the two unity eigenvalues from the state transition matrix (STM) to find a robust, non-singular Poincaré map to solve for the periodic orbits. The algorithm converges well, especially for stable periodic orbits. As we give the initial variations a Jacobi constraint, the procedure automatically searches for a periodic orbit at a fixed energy level. By calculating the STM for the periodic orbit, we find the characteristic multipliers which are the indices of stability of the periodic orbit. These are used to test the stability of the periodic orbits. Then, by using a relatively automatic searching procedure for the periodic orbits, we find five basic families of periodic orbits and discuss their existence and stability at different central body rotation rates. We call these five basic families the near direct, far direct, 1:1 resonant, 1:2 resonant and retrograde periodic orbits. There are also other "special" periodic orbits which lie between these basic periodic orbit families. A conference paper [21] has been published from this chapter.

In Chapter VI, we give a summary of the dissertation and indicate future research topics. We see that by using these three different methods, averaging, resonance analysis and periodic orbit computation, we can reveal different aspects of the nature of spacecraft motion in a uniformly rotating, second degree and order gravity field. We also find that they are closely related, and that some results in our secular and resonant analyses can be used to discuss the existence and stability of periodic orbits.

CHAPTER II

PROBLEM STATEMENT

In this chapter we will first review some basic notation and equations which we will use in this dissertation. Then we propose a definition for size-shape stability and present two facts which are related to the orbital stability of spacecraft motion around an asteroid. Finally, we give a preliminary analysis to some basic questions of our problem with a numerical study. These questions will be discussed throughout the dissertation.

2.1 Gravity Potential

This dissertation studies the orbital motion of a spacecraft about a non-spherical, uniformly rotating asteroid. The first non-trivial perturbation terms from the asteroid gravity field is represented by the 2nd degree and order gravity coefficients, C_{20} and C_{22}. Before discussing these important coefficients, we give some remarks about higher order gravity potential expansions.

2.1.1 Expansion of the gravity potential

The spherical harmonic expansion of a gravitational force potential is [23]:

$$U = \sum_{l=0}^{\infty} \sum_{m=0}^{n} \frac{\mu}{r^{l+1}} P_{lm}(\sin\delta) \left[C_{lm} \cos m\lambda + S_{lm} \sin m\lambda\right], \qquad (2.1)$$

where μ is gravitational parameter, r is the radius of the particle measured from the center of mass of the body, δ is the particle declination measured from the x-y plane, and λ is the particle longitude in the body-fixed frame, measured counter-clockwise from the x axis. See Figure 2.1 for the geometry of the above definitions.

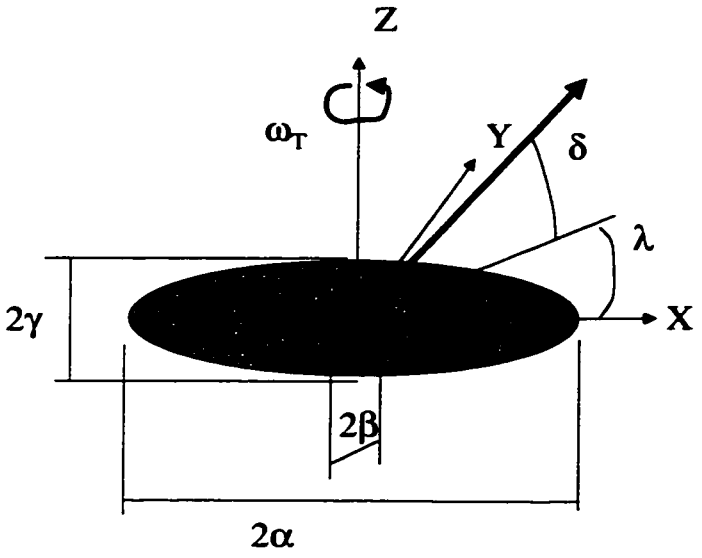

Figure 2.1: Position geometry of a mass point about an asteroid(ellipsoid here) in the body-fixed space.

The $P_{lm}(\sin\delta)$ are Associated Legendre Functions of degree l and order m.

$$P_{lm}(\sin\delta) = \cos^m\delta\sum_{t=0}^{k} T_{lmt}\sin^{l-m-2t}\delta, \tag{2.2}$$

where k is the integer part of $(l-m)/2$, $m \le l$. For $t \neq 0$

$$T_{lmt} = \frac{(-1)^t(2l-2t)!}{2^l t!(l-t)!(l-m-2t)!}. \tag{2.3}$$

For $t = 0$

$$T_{lm0} = \frac{(2l)!}{2^l l!(l-m)!}. \tag{2.4}$$

In general

$$P_{lm}(x) = \frac{(1-x^2)^{m/2}}{2^l l!}\cdot\frac{\mathrm{d}^{(l+m)}(x^2-1)^l}{\mathrm{d}x^{(l+m)}}. \tag{2.5}$$

The expansions of the potential $U = U_0 + U_1 + U_2 + U_3 + U_4 + \ldots$ up to order four are shown here

$$U_0 = \frac{\mu}{r}, \tag{2.6}$$

$$U_1 = \frac{\mu}{r^2}\Big[C_{10}\sin\delta + \cos\delta(C_{11}\cos\lambda + S_{11}\sin\lambda)\Big], \tag{2.7}$$

$$\begin{aligned} U_2 = \frac{\mu}{r^3}\Big[&C_{20}(1-\frac{3}{2}\cos^2\delta) \\ &+\frac{3}{2}\cos 2\delta(C_{21}\cos\lambda + S_{21}\sin\lambda) \\ &+3\cos^2\delta(C_{22}\cos 2\lambda + S_{22}\sin 2\lambda)\Big], \end{aligned} \tag{2.8}$$

$$\begin{aligned} U_3 = \frac{\mu}{r^4}\Big[&C_{30}\sin\delta(1-\frac{5}{2}\cos^2\delta) \\ &-\frac{3}{2}(1-5\sin^2\delta)\cos\delta(C_{31}\cos\lambda + S_{31}\sin\lambda) \\ &+15\sin\delta\cos^2\delta(C_{32}\cos 2\lambda + S_{32}\sin 2\lambda) \\ &+15\cos^3\delta(C_{33}\cos 3\lambda + S_{33}\sin 3\lambda)\Big], \end{aligned} \tag{2.9}$$

$$U_4 = \frac{\mu}{r^5}\Big[C_{40}(\frac{35}{8}\sin^4\delta - \frac{15}{4}\sin^2\delta + \frac{3}{8})$$

$$+(\frac{35}{2}\sin^3\delta - \frac{15}{2}\sin\delta)\cos\delta(C_{41}\cos\lambda + S_{41}\sin\lambda)$$
$$+(\frac{105}{2}\sin^2\delta - \frac{15}{2})\cos^2\delta(C_{42}\cos 2\lambda + S_{42}\sin 2\lambda)$$
$$+105\sin\delta\cos^3\delta(C_{43}\cos 3\lambda + S_{43}\sin 3\lambda)$$
$$+105\cos^4\delta(C_{44}\cos 4\lambda + S_{44}\sin 4\lambda)\Big]. \qquad (2.10)$$

If the origin of the coordinate frame is at the center of mass of the asteroid, then $C_{10} = C_{11} = S_{11} = 0$. Also, if the body-fixed coordinate axes are assumed to be aligned along the body's principal moments of inertia (see Figure 2.1) then $C_{21} = S_{21} = S_{22} = 0$. So for these two conditions, the gravity field can be represented by two coefficients C_{20} and C_{22} for a second degree and order gravity expansion.

Shown in Table 2.1 are the gravity coefficients of asteroid 4769 Castalia through order 4 [36]. The coefficients are normalized by a radius $r_0 = 0.5431$ km and by normalizing factors, defined by

$$\bar{S}_{lmi} = \left[\frac{(l-m)!(2l+1)(2-\delta_{0m})}{(l+m)!}\right]^{1/2} S_{lmi}, \qquad (2.11)$$

where $\delta_{0m} = 1$ when $m = 0$, and $\delta_{0m} = 0$ when $m \neq 0$. We see from the Table 2.1 that C_{20} and C_{22} are much larger than the other coefficients.

Conventionally, the C_{l0} are called zonal harmonic coefficients and the C_{lm}, S_{lm} are called sectoral harmonic coefficients when $l = m$ and tesseral harmonic coefficients when $l \neq m$.

2.1.2 Relation to moments of inertia

For definiteness we will specify the frame so that $C_{20} \leq 0$ and $C_{22} \geq 0$, implying that the principal moments of inertia are ordered as $I_{xx} \leq I_{yy} \leq I_{zz}$ with axes x, y and z (See Figure 2.1). The relations between the gravity coefficients and the

Order	Degree	C coefficient	S coefficient
0	0	1.0	-
1	0	0.0	-
1	1	0.0	0.0
2	0	-0.110298	-
2	1	0.0	0.0
2	2	0.156733	0.0
3	0	-0.015112	-
3	1	-0.037935	0.001211
3	2	0.006325	0.000616
3	3	0.020568	-0.013715
4	0	0.036630	-
4	1	0.002706	0.000407
4	2	-0.051363	0.003949
4	3	0.006140	-0.001747
4	4	0.050334	-0.006839

Table 2.1: The gravity coefficients for Castalia

principal moments of inertia of the body (normalized by the body mass) are [9], [43]:

$$C_{20} = -\frac{1}{2}(2I_{zz} - I_{xx} - I_{yy}), \tag{2.12}$$

$$C_{22} = \frac{1}{4}(I_{yy} - I_{xx}). \tag{2.13}$$

A mass-distribution parameter σ can be defined as:

$$\sigma = \frac{I_{yy} - I_{xx}}{I_{zz} - I_{xx}} = -\frac{4C_{22}}{C_{20} - 2C_{22}}, \tag{2.14}$$

where $0 \leq \sigma \leq 1$ for any mass distribution. A value of $\sigma = 0$ denotes a body with rotational symmetry about the z-axis ($I_{yy} = I_{xx}$) and a value of $\sigma = 1$ denotes a body with rotational symmetry about the x-axis ($I_{yy} = I_{zz}$). This parameter will be introduced into the gravitational potential once averaging is performed in Chapter III. The gravity coefficients in terms of this parameter are:

$$C_{20} = -\frac{1}{2}(I_{zz} - I_{xx})(2 - \sigma) \tag{2.15}$$

$$C_{22} = \frac{1}{4}(I_{zz} - I_{xx})\sigma \tag{2.16}$$

2.1.3 Ellipsoid example

To give a more physically motivated example for the gravity potential we assume that the second degree and order gravity coefficients are derived from a constant density, tri-axial ellipsoid shape. This assumption is not necessary, but provides a physical realization of our system. Assume a central body with semi-axes of $\alpha \geq \beta \geq \gamma$. According to our coordinate frame definitions α is along the x-axis while β is measured along the y-axis and γ is measured along the z-axis (See Figure 2.1). Instead of using the semi-major axes β and γ we can also use the ellipticities of the ellipsoid:

$$\beta = \alpha\sqrt{1 - \epsilon_b^2}, \tag{2.17}$$

$$\gamma = \alpha\sqrt{1 - \epsilon_c^2}. \tag{2.18}$$

Thus, with our ordering convention we have $\epsilon_b \leq \epsilon_c$ and $\sigma = \epsilon_b^2/\epsilon_c^2$. With these definitions the gravity coefficients can be re-written in terms of ϵ_c and σ as [35]:

$$C_{20} = -\frac{\alpha^2\epsilon_c^2}{10}(2-\sigma), \tag{2.19}$$

$$C_{22} = \frac{\alpha^2\epsilon_c^2}{20}\sigma. \tag{2.20}$$

2.2 The Equations of Motion of orbiging body

In inertial coordinates the position vector of orbiting body is $\mathbf{r}_i = [x_i, y_i, z_i]^T$ satisfies,

$$\ddot{\mathbf{r}}_i = \frac{\partial U_i}{\partial \mathbf{r}_i}, \tag{2.21}$$

where the gravity potential $U_i = \mu/r + U_2$. As we show later, the equations are time varying if we include the angular velocity in the rotating asteroid. To avoid this inconvenience, we transform the above equations into a rotating coordinate frame that is fiexed to the asteroid.

2.2.1 Motion in body-fixed coordinates

Let $\mathbf{r} = [x, y, z]^T$, $\boldsymbol{\omega} = [0, 0, \omega_T]^T$ both expressed in body-fixed coordinate, then[15]

$$\ddot{\mathbf{r}} + 2\boldsymbol{\omega} \times \dot{\mathbf{r}} + \boldsymbol{\omega} \times (\boldsymbol{\omega} \times \mathbf{r}) = -\frac{\mu}{r^3}\mathbf{r} + \frac{\partial U_2}{\partial \mathbf{r}}, \tag{2.22}$$

where U_2 is Equation 2.8. The scalar form of the above equation is:

$$\ddot{x} - 2\omega_T\dot{y} = \omega_T^2 x - \frac{\mu x}{r^3} + \frac{\partial U_2}{\partial x}, \tag{2.23}$$

$$\ddot{y} + 2\omega_T\dot{x} = \omega_T^2 y - \frac{\mu y}{r^3} + \frac{\partial U_2}{\partial y}, \tag{2.24}$$

$$\ddot{z} = -\frac{\mu z}{r^3} + \frac{\partial U_2}{\partial z}. \tag{2.25}$$

These equations are defined in the body-fixed coordinate frame whose rotation rate is a constant ω_T, and thus includes the effect of coriolis and centripetal accelerations. Here we assume that the asteroid is in uniform rotation about its maximum moment of inertia (the z-axis) with a rotation rate ω_T and a corresponding rotation period $T = 2\pi/\omega_T$. More complete discussions of these equations as applied to motions about an asteroid have been reported in [35]. Figure 2.2 shows the relation between the inertial coordinates and the body-fixed coordinates with rotation rate ω_T.

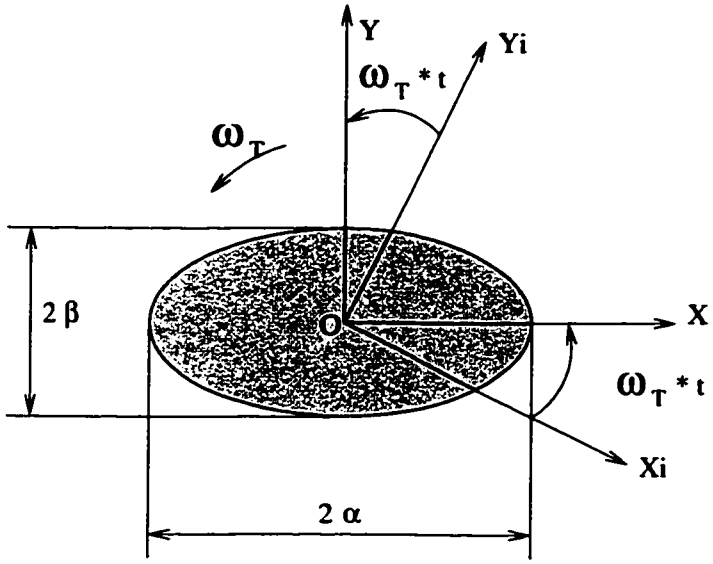

Figure 2.2: Plane geometry of the inertial X_iOY_i and the body-fixed XOY coordinates.

In Equation 2.22-2.25 the gravitational perturbation potential of the 2nd degree and order in the body-fixed frame is

$$U_2 = \frac{\mu}{r^3}\left[C_{20}\left(1 - \frac{3}{2}\cos^2\delta\right) + 3C_{22}\cos^2\delta\,\cos 2\lambda\right]. \tag{2.26}$$

In Cartesian coordinates it becomes

$$U_2 = -\frac{\mu C_{20}(x^2+y^2-2z^2)}{2r^5} + \frac{3\mu C_{22}(x^2-y^2)}{r^5}, \tag{2.27}$$

where $r = \sqrt{x^2+y^2+z^2}$, $\sin\delta = z/r$ and $\tan\lambda = y/x$, or $\lambda = \arctan(y_i/x_i) - \omega_T t = \arctan(y/x)$.

First order partial derivatives of the potential are

$$\begin{aligned}\frac{\partial U_2}{\partial x} &= -\frac{\mu C_{20} x}{r^5} + \frac{5\mu C_{20} x(x^2+y^2-2z^2)}{2r^7} \\ &\quad + \frac{6\mu C_{22} x}{r^5} - \frac{15\mu C_{22} x(x^2-y^2)}{r^7}, \end{aligned} \tag{2.28}$$

$$\begin{aligned}\frac{\partial U_2}{\partial y} &= -\frac{\mu C_{20} y}{r^5} + \frac{5\mu C_{20} y(x^2+y^2-2z^2)}{2r^7} \\ &\quad - \frac{6\mu C_{22} y}{r^5} - \frac{15\mu C_{22} y(x^2-y^2)}{r^7}, \end{aligned} \tag{2.29}$$

$$\begin{aligned}\frac{\partial U_2}{\partial z} &= \frac{2\mu C_{20} z}{r^5} + \frac{5\mu C_{20} z(x^2+y^2-2z^2)}{2r^7} \\ &\quad - \frac{15\mu C_{22} z(x^2-y^2)}{r^7}. \end{aligned} \tag{2.30}$$

2.2.2 Numerical calculation

For numerical analyses in this dissertation we use a variable-step Runge-Kutta 7(8) method to integrate Equation 2.23-2.25. The calculated orbital position (x, y, z) and velocity $(\dot{x}, \dot{y}, \dot{z})$ in the rotating coordinate frame can then be transformed into position (x_i, y_i, z_i) and velocity $(\dot{x}_i, \dot{y}_i, \dot{z}_i)$ in the inertial coordinates by the transformation

$$\begin{bmatrix} x_i \\ y_i \\ z_i \end{bmatrix} = \begin{bmatrix} \cos\omega_T t & -\sin\omega_T t & 0 \\ \sin\omega_T t & \cos\omega_T t & 0 \\ 0 & 0 & 1 \end{bmatrix} \begin{bmatrix} x \\ y \\ z \end{bmatrix}, \tag{2.31}$$

$$\begin{bmatrix} \dot{x}_i \\ \dot{y}_i \\ \dot{z}_i \end{bmatrix} = \begin{bmatrix} \cos\omega_T t & -\sin\omega_T t & 0 \\ \sin\omega_T t & \cos\omega_T t & 0 \\ 0 & 0 & 1 \end{bmatrix} \begin{bmatrix} \dot{x} - \omega_T y \\ \dot{y} + \omega_T x \\ \dot{z} \end{bmatrix}. \tag{2.32}$$

Then using the position and velocity in the inertial coordinate frame we can evaluate the six orbital elements [4],[32]. When necessary the elements can be transformed

into a rotating coordinate frame again. Since the elements a, e, i, ω, τ in rotating coordinates are the same as in inertial coordinates, the only changed element is the longitude of ascending node. The relation between the longitude of ascending node in rotating coordinates and inertial coordinates is $\Omega_R = \Omega - \omega_T t$. More detailed discussions about the six orbital elements can be found in Section 3.1.1.

By the inverse transformations of Equation 2.31 and 2.32, the equations of motion of 2.23-2.25 can be transformed into inertial coordinates

$$\begin{aligned}
\ddot{x}_i &= -\frac{\mu x_i}{r^3} - \frac{\mu C_{20} x_i}{r^5} - \frac{5\mu C_{20} x_i (x_i^2 + y_i^2 - 2z_i^2)}{2r^7} + \frac{6\mu C_{22} x_i}{r^5} \\
&\quad - \frac{15\mu C_{22} x_i}{r^7}\Big[\cos(2\omega_T t)(x_i^2 - y_i^2) + 2\sin(2\omega_T t) x_i y_i\Big], \qquad (2.33) \\
\ddot{y}_i &= -\frac{\mu y_i}{r^3} - \frac{\mu C_{20} y_i}{r^5} - \frac{5\mu C_{20} y_i (x_i^2 + y_i^2 - 2z_i^2)}{2r^7} - \frac{6\mu C_{22} y_i}{r^5} \\
&\quad - \frac{15\mu C_{22} y_i}{r^7}\Big[\cos(2\omega_T t)(x_i^2 - y_i^2) + 2\sin(2\omega_T t) x_i y_i\Big], \qquad (2.34) \\
\ddot{z}_i &= -\frac{\mu z_i}{r^3} + \frac{2\mu C_{20} z_i}{r^5} + \frac{5\mu C_{20} z_i (x_i^2 + y_i^2 - 2z_i^2)}{2r^7} \\
&\quad - \frac{15\mu C_{22} z_i}{r^7}\Big[\cos(2\omega_T t)(x_i^2 - y_i^2) + 2\sin(2\omega_T t) x_i y_i\Big]. \qquad (2.35)
\end{aligned}$$

We see that these equations are explicit functions of time t.

2.2.3 Jacobi integral and Hamiltonian function

Since the force potential U_2 is time invariant in the rotating coordinates, a Jacobi integral exists for our problem:

$$\begin{aligned}
J &= \frac{1}{2}\left(\dot{x}^2 + \dot{y}^2 + \dot{z}^2\right) - \frac{1}{2}\omega_T^2 (x^2 + y^2) - U_2 - \frac{\mu}{r} \qquad (2.36) \\
&= -\frac{\mu}{2a} - \omega_T \sqrt{\mu a (1 - e^2)}\cos i - U_2, \qquad (2.37)
\end{aligned}$$

where a is the osculating semi-major axis of the orbit, e is the osculating eccentricity, and i is the osculating inclination. This relation is conserved for all solutions to the equations of motion.

It can be shown that the system we study can be expressed as a Hamiltonian system. If we assume $\mathbf{q} = [x\ y\ z]^T$, $\mathbf{p} = [p_x\ \ p_y\ \ p_z]^T$, then

$$H(\mathbf{p},\mathbf{q}) = \frac{1}{2}(p_x^2 + p_y^2 + p_z^2) - \omega_T y p_x + \omega_T x p_y - \frac{\mu}{r} - U_2 \tag{2.38}$$

$$= H(x, y, z, \dot{x}, \dot{y}, \dot{z}) = \frac{1}{2}(\dot{x}^2 + \dot{y}^2 + \dot{z}^2) - U_e, \tag{2.39}$$

where U_e is the effective potential function,

$$U_e = \frac{1}{2}\omega_T^2(x^2 + y^2) + \frac{\mu}{r} + U_2. \tag{2.40}$$

And the p_x, p_y, p_z are

$$p_x = \dot{x} - \omega_T y, \tag{2.41}$$

$$p_y = \dot{y} + \omega_T x, \tag{2.42}$$

$$p_z = \dot{z}. \tag{2.43}$$

We see that the Hamiltonian function (Equation 2.39) is just the Jacobi integral (Equation 2.36), for

$$\dot{\mathbf{q}} = \frac{\partial H}{\partial \mathbf{p}}, \tag{2.44}$$

$$\dot{\mathbf{p}} = -\frac{\partial H}{\partial \mathbf{q}}. \tag{2.45}$$

2.3 Stability Analysis

Conventionally, a perturbed orbit is said to be stable if its motion remains near to its unperturbed orbit. This definition is not convenient for the discussion of our problem; thus we define a specific type of orbital stability for our problem.

2.3.1 Size-shape stability definition

For an unperturbed Keplerian orbit, five of its six elements are constant(assuming the true anomally as its 6th element): semi-major axis a, eccentricity e, longitude of

ascending node Ω, argument of periapsis ω, inclination i. These five elements can be classified into two groups, a size-shape group including a, e, and an orientation group including Ω, ω, i. For spacecraft motion about the Earth (nonzero $C_{20}, C_{22} \approx 0$), an orbit's size and shape are constant on average and the only changes in an orbit are in its orientation. But for the case of orbits close to asteroids, both orientation and size-shape changes occur, making the study of the motion around a rotating asteroid complicated.

If an orbit's semi-major axis and eccentrity are constant on average, the orbit is said to be *size-shape stable.* Sometimes this motion is regarded as a regular motion. For this situation, we usually use an averaging method to analyze the secular orientation of the orbit.

If an orbit's semi-major axis or eccentrity is not constant on average, the orbit is said to be *size-shape unstable.* Often, this motion can be regarded as chaotic.

Figure 2.3 shows two examples of orbits; one is size-shape stable and one is size-shape unstable. Their initial orbits are both near circular. The orbit whose initial semi-major axis $a_{0s} = 1.8$ is stable; the other orbit whose initial semi-major axis $a_{0u} = 1.6$ is unstable.

If an orbit is size-shape stable, its averaged orbit is said to be its *nominal orbit*, whose semi-major axis a_0 and eccentrity e_0 are constant on average. Then our problem is to study the oscillations of $a(t)$ and $e(t)$ about their nominal values. When our orbit is size-shape unstable we find that, at least, $a(t)$ and $e(t)$ rapidly depart from their initial specification.

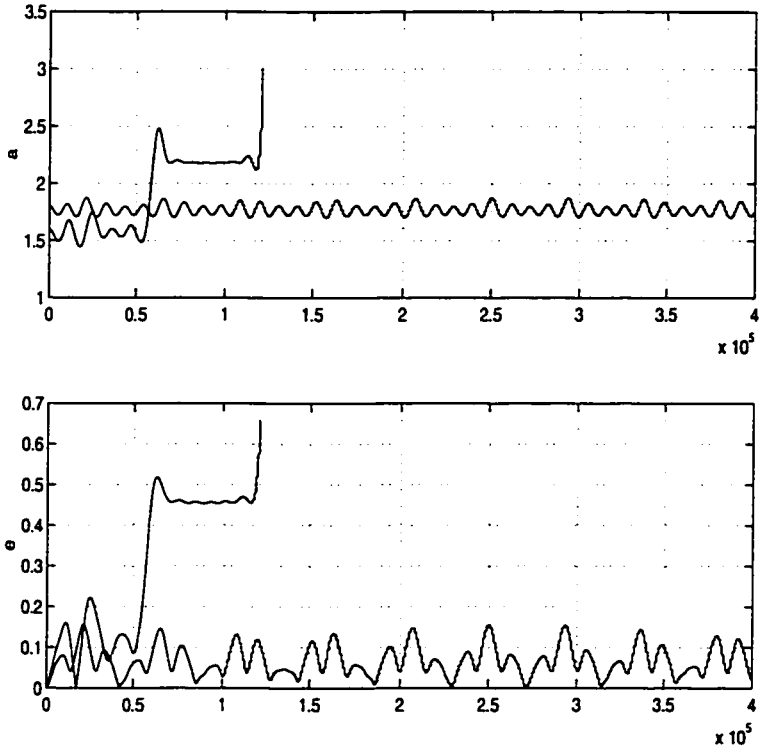

Figure 2.3: Examples of size-shape stable and unstable orbits

2.3.2 Two facts

With our definitions of size-shape stability and nominal orbit, we can state two qualitative facts concerning spacecraft motion in our uniformly rotating 2nd degree and order gravity field based on numerical calculations and analysis without rigorous proof.

Fact one: For an orbit in the uniformly rotating second degree and order gravity field, if changes in semi-major axis $\Delta a(T)$ and eccentricity $\Delta e(T)$ over one nominal orbit are "small enough", the orbit will "mostly" keep its semi-major axis and eccentricity constant on average, i.e., it will be size-shape stable; when $\Delta a(T)$ or $\Delta e(T)$ is large enough, the orbit will be size-shape unstable.

The above fact can be regarded as a specific version of the general KAM theory for our problem, but we give explicit stability estimates (More discussion is given in Section 4.4.1). Consider an n-Degree-of-Freedom, smooth Hamiltonian system ($n > 1$) written as a function of actions $\mathbf{I}$ and angle coordinates $\boldsymbol{\theta}$. The Hamiltonian consists of an integrable term H_0 being perturbed by a term H_1

$$H = H_0(\mathbf{I}) + \epsilon H_1(\mathbf{I}, \boldsymbol{\theta}). \tag{2.46}$$

The KAM theorem states that if H_0 is sufficiently nonlinear ($|\partial^2 H_0/\partial \boldsymbol{I}^2 \neq 0|$), and the system initial condition are sufficiently far from resonance, then there exist a smooth, near-identity change of coordinates from the integrable solution to the non-integrable solution, and the motion of the perturbed system will produce quasiperiodic trajectories associated with the integrable motion [10],[8]. The integrable motion here corresponds to our averaged nominal orbits.

Fact two: When a particle is moving in a uniformly rotating 2nd degree and order gravity field, if it is size-shape stable, the particle will normally not escape or collide

with the central body; conversely, if it is size-shape unstable, it will "usually" escape or impact the central body, sooner or later.

Figure 2.4 shows two examples of orbits, one of them escaping from the asteroid, the other colliding into the asteroid. Both of these orbits are size-shape unstable, though their initial orbits are nearly circular. We note that the center of mass of the asteroid is at the origin $(0, 0)$.

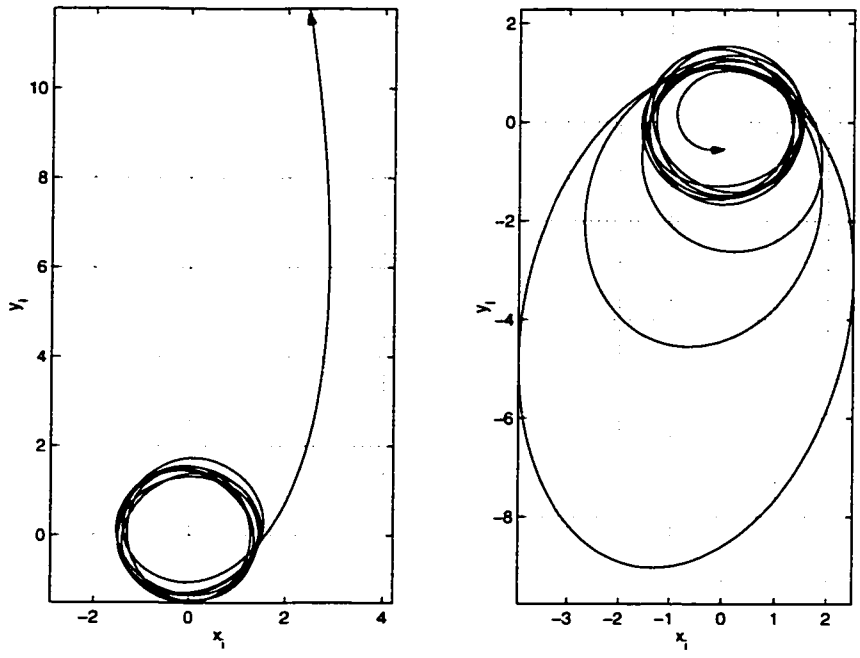

Figure 2.4: Examples of ejection and collision orbits

Here we make some discussion concerning the words "usually", and "small enough". Similar to the celebrated KAM theorem, we also use the world "usually" which means that occasionally some anomalies appear, but almost all, if not all, will follow the law. And also, the phrase "small enough" is used to mean the oscillation amplitude of the semi-major axis and eccentricity will have limits which correspond to KAM stability estimates when the orbits are size-shape stable. Wiggins [45] gives some mathematical remarks about these "ambiguous" words when he states the KAM

theorem.

It is evident that the stable orbits with "small enough" oscillation do exist in our problem. For example, when the orbiting body is far from the asteroid, the perturbation from the asteroid on the orbiting body is weak and the orbit is size-shape stable. The radius is one factor that affects the strength of the perturbation, but the asteroid rotation rate ω_T and the asteroid gravity coefficient C_{22} also are important [38].

2.3.3 Size-shape stability of motions

There are some basic questions we can ask about the size-shape stability of motion in our uniformly rotating second degree and order gravity field.

- What are the parameters which determine the size-shape stability of an orbit?
- Over what initial conditions do stable and unstable orbits exist?
- How does the trajectory behave when an orbit is size-shape stable or size-shape unstable?

We will discuss these questions throughout this dissertation and answer them at different points, both numerically and analytically. Here we provide a preliminary analysis using a numerical study.

In the above sections we qualitatively discussed the phenomena of general instability. The mechanism which causes these instabilities is resonance. Resonance occurs when the ratio of the asteroid rotation rate, ω_T, to the nominal mean motion, n_0, of a orbiting body is near a rational number, i.e., the ratio of two integers such as 1:2, 1:1, 3:2.

Near resonance, the size and shape of the orbit often experience large changes. In the uniformly rotating second degree and order gravity field, if the oscillation of the semi-major axis or eccentricity over one nominal orbit is "large enough", the orbit is size-shape unstable.

Recall from Figure 2.3 that one orbit whose initial semi-major axis $a_{0s} = 1.8$ is size-shape stable; the other orbit whose initial semi-major axis $a_{0u} = 1.6$ is size-shape unstable. In between these two near-circular initial orbits there exists a critical near circular orbit whose semi-major axis is a_{0c}. For another initially near circular orbit, if its semi-major axis satisfies $a_0 \geq a_{0c}$, it is stable, and for an orbit whose semi-major axis satisfies $a_0 < a_{0c}$, it is unstable. Hence, a_{0c} can be regarded as the minimum initial semi-major axis for a stable, near circular orbit.

We performed a numerical analysis to find the boundary between the size-shape stable and unstable regions for initially near circular orbits for fixed values of the coefficients C_{20} and C_{22}, but with different central body rotation rates, ω_T. The boundary represents the relation between ω_T and the minimum initial semi-major axis a_{0c}. Figure 2.5 shows the critical line between stable and unstable initially circular orbits for different values of ω_T. And it shows the relation to resonant orbits when ω_T/n_0 is a ratio of two integers.

The stable orbits defined in the plots are the orbits whose semi-major axis and eccentrity are near constant on average, which means the energy and angular momentum magnitude of the orbit do not change much on average. The orientation of these orbits may change. If there are large semi-major axis and eccentrity changes within one nominal orbit, we regard the nominal orbit as unstable. We see in this picture that when the line is crossed, the system is in a region with a more strongly varying semi-major axis and eccentrity. The plot is made using the Castalia

model with a varying rotation rate. For the asteroid, $\mu = 9.40 \times 10^{-8}\text{km}^3/\text{sec}^2$, $C_{20} = -7.275 \times 10^{-2}\text{km}^2$, $C_{22} = 2.984 \times 10^{-2}\text{km}^2$ and $\omega_T = 4.2883 \times 10^{-4}$ radians/sec.

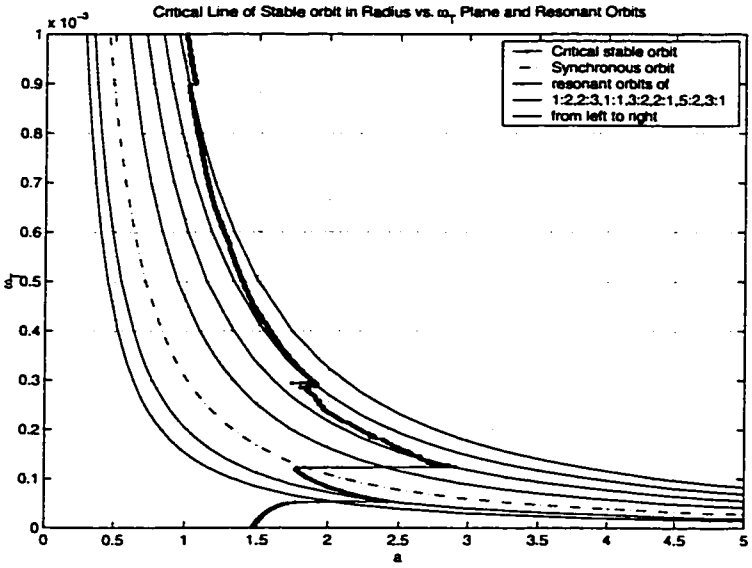

Figure 2.5: The boundary line between the size-shape stable and the size-shape unstable regions for near circular orbits

In Figure 2.5, when orbits are near the asteroid and the asteroid rotates slowly, then $|(n_0 - \omega_T)/\omega_T| \gg 1$. These orbits are usually in a size-shape stable region(lower-right). When orbits are far away and the asteroid rotates rapidly, then $(\omega_T - n_0)/n_0 \gg 1$. These orbits are also usually in the stable region(upper-right). For both of these cases, averaging theory can be used to analyze their secular motions. We will give comprehensive discussions of this in Chapter III.

In the middle part of the figure, which is the *resonance region*, the orbits are usually unstable. We will give more discussions about this in Chapter IV, both numerically and analytically, where Fourier expansions for the semi-major axis and the eccentrity are used to derived the short period oscillation.

Analyses of secular motion and short period oscillations also help us to find and analyze stable and unstable periodic orbits. In Chapter V, we determine families of periodic orbits in both the stable and resonant regions. In this chapter we also introduce a control law to stabilize some of the size-shape unstable orbits in the resonance region.

CHAPTER III

ANALYSIS OF SECULAR MOTION

3.1 Introduction

For size-shape stable orbits in our uniformly rotating second degree and order gravity field, we can use averaging methods to filter the rapidly changing effects while keeping the slowly changing effects that describe the secular motion. The averaging method has been used extensively for orbital motion about an oblate planet (or gravity field with C_{20} term only), starting in the early 1960's [11],[25],[7]. Most studies that have included the equatorial ellipticity of the central body (i.e., the C_{22} gravity term) have made the assumption that the ellipticity is small, as is appropriate for planets in the solar system [23],[13],[10]. Our current problem is a significant departure, however, in that it considers values of the C_{22} gravity coefficient that are significantly larger than those found for all solar system planets, making this analysis applicable to asteroids and comets which can have large values of equatorial ellipticity. As has been shown, the basic nature of orbit dynamics about distended, rotating bodies has fundamental differences as compared to orbit dynamics about slightly elliptical bodies [35]. In this chapter, we study the averaged motion for three cases when the asteroid does not rotate, rotates slowly and rotates rapidly. We first introduce some basic notation and equations used in this chapter.

3.1.1 Potential in orbital element form

For convenience, we recall the gravity potential.

$$U_2 = \frac{\mu}{r^3}\left[C_{20}\left(1-\frac{3}{2}\cos^2\delta\right)+3C_{22}\cos^2\delta\cos 2\lambda\right]. \tag{3.1}$$

The angles δ and λ can be specified in terms of orbital elements:

$$\sin\delta = \sin i\sin u, \tag{3.2}$$

$$\tan\lambda = \frac{\sin\Omega_R\cos u+\cos\Omega_R\sin u\cos i}{\cos\Omega_R\cos u-\sin\Omega_R\sin u\cos i}, \tag{3.3}$$

$$u = \omega+f, \tag{3.4}$$

$$\Omega_R = \Omega-\omega_T t, \tag{3.5}$$

where i is the inclination, ω is the argument of periapsis, f is the true anomaly, Ω_R is the longitude of the ascending node in the body-fixed frame and Ω is the longitude of ascending node in the inertial frame. For a slowly rotating asteroid, the elements (a,e,i,ω,f) in the rotating coordinate frame are the same as they are in the inertial coordinate frame, the only difference being the longitude of ascending node. The relation between the longitude of ascending node in a rotating coordinate frame and in an inertial coordinate frame is $\Omega_R=\Omega-\omega_T t$. When a central body does not rotate($\omega_T=0$), these two longitudes of the ascending node are the same($\Omega_R=\Omega$).

Figure 3.1 shows a spacecraft orbit in both inertial coordinates $X_iY_iZ_iO$ and body-fixed, rotating coordinates $XYZO$.

In inertial coordinates, the gravity potential can be shown to be

$$\begin{aligned} U_2 = \frac{\mu}{r^3}\Bigg\{ & C_{20}\left[\frac{3}{4}\sin^2 i\big(1-\cos 2(\omega+f)\big)-\frac{1}{2}\right]+ \\ & +3C_{22}\Big[\frac{1}{2}\sin^2 i\cos 2(\Omega-\omega_T t)+\cos^4\frac{i}{2}\cos 2(\Omega+\omega+f-\omega_T t) \\ & +\sin^4\frac{i}{2}\cos 2(\Omega-\omega-f-\omega_T t)\Big]\Bigg\}. \end{aligned} \tag{3.6}$$

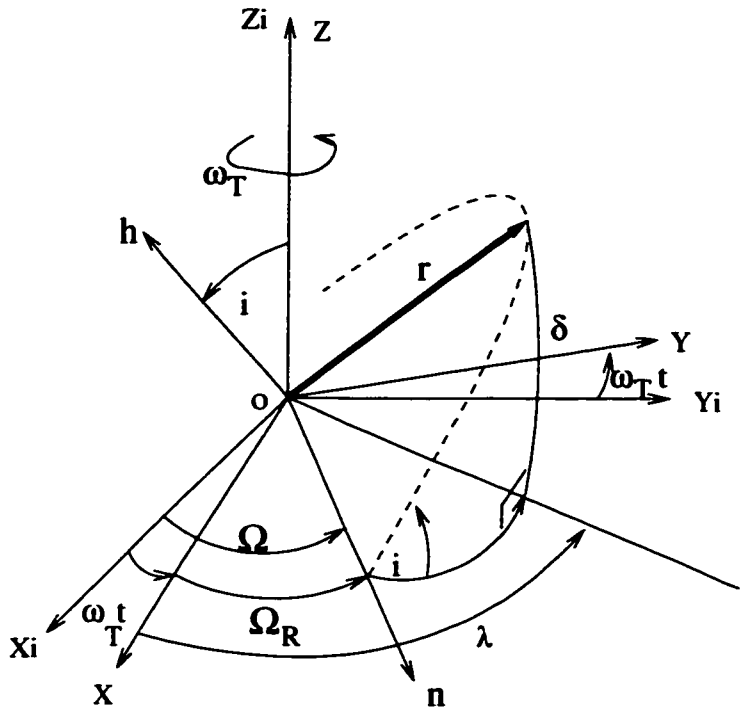

Figure 3.1: The geometry of an orbit in both inertial and rotating coordinates.

3.1.2 Averaging condition

We now review the fundamentals of the averaging method; consider[24]:

$$\dot{\mathbf{x}} = \epsilon \mathbf{f}(t, \mathbf{x}, \epsilon), \tag{3.7}$$

where $\mathbf{x}$ is a vector of slow varibles compared to t and ϵ is a small positive number, and $\mathbf{f}(t, \mathbf{x}, \epsilon)$ is a T-periodic or quasi-periodic vector in t. The corresponding averaged system is defined as

$$\dot{\mathbf{x}}_{av} = \epsilon \mathbf{f}_{av}(\mathbf{x}_{av}, \epsilon), \tag{3.8}$$

where

$$\mathbf{f}_{av} = \frac{1}{T} \int_0^T \mathbf{f}(\tau, \mathbf{x}, 0) \mathrm{d}\tau. \tag{3.9}$$

Then, under some non-resonance conditions[3], it can be shown that

$$\| \mathbf{x}(t, \epsilon) - \mathbf{x}_{av}(t, \epsilon) \| = O(\epsilon). \tag{3.10}$$

For our system, the slow variables are $a, e, i, \Omega, \omega, n$, and the fast variable is the mean motion M for the central body slowly or non-rotating case; and the fast mode is $\omega_T t$ for the rapidly rotating case.

3.2 When The Central Body Does Not Rotate: $\omega_T = 0$

In this section the motion of a particle about a non-rotating second degree and order gravity field is investigated. Averaging conditions are applied to the orbit motion and a qualitative analysis which reveals the general character of motion in this system is given. It is shown that the orbit plane will either be stationary or precess about the body's axis of minimum or maximum moment of inertia. We then show that the secular equations for this system can be integrated in terms of trigonometric, hyperbolic or elliptic functions. Explicit solutions are derived in all cases of interest.

3.2.1 Averaged Lagrange equations

To formulate our approach to this problem we average the perturbing potential (Equation 2.26) over the mean anomaly M:

$$\bar{U}_2 = \frac{1}{2\pi}\int_0^{2\pi} U_2 \mathrm{d}M, \tag{3.11}$$

to find the averaged gravity potential:

$$\bar{U}_2 = \frac{\mu(I_{zz}-I_{xx})}{2a^3(1-e^2)^{\frac{3}{2}}}\left[-\frac{2-\sigma}{2}\left(\frac{3}{2}\sin^2 i - 1\right) + \frac{3}{4}\sigma \sin^2 i \cos 2\Omega\right], \tag{3.12}$$

where the relations (Equation 2.19-2.20) are used.

Before substituting into Lagrange planetary equations a few points should be made. First, as with most averaged potential theories, the semi-major axis will be constant as the mean motion has been removed from the perturbation function.

Also, due to the absence of the argument of periapsis ω in the averaged potential, the eccentricity e will also be constant. This corresponds to our size-shape stability condition.

The energy integral can be re-evaluated for the averaged case. Performing the averaging on the integral yields:

$$\bar{J} = -\frac{\mu}{2a} - \bar{U}_2. \tag{3.13}$$

and we immediately note that $\bar{U}_2$ must be constant on average, specifically that the terms within the square brackets in Equation 3.12 are constant. Simplifying the expression we find a new form of the integral:

$$C = \sin^2 i \left(1 - \sigma \cos^2 \Omega\right). \tag{3.14}$$

This quantity is conserved for the averaged orbital elements only and not for the unaveraged elements.

Next, averaging the Lagrange planetary equations[7],[32] for the inclination, longitude of the ascending node, argument of periapsis, and mean motion yields:

$$\frac{\mathrm{d}i}{\mathrm{d}t} = \frac{1}{2} B\sigma \sin i \sin 2\Omega, \tag{3.15}$$

$$\frac{\mathrm{d}\Omega}{\mathrm{d}t} = -B \cos i \left(1 - \sigma \cos^2 \Omega\right), \tag{3.16}$$

$$\frac{\mathrm{d}\omega}{\mathrm{d}t} = -\frac{B}{2}\left(5C - 4 + \sigma + 2\sigma \cos^2 \Omega\right), \tag{3.17}$$

$$\frac{\mathrm{d}M}{\mathrm{d}t} = n\left[1 - \frac{B}{2}\sqrt{a^3(1-e^2)}\,(3C - 2 + \sigma)\right], \tag{3.18}$$

where

$$B = \frac{3n(I_{zz} - I_{xx})}{2a^2(1-e^2)^2}, \tag{3.19}$$

$$n = \sqrt{\frac{\mu}{a^3}}. \tag{3.20}$$

It is important to note that the mean anomaly rate in Equation 3.18 is a constant, implying that it can be used to define a new, effective semi-major axis value. Integrating this equation over one period of the mean anomaly yields:

$$2\pi = n\left[1 - \frac{B}{2}\sqrt{a^3(1-e^2)}\,(3C - 2 + \sigma)\right]\tilde{T}, \tag{3.21}$$

where $\tilde{T}$ is the new period of motion and is explicitly equal to:

$$\tilde{T} = \frac{T}{1 - \frac{1}{2}B\sqrt{a^3(1-e^2)}\,(3C - 2 + \sigma)}, \tag{3.22}$$

where $T = 2\pi/n$ is the unperturbed orbit period. We can define a new semi-major axis for our system as $\tilde{a}$ from the relation $\tilde{T} = 2\pi\tilde{a}^{3/2}/\sqrt{\mu}$ to find:

$$\tilde{a} = a\left[1 - \frac{1}{2}B\sqrt{a^3(1-e^2)}\,(3C - 2 + \sigma)\right]^{-2/3}. \tag{3.23}$$

We can then redefine the constant B using this new semi-major axis.

We also note that the argument of periapsis does not appear in any of the right-hand sides of Equations 3.15 - 3.17 and thus can be solved for by quadrature once solutions for i and Ω are found. Finally, we see that the equations for the inclination i and node Ω (Equations 3.15 and 3.16, respectively) are coupled - however Equation 3.14 can be used to decouple them. We will do so later when we explicitly integrate these equations.

When the inclination of the orbit is equal to 0° or 180° the longitude of the ascending node and argument of periapsis are combined into the longitude of periapsis, defined as $\varpi_\pm = \Omega \pm \omega$, where the + sign is used for orbits with an inclination of 0° and the − sign for orbits with an inclination of 180°. The general equation of motion for $\varpi_\pm$ is defined as:

$$\frac{d\varpi_\pm}{dt} = \mp\frac{B}{2}\left[5C - 2 + \sigma\right] \pm B\,(1 \mp \cos i)\left[1 - \sigma\cos^2\Omega\right], \tag{3.24}$$

where the second term containing Ω disappears in $\dot{\varpi}_+$ when $i = 0°$, and disappears in $\dot{\varpi}_-$ when $i = 180°$. Inspection of both cases shows that the longitude of periapsis changes at a constant rate for equatorial orbits.

Once we find explicit relations for Ω, i, and ω we will use them to express the unit vector normal to the orbit plane, $\mathbf{h}$, and the unit vector that lies along the longitude of the ascending node, $\mathbf{n}$, defined as:

$$\mathbf{h} = \begin{bmatrix} \sin i \sin \Omega \\ -\sin i \cos \Omega \\ \cos i \end{bmatrix}, \tag{3.25}$$

$$\mathbf{n} = \begin{bmatrix} \cos \Omega \\ \sin \Omega \\ 0 \end{bmatrix}. \tag{3.26}$$

From these two vectors we can construct the (normalized) eccentricity vector $\mathbf{e}$ as:

$$\mathbf{e} = \cos \omega \mathbf{n} + \sin \omega (\mathbf{h} \times \mathbf{n}). \tag{3.27}$$

This set of vectors provide a different way in which to express the secular motion of the orbit and orbit plane.

The averaged dynamics of the momentum can be found by using Equation 3.15 and 3.16.

$$\frac{dh_x}{dt} = B(1-\sigma)h_y h_z, \tag{3.28}$$

$$\frac{dh_y}{dt} = -Bh_z h_x, \tag{3.29}$$

$$\frac{dh_z}{dt} = B\sigma h_x h_y. \tag{3.30}$$

The averaged equations of momentum are quite similar to the well-known dynamics

of a free-rigid-body rotation.

$$\frac{d\omega_x}{dt} = \frac{I_{yy} - I_{zz}}{I_{xx}}\omega_y\omega_z, \tag{3.31}$$

$$\frac{d\omega_y}{dt} = \frac{I_{zz} - I_{xx}}{I_{yy}}\omega_z\omega_x, \tag{3.32}$$

$$\frac{d\omega_z}{dt} = \frac{I_{xx} - I_{yy}}{I_{zz}}\omega_x\omega_y. \tag{3.33}$$

More discussions about this are given in Section 3.3.6

3.2.2 Qualitative analysis

Before we explicitly integrate Equations 3.15-3.17, the averaged integral of motion in Equation 3.14 can be used to understand the qualitative motion of orbits.

First, we note by inspection of Equation 3.14 that the constant C lies in the interval $[0, 1]$, as it is the product of two quantities that lie within this same interval. Then we can understand the relationship between changes in i and Ω by plotting the contour curves for different values of C in this interval. Given our single mass-distribution parameter σ which is defined in Equation 2.14 we need only consider three different qualitative situations: $\sigma = 0$, $0 < \sigma < 1$, and $\sigma = 1$. The case $\sigma = 0$ yields i constant for all values of Ω, which just recovers the classic result that the inclination is constant on average for the C_{20}-only potential field. In Figure 3.2 we show the contour lines generated for a generic case of $0 < \sigma < 1$ and in Figure 3.3 we show the case for $\sigma = 1$. Motion in the averaged system will follow the contour lines in the clock wise direction.

Motion for $0 < \sigma < 1$

For $C = 0$ the inclination is constrained to equal 0 or 180°. In this case the orbit plane is fixed and only the argument of periapsis will have a secular change

$$\frac{d\varpi_\pm}{dt} = \pm B\left(1 - \frac{\sigma}{2}\right), \tag{3.34}$$

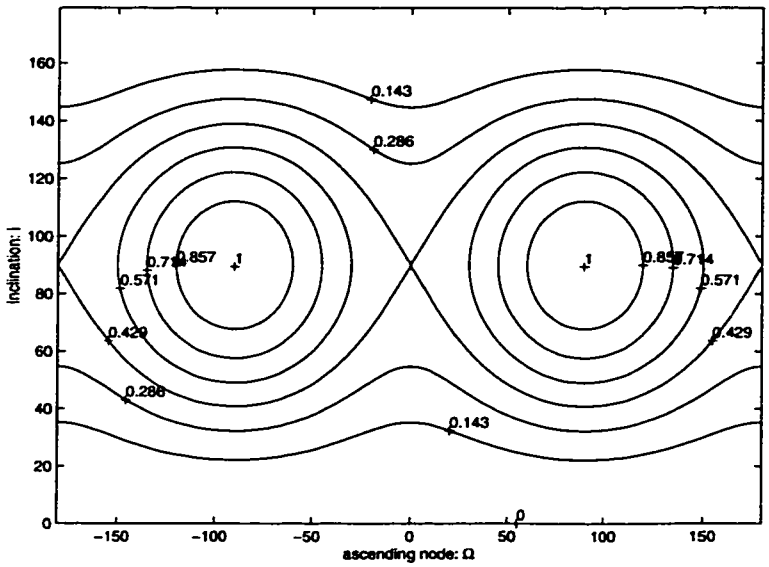

Figure 3.2: Contour plots of the averaged integral Equation 3.14 as a function of inclination i and node Ω for the case of $\sigma = 0.571$.

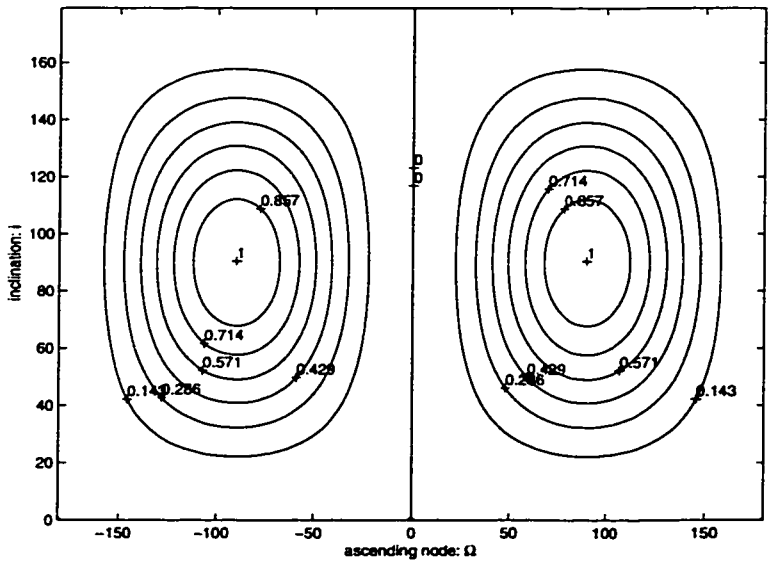

Figure 3.3: Contour plots of the averaged integral Equation 3.14 as a function of inclination i and node Ω for the case of $\sigma = 1$.

where the + is for $i = 0°$ and the − is for $i = 180°$. Conversely, for $C = 1$ the integral demands that $i = 90°$ and $\Omega = \pm 90°$, yielding a stationary value of Ω and i, with the argument of periapsis having a constant secular decrease:

$$\frac{\mathrm{d}\omega}{\mathrm{d}t} = -\frac{B}{2}(1+\sigma). \tag{3.35}$$

For values of C not equal to 0 or 1 we find, in general, a time periodic variation in the orbit plane (see Fig. 3.2). For values of C sufficiently close to zero the orbit plane will precess about the z-axis of the body (the maximum moment of inertia). For values of C sufficiently close to 1 the orbit plane will precess about the x-axis (the minimum moment of inertia). In both cases, the orbit precession occurs in the clock-wise direction, as measured from the orbit normal. For both of these general cases the argument of periapsis will be driven by a time periodic differential equation, in general. Depending on the parameters C and σ this variation may even switch between clockwise and counter clockwise within one secular period of motion. A general rule, however, is that when C is near zero the argument of periapsis will decrease on average and when C is near 1 the argument of periapsis will increase on average.

As C decreases from 1 or increases from 0 we see that there must be a boundary between precession about the x and z axes. In the contour plots of Ω and i this appears as a heteroclinic connection between two equilibrium points located at $i = 90°$ and $\Omega = 0, 180°$. These equilibrium points correspond to an energy of $C = 1 - \sigma$ and are hyperbolic, with their stable and unstable manifolds forming heteroclinic connections to the other equilibrium point. These manifolds serve as a separatrix between the two modes of orbit normal precession.

Motion for $\sigma = 1$

For $\sigma = 1$ we note that the orbit normal is either stationary or precesses about the x-axis (the minimum moment of inertia, see Fig. 3.3). Motion in this case corresponds to orbital motion about a prolate body. We note that Ω is now constrained to lie in one of the intervals $(-180°, 0)$ or $(0, 180°)$. Exceptions to this occur if the orbit is in the equatorial plane or has $\Omega = 0, 180°$. If the orbit is in the equatorial plane the situation is similar to the case when $\sigma < 1$. If the orbit has an initial value of $\Omega = 0, 180°$ we see, from Equations 3.15 and 3.16, that the inclination and node are frozen at their given values and from Equation 3.14 that $C = 0$. Thus, the vertical lines in the contour plot correspond to a locus of equilibrium points. Essentially, the unstable equilibrium point and manifolds for $\sigma < 1$ degenerate into a locus of fixed points for $\sigma = 1$.

Additional considerations

The contours in Figures 3.2 and 3.3 can be mapped onto the surface of a sphere. To show this, first identify the $\Omega = 180°$ and $\Omega = -180°$ lines to form a cylinder. Then the two lines $i = 0$ and $i = 180°$ can be identified with themselves, respectively, to form a topological sphere. Performing these identifications brings to light a connection between the geometry of the polhodes of the torque-free rotation of a rigid body (cf [15], pg 391) and the geometry of our current analysis. The principal axes are similarly aligned in each case with the x and z-axes surrounded by level curves, and the y-axis lying at the intersection of hyperbolic manifolds. Thus we have the interesting result that motion in our averaged system has similarities to the rigid body rotation of a torque-free body. As the equations of motion are similar (see Equation 3.28-3.30 and Equation 3.31-3.33), even though the underlying physical

meanings are different. Additionally, the contours maintain their similarity in the case of a rotationally symmetric inertia tensor about either the x or z-axes.

3.2.3 Analytical solutions

Given a qualitative understanding of motion for the averaged system we now proceed to integrate the equations for i, Ω, and ω explicitly. We first discuss a number of special cases in which the motion can be expressed in terms of elementary functions, and then progress to the cases which can be solved in terms of elliptic functions. In the discussion we state the elliptic functions and integrals with minimal definition. See the Appendix A.1, A.2, for a brief definition of the special functions used in this analysis.

Before proceeding we discard the case $C = 1$ as this corresponds to stable equilibra ($i = 90°$, $\Omega = \pm 90°$) that exist in both cases of interest, $0 < \sigma < 1$ and $\sigma = 1$. Similarly we dispose of the case $C = 0$ as this corresponds to an inclination equals to 0 or 180° and the longitude of periapsis $\varpi_{\pm}$ increasing at a constant rate of $\pm B(1 - \sigma/2)$, where the + corresponds $i = 0$ and the − corresponds $i = 180°$. If $\sigma = 1$ we also note that $C = 0$ allows a frozen orbit with $\Omega = 0, 180°$ and an arbitrary inclination i. Thus we can constrain C to the interval $0 < C < 1$. The remainder of the discussion treats the cases $\sigma = 0$, $0 < \sigma < 1$, and $\sigma = 1$ separately. We include the case $\sigma = 0$ for completeness.

Analytical solution for $\sigma = 0$

As noted above, this corresponds to the classical example of secular motion about a body with C_{20} only ([9], pg 345). From Equation 3.14 we see that $\sin i = \sqrt{C}$, and is constant. The solutions for Ω and ω can be immediately found as: $\Omega = \mp\sqrt{1 - C}B(t - t_o)$ and $\omega = \frac{1}{2}(4 - 5C)B(t - t_o)$, the $\pm$ in Ω denoting whether the

initial inclination is less than or greater than 90°. Using this solution, the orbit normal and node vectors are found to be:

$$\mathbf{h} = \begin{bmatrix} \mp\sqrt{C}\sin\left(\sqrt{1-C}B(t-t_o)\right) \\ -\sqrt{C}\cos\left(\sqrt{1-C}B(t-t_o)\right) \\ \pm\sqrt{1-C} \end{bmatrix}, \tag{3.36}$$

$$\mathbf{n} = \begin{bmatrix} \cos\left(\sqrt{1-C}B(t-t_o)\right) \\ \mp\sin\left(\sqrt{1-C}B(t-t_o)\right) \\ 0 \end{bmatrix}. \tag{3.37}$$

This corresponds to the precession of the orbit plane at a constant rate about the z-axis (the maximum moment of inertia), in the clock-wise direction relative to the orbit normal.

Analytical solution for $\sigma = 1$

In this case Equations 3.15, 3.16, and 3.14 simplify to:

$$\frac{\mathrm{d}i}{\mathrm{d}t} = B\sin i\sin\Omega\cos\Omega, \tag{3.38}$$

$$\frac{\mathrm{d}\Omega}{\mathrm{d}t} = -B\cos i\sin^2\Omega, \tag{3.39}$$

$$C = \sin^2 i\sin^2\Omega. \tag{3.40}$$

Define a new variable $v = \cot\Omega$, noting that $1 + v^2 = 1/\sin^2\Omega$ and:

$$\frac{\mathrm{d}v}{\mathrm{d}t} = -(1+v^2)\frac{\mathrm{d}\Omega}{\mathrm{d}t} \tag{3.41}$$

$$= B\cos i. \tag{3.42}$$

Then $\cos i$ can be solved for from Equation 3.40 to find:

$$\cos i = (\pm)_i\sqrt{1-C}\sqrt{1-\frac{Cv^2}{1-C}}. \tag{3.43}$$

The sign of $(\pm)_i$ is equal to the sign of $\cos i$, and hence is positive when the inclination is less than 90°, negative when greater than 90°, and indeterminant when equal to 90°. Rewriting the equation for dv/dt and separating the variables yields the differential equation:

$$\frac{dv}{\sqrt{1-\frac{Cv^2}{1-C}}} = (\pm)_i B\sqrt{1-C}dt. \tag{3.44}$$

Perform a final change of variable to $u = \sqrt{C/(1-C)}v$ to find:

$$\frac{du}{\sqrt{1-u^2}} = (\pm)_i B\sqrt{C}dt. \tag{3.45}$$

For an initial condition we choose a value of inclination equal to 90° as the motion we are investigating always passes through this value. Then we find that $u(t_o) = \pm 1$ and we choose the positive sign so that $\cot\Omega(t_o) = \sqrt{(1-C)/C}$, meaning that Ω begins in either quadrants I or III. From Equation 3.38 we note that the inclination initially increases, leading to the negative root for $\cos i$. Evaluating the separated differential equation we find:

$$\arcsin(u) = \frac{\pi}{2} - B\sqrt{C}(t-t_o). \tag{3.46}$$

Completing the solution, evaluating $\cos i$, and performing the quadrature for ω yields:

$$\cot\Omega = \sqrt{\frac{1-C}{C}}\cos\left[B\sqrt{C}(t-t_o)\right], \tag{3.47}$$

$$\cos i = -\sqrt{1-C}\sin\left[B\sqrt{C}(t-t_o)\right], \tag{3.48}$$

$$\omega - \omega_o = -\frac{B}{2}(5C-1)(t-t_o) + \arctan\left[\sqrt{C}\tan\left(B\sqrt{C}(t-t_o)\right)\right]. \tag{3.49}$$

The solution holds identically when Ω is shifted by $\pm 180°$, generating both families in the contour plots for this case.

Evaluting the orbit normal vector with this solution yields:

$$\mathbf{h} = \begin{bmatrix} (\pm)_i\sqrt{C} \\ -(\pm)_i\sqrt{1-C}\cos\left[\sqrt{C}B(t-t_o)\right] \\ -\sqrt{1-C}\sin\left[\sqrt{C}B(t-t_o)\right] \end{bmatrix}, \tag{3.50}$$

$$\mathbf{n} = \frac{(\pm)_\Omega}{\sqrt{\cos^2\left[\sqrt{C}B(t-t_o)\right] + C\sin^2\left[\sqrt{C}B(t-t_o)\right]}} \times \begin{bmatrix} \sqrt{1-C}\cos\left[\sqrt{C}B(t-t_o)\right] \\ \sqrt{C} \\ 0 \end{bmatrix}, \tag{3.51}$$

where $(\pm)_\Omega$ is positive for an initial node in quadrant I and negative for an initial node in quadrant III. Here we note that the projection of the orbit normal on the x axis remains constant, and the amplitude of the projection on the y-z plane is constant. Thus we see that this case reduces to a uniform precession of the orbit plane about the axis of symmetry, analogous to the case of $\sigma = 0$, except now applying to a prolate body.

Analytical solution for $0 < \sigma < 1$

Now the general form of the equations for $\mathrm{d}i/\mathrm{d}t$, $\mathrm{d}\Omega/\mathrm{d}t$, and C from Equations 3.15, 3.16, and 3.14 hold, respectively. Define a new variable $s = \tan\Omega$ with $1+s^2 = 1/\cos^2\Omega$ and $\mathrm{d}s/\mathrm{d}\Omega = 1+s^2$. Rewriting the differential equation for s yields:

$$\frac{\mathrm{d}s}{\mathrm{d}t} = -(\pm)_i B\sqrt{[1-C-\sigma+(1-C)s^2]\,(1-\sigma+s^2)}, \tag{3.52}$$

where the $(\pm)_i$ is defined as before.

For notational convenience we also define two constant parameters:

$$m^2 = 1-\sigma, \tag{3.53}$$

$$\theta = \frac{1-C-\sigma}{1-C}, \tag{3.54}$$

where $0 < m^2 < 1$, and $-\infty < \theta < 1$ for the cases of interest.

Equation 3.52 can then be separated into:

$$\frac{\mathrm{d}s}{\sqrt{(\theta + s^2)(m^2 + s^2)}} = \mp\sqrt{1 - C}B\mathrm{d}t. \tag{3.55}$$

The three cases $\theta < 0$, $\theta = 0$, and $\theta > 0$ yield three different fundamental solutions, corresponding to precession about the x-axis (minimum moment of inertia), motion on the separatrix, and precession about the z-axis (maximum moment of inertia), respectively. These analytical solutions can be expressed in terms of elliptic integrals, as shown in Appendix A.3.

3.3 When The Central Body Rotates Slowly: $n >> \omega_T$

When the central body rotates slowly and the spacecraft is near the central body, $|n - \omega_T|/\omega_T \gg 1$, and the averaging conditions apply. This section investigates how the orbital dynamics are modified when the central body rotates slowly. There are a significant number of asteroids that fall into this classification[30],[16]. Some of these asteroids, such as Toutatis, are potential mission targets[22]. Thus, in addition to being a problem of theoretical interest, this analysis is also of practical interest for future missions.

To give a physically motivated example of what we mean by "slow rotation", assume the mean radius of an asteroid is R_A, its density lies in the range $1 < \rho < 4$ g/cm^3, and a spacecraft is orbiting it in a circular orbit with radius r_S. Then the gravity parameter is $\mu = (4/3)\pi\rho G R_A^3$, where G is the universal gravity constant, the mean orbital motion of the spacecraft is $n = \sqrt{\mu/r_S^3}$, and the period of the spacecraft is

$$T_{S/C} = \frac{2\pi}{n} = \frac{2\pi}{\sqrt{(4/3)\pi\rho G(R_A/r_S)^3}}. \tag{3.56}$$

For close asteroid orbits with $r_S \approx R_A$, if we choose $\rho = 2.5$, then $T_{S/C} \approx 2$hr. If an asteroid's rotation period T is more than 20hr, then we can regard this asteroid as "slow rotating" since $T \gg T_{S/C}$. About 10% of the asteroids in the Solar system fall into this category[30]. Actually, the Earth can also be considered to be slowly rotating for low altitude orbits, but its C_{22} is very small and the phenomenon we describe here is not evident. However, Mars' C_{22} is 34 times larger than the Earth's [48], so the secular motion for a close Mars orbit could be more significant.

In the following the averaged Lagrange planetary equations for a slowly rotating asteroid are derived and used, in conjunction with the Jacobi integral, to give a complete description of orbital motion. Under the averaging assumptions, the problem is completely integrable and can be reduced to quadratures. For this problem the orbit plane will experience nutation in addition to the precession that is found for orbital motion about an oblate body. It is possible for the orbit plane to be trapped in a 1:1 resonance with the rotating body, the plane essentially being dragged by the rotating asteroid. As the asteroid rotation rate is increased this resonant motion disappears for rotation rates greater than a specific value. Finally, the analysis is validated with numerical integrations for cases of interest, showing that the averaging assumptions apply and give a correct prediction. These results are applicable to understanding spacecraft and particle orbital motion about slowly rotating asteroids.

3.3.1 Averaged equations

The discussion in this section has some similarities to the discussion in Section 3.2.1. Actually, the result in Section 3.2.1 is a special case of the result in this section when $\omega_T = 0$ and $\Omega_R = \Omega$. For convenience, the discussions are given separately.

This section studies the "slowly" rotating problem which means that over one

spacecraft orbit period all of the elements, including Ω_R, can be regarded as constant, as most averaging theories require. This assumption implies that the mean motion of the spacecraft is much faster than the central body rotation rate, or $n = \sqrt{\mu/a^3} \gg \omega_T$. When these rates become close to each other, resonant phenomenon invalidate our basic assumptions.

To formulate an analytical approach to the problem the perturbing potential is averaged over the mean anomaly M:

$$\bar{U}_2 = \frac{1}{2\pi}\int_0^{2\pi} U_2 \mathrm{d}M, \tag{3.57}$$

to find:

$$\bar{U}_2 = \frac{\mu}{2\bar{a}^3(1-\bar{e}^2)^{\frac{3}{2}}}\left[C_{20}\left(\frac{3}{2}\sin^2\bar{i}-1\right)+3C_{22}\sin^2\bar{i}\cos 2\bar{\Omega}_R\right], \tag{3.58}$$

where the over-bars indicate that the orbital elements are now mean orbit elements. At this point it is useful to use the mass-distribution parameter σ which is defined in Equation 2.14, changing the form of the potential to:

$$\bar{U}_2 = \frac{-\mu\,(I_{zz}-I_{xx})}{4\bar{a}^3(1-\bar{e}^2)^{\frac{3}{2}}}\left[\sigma-2+3\sin^2\bar{i}(1-\sigma\cos^2\bar{\Omega}_R)\right]. \tag{3.59}$$

In the remainder of this section, we drop the over-bar notation, implicitly assuming that all orbit elements referenced from this point on, unless otherwise defined, are mean (or averaged) orbital elements. Then, substituting the averaged potential into the Lagrange planetary equations yields[7],[32](See Equation C.1-C.6):

$$\frac{\mathrm{d}a}{\mathrm{d}t} = 0, \tag{3.60}$$

$$\frac{\mathrm{d}e}{\mathrm{d}t} = 0, \tag{3.61}$$

$$\frac{\mathrm{d}i}{\mathrm{d}t} = \frac{1}{2}B\sigma\sin i\,\sin 2\Omega_R, \tag{3.62}$$

$$\frac{\mathrm{d}\Omega_R}{\mathrm{d}t} = -B\cos i\left(1-\sigma\cos^2\Omega_R\right)-\omega_T, \tag{3.63}$$

$$\frac{\mathrm{d}\omega}{\mathrm{d}t} = -\frac{B}{2}\left[\sigma - 4 + 2\sigma\cos^2\Omega_R + 5\sin^2 i(1-\sigma\cos^2\Omega_R)\right], \quad (3.64)$$

$$\frac{\mathrm{d}M}{\mathrm{d}t} = n - \frac{B}{2}\sqrt{1-e^2}\left[\sigma - 2 + 3\sin^2 i(1-\sigma\cos^2\Omega_R)\right], \quad (3.65)$$

where

$$B = 3\mu^{\frac{1}{2}}\left(I_{zz} - I_{xx}\right)\Big/\left[2a^{\frac{7}{2}}(1-e^2)^2\right] = \frac{3n}{2p^2}\left(I_{zz} - I_{xx}\right), \quad (3.66)$$

and where $p = a(1-e^2)$ is the semi-latus rectum. We note that the semi-major axis and eccentricity are constant on average, thus implying that orbital energy and angular momentum magnitude will be constant on average. Also, the equations for inclination i and node Ω_R are coupled with each other, whereas the argument of periapsis does not appear in any of the right-hand sides of Equations 3.62 – 3.65.

In some situations the longitude of periapsis will be needed, defined here as $\varpi_\pm = \omega \pm \Omega_R$, the "-" branch is used when $i > 90°$.

$$\dot{\varpi}_\pm = (B/2)\left[2 - \sigma - (3 \pm 5\cos i)(1 \mp \cos i)\left(1 - \sigma\cos^2\Omega_R\right)\right] \mp \omega_T, \quad (3.67)$$

where the term containing Ω_R will disappear whenever $i = 0, 180°$ (i.e., whenever it isn't defined). Thus, for motion in the equatorial plane ($i = 0, 180°$) the longitude of periapsis has a constant secular rate: $\dot{\varpi}_\pm = B(2-\sigma)/2 \mp \omega_T$.

By setting $\sigma = 0$ while keeping $I_{xx} = I_{yy} \leq I_{zz}$ these averaged equations reduce to the classical equations describing the averaged orbit elements about a body with C_{20}[11]. Thus, we see that the effect of the body's equatorial ellipticity is to cause a nutation in the orbit plane (i.e., a change in inclination) in addition to the precession of the orbit plane which is already present for the $\sigma = 0$ case.

Since the Jacobi integral is a constant, it can be averaged to yield the same value. It is important to note, however, that averaging the functional side of the integral does introduce some subtle, but important, changes. Performing the averaging on

the integral yields:

$$\bar{J} \;=\; -\mu/(2a) - \omega_T\sqrt{\mu a(1-e^2)}\cos i - \bar{U}_2, \tag{3.68}$$

where the orbital elements on the right hand side are interpreted as mean elements. From Equations 3.60 and 3.61 we note that the semi-major axis a and eccentricity e are conserved on average and can be removed to define a new, simplified form of the constant:

$$C \;=\; \left(1 - \sigma\cos^2\Omega_R\right)\sin^2 i - (2\omega_T/B)\cos i. \tag{3.69}$$

The quantity in Equation 3.69 is conserved among the mean orbital elements only, and not among the unaveraged osculating elements.

Even though the averaged orbit dynamics can be reduced to quadratures, this does not give us any direct insight into how the orbit will evolve. Such insight can be obtained, however, by plotting Equation 3.69 along contours of constant C as a function of i and Ω_R. In Figures 3.4-3.7 we show a sequence of contours for a generic situation with $\sigma \in (0,1)$ for values of ω_T increasing from zero. In these figures the inclination i and relative node Ω_R follow curves of constant contour.

Figure 3.4 recreates a figure for the case $\omega_T = 0$[40] (See Figure 3.2). Here we note that there are two fundamental types of motion possible for the inclination and longitude of the ascending node (in the body-fixed frame). The orbit plane will either be in circulation, corresponding to a secularly changing Ω_R, or in libration, corresponding to the inclination oscillating about 90° and the node oscillating about ±90°. We note four points at which the inclination and node will remain stationary: $i = 90°$ and $\Omega_R = 0, \pm 90, 180°$. From the contours it is evident that two of these solutions ($\Omega_R = \pm 90°$) are stable and two ($\Omega_R = 0, 180°$) are unstable. It should be noted that, even though i and Ω_R can have stationary values in the body-fixed

frame, the argument of periapsis will not be stationary in general, but instead has a constant secular increase when at these points.

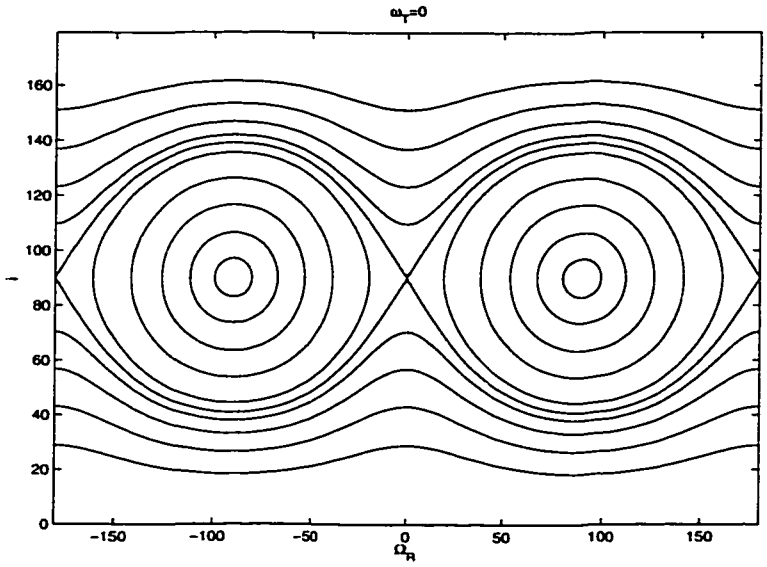

Figure 3.4: Contour plots of Equation 3.69 as a function of inclination i and node Ω_R for the case of no rotation ($\omega_T = 0$).

In Figures 3.5 - 3.7 we show the Jacobi contours when $\omega_T > 0$. We note that the zones of libration are pushed to higher inclinations. As ω_T increases the unstable point eventually disappears when it is pushed into a retrograde, equatorial orbit. As ω_T is increased further the stable point also disappears in the same fashion. For rotation rates larger than this the orbit plane always has a secular precession in the body-fixed frame. In Figure 3.6 we note that the separation line between circulation and libration terminates in the line of equatorial, retrograde orbits ($i = 180°$). The separation line acts as a heteroclinic orbit connecting these equatorial, retrograde orbits to themselves – although the orbital dynamics in the equator have a fundamental separation from motion out of the equator. This separatrix exists for rotation rates between the two critical values where the unstable and stable equilibra disappear.

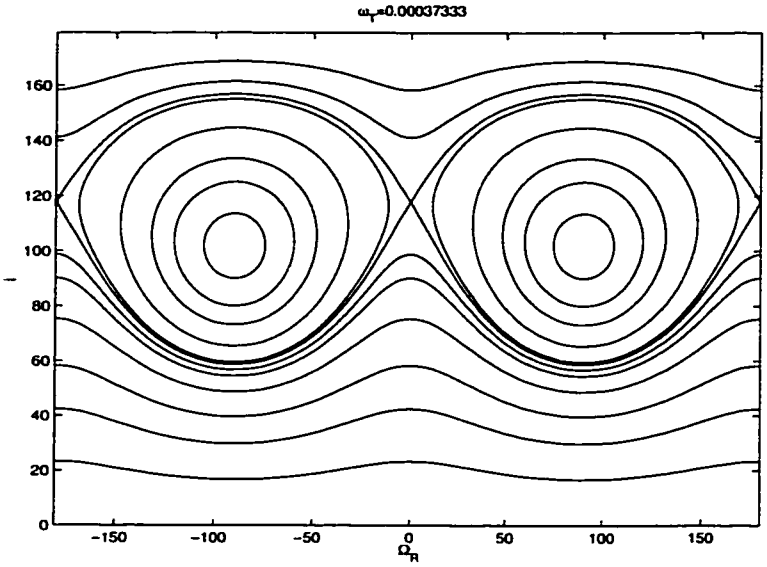

Figure 3.5: Contour plots of Equation 3.69 as a function of inclination i and node Ω_R for the case $0 < \omega_T < \omega_{T_u}$.

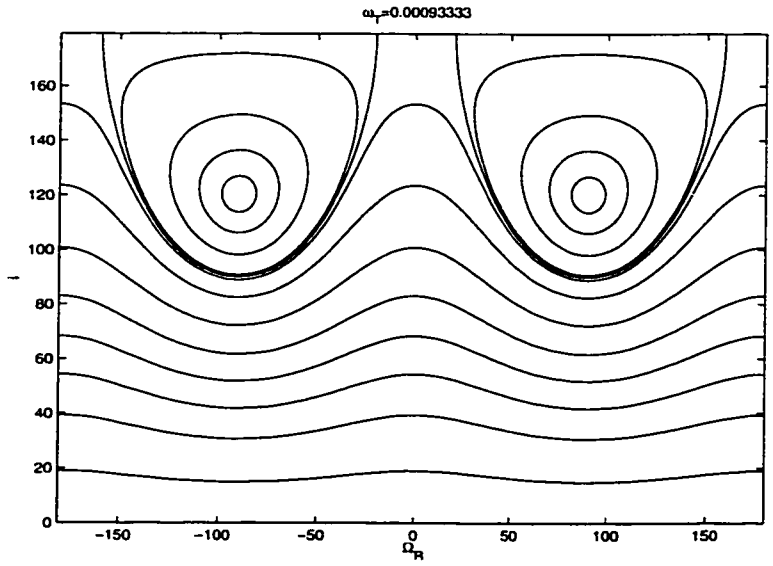

Figure 3.6: Contour plots of Equation 3.69 as a function of inclination i and node Ω_R for the case $\omega_{T_u} < \omega_T < \omega_{T_s}$.

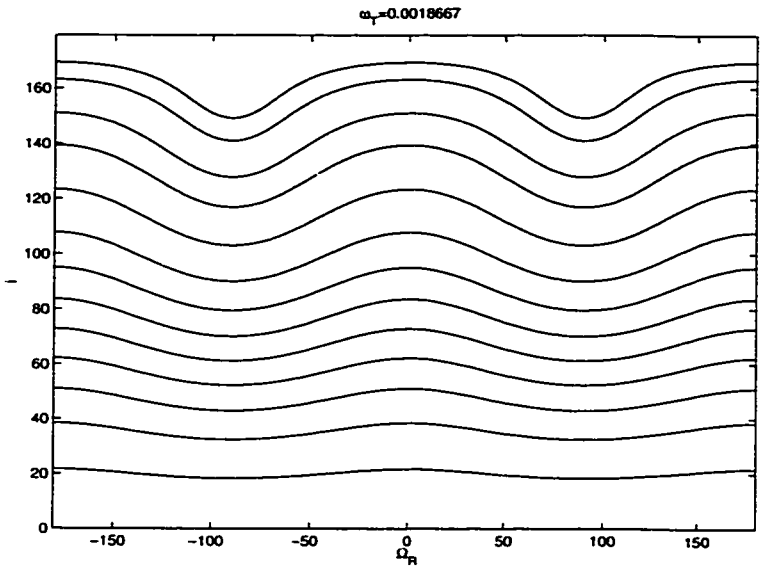

Figure 3.7: Contour plots of Equation 3.69 as a function of inclination i and node Ω_R for the case $\omega_T > \omega_{T_s}$.

3.3.2 Partially frozen orbits

A frozen orbit is generally defined as an orbit with no secular motion – or as an equilibrium to the averaged Lagrange planetary equations. We do not find completely frozen orbits in general, as the argument of periapsis usually has a non-zero secular increase. We do find, however, families of orbits where the orbital plane of the spacecraft is frozen in the body-fixed frame, corresponding to stationary values for the inclination i and longitude of the ascending node Ω_R. These points are clearly seen in the Jacobi contours and can be explicitly found from the Lagrange equations as well. We will look at the unstable and stable points separately.

Unstable orbit

Setting $\Omega_R = 0$ or 180° we see from Equation 3.62 and 3.63:

$$\frac{\mathrm{d}i_0}{\mathrm{d}t} = 0, \tag{3.70}$$

$$\frac{\mathrm{d}\Omega_{R0}}{\mathrm{d}t} = -B(1-\sigma)\cos i_0 - \omega_T. \tag{3.71}$$

Thus we derive a simple condition on inclination for the relative node to be frozen:

$$\cos i_0 = -\frac{\omega_T}{B(1-\sigma)}. \tag{3.72}$$

A simple analysis of this solution shows that it is unstable. We assume $\Delta\Omega_R = \Omega_R - \Omega_{R0}$, $\Delta i = i - i_0$ at these frozen points. The local linearized equations are

$$\frac{\mathrm{d}\Delta i}{\mathrm{d}t} = B\sigma \sin i_0 \Delta\Omega_R, \tag{3.73}$$

$$\frac{\mathrm{d}\Delta\Omega_R}{\mathrm{d}t} = B(1-\sigma)^2 \sin i_0 \Delta i. \tag{3.74}$$

Their characteristic equation is $\lambda^2 - B^2\sigma(1-\sigma)^2 \sin^2 i_0 = 0$. So, the equilibrium is a saddle point. The argument of periapsis will have a constant secular rate at this point equal to:

$$\frac{\mathrm{d}\omega}{\mathrm{d}t} = -\frac{B}{2}(1-2\sigma) + \frac{5}{2}\frac{\omega_T^2}{B(1-\sigma)}. \tag{3.75}$$

Thus as ω_T is increased from zero, the inclination of the frozen orbit in Equation 3.72 is pushed to higher values. When the inclination is pushed to 180° the equation for the relative node is no longer defined and the frozen orbit disappears (note that the longitude of periapsis for an equatorial, retrograde orbit has a constant secular rate). The critical value of the asteroid rotation rate when the unstable equilibrium point disappears is:

$$\omega_{T_u} = (1-\sigma)B, \tag{3.76}$$

or in terms of the orbit period of the spacecraft:

$$T_u = T_{S/C}\frac{2a^2(1-e^2)^2}{3(I_{zz}-I_{xx})(1-\sigma)} = T_{S/C}\frac{2p^2}{3(I_{zz}-I_{yy})}. \tag{3.77}$$

Thus we see that the critical rotation period depends on the spacecraft orbit period, orbit parameter, and the mass distribution of the rotating asteroid.

For asteroid rotation rates greater then ω_{T_u} we can still use Equation 3.63 to delineate where the line between circulation and libration of the orbit plane occurs. This is done by artificially treating an equilibrium point for Equation 3.63 when $i = 180°$, yielding an explicit solution for the relative node:

$$\cos^2 \Omega_R = \frac{B - \omega_T}{\sigma B}. \tag{3.78}$$

We see that $\cos^2 \Omega_R = 1$ at the critical rotation rate $\omega_{T_u} = B(1 - \sigma)$, and that $\cos^2 \Omega_R = 0$ when the rotation rate is increased to a value equal to B. In the next subsection we shall see that this corresponds to the disappearance of the stable frozen orbit. The value of Ω_R computed from this relation predicts the intersection of the separatrix between circulation and libration with $i = 180°$.

Stable Orbit

Next, setting $\Omega_R = \pm 90°$, Equations 3.62 and 3.63 reduce to:

$$\frac{\mathrm{d}i_0}{\mathrm{d}t} = 0, \tag{3.79}$$

$$\frac{\mathrm{d}\Omega_{R0}}{\mathrm{d}t} = -B \cos i_0 - \omega_T. \tag{3.80}$$

Thus the condition to freeze the relative node reduces to the condition on inclination:

$$\cos i_0 = -\frac{\omega_T}{B}. \tag{3.81}$$

Again, by assuming $\Delta\Omega_R = \Omega_R - \Omega_{R0}$, $\Delta i = i - i_0$ at these frozen points, we have the local linearized equations

$$\frac{\mathrm{d}\Delta i}{\mathrm{d}t} = -B\sigma \sin i_0 \Delta\Omega_R, \tag{3.82}$$

$$\frac{\mathrm{d}\Delta\Omega_R}{\mathrm{d}t} = B(1 - \sigma) \sin i_0 \Delta i. \tag{3.83}$$

Their characteristic equation is $\lambda^2 + B^2\sigma(1 - \sigma)\sin^2 i_0 = 0$. So, the equilibrium is a center. The argument of periapsis has a constant secular rate at this point which

equals to:

$$\frac{d\omega}{dt} = -\frac{B}{2}(1+\sigma)+\frac{5}{2}\frac{\omega_T^2}{B}. \tag{3.84}$$

As ω_T is increased from zero the inclination in Equation 3.81 is pushed from 90 degrees to higher values. The critical rotation period, where the stable orbit ceases to exist, now occurs when:

$$\omega_{T_s} = B, \tag{3.85}$$

or in terms of the orbit period of the spacecraft as:

$$T_s = T_{S/C}\frac{2p^2}{3(I_{zz}-I_{xx})} = T_u(1-\sigma). \tag{3.86}$$

For asteroids rotating at a faster rate (with a shorter period) we see that the orbit plane can only be in circulation, albeit with a predictable nutation amplitude as a function of inclination.

Direct and retrograde orbit

In the above two sections, we briefly discussed the stability of the direct orbit when $i = 0°$ and the retrograde orbit when $i = 180°$. Strictly speaking, there is no definition of Ω_R for these two cases. Let us use new variables p_1 and q_1 instead of the traditional i and Ω_R to study the stability of these two special orbits. From the definition of inclination and ascending node, $i = 0, \omega_T < 0$ is equivalent to $i = 180°, \omega_T > 0$, so we can just study direct orbits and include retrograde orbits by considering the case $\omega_T < 0$, $i = 0°$. Let

$$p_1 = \tan(\frac{i}{2})\sin\Omega_R, \tag{3.87}$$

$$q_1 = \tan(\frac{i}{2})\cos\Omega_R. \tag{3.88}$$

The secular rate of p_1 and q_1 can be found by using the averaged equation 3.62-3.63

$$\frac{dp_1}{dt} = \frac{Bq_1}{1+p_1^2+q_1^2}[\sigma(1+p_1^2-q_1^2)-(1-p_1^2-q_1^2)]-\omega_T q_1, \quad (3.89)$$

$$\frac{dq_1}{dt} = \frac{Bp_1}{1+p_1^2+q_1^2}[2\sigma q_1^2+(1-p_1^2-q_1^2)]+\omega_T p_1. \quad (3.90)$$

The equilibrium point of the above equation is $p_{10} = q_{10} = 0$ when $i = 0°$. By linearization using $\Delta p_1 = p_1 - p_{10}$, $\Delta q_1 = q_1 - q_{10}$, we have

$$\frac{d\Delta p_1}{dt} = -[B(1-\sigma)+\omega_T]\Delta q_1, \quad (3.91)$$

$$\frac{d\Delta q_1}{dt} = (B+\omega_T)\Delta p_1. \quad (3.92)$$

The stability condition on this equations is

$$[B(1-\sigma)+\omega_T](B+\omega_T) > 0. \quad (3.93)$$

Since $B > 0$ and $\sigma < 1$, Equation 3.93 implies that the direct orbit for $i = 0$ and $\omega_T > 0$ is always stable independent of the central body rotation rate ω_T; whereas, the retrograde orbit for $i = 0$ and $\omega_T < 0$ is stable only when $|\omega_T| < B(1-\sigma)$ or $|\omega_T| > B$, and is unstable in the interval $B(1-\sigma) < |\omega_T| < B$. The unstable situation occurs when the stable frozen orbit exists and the unstable frozen orbit disappears, i.e. $\omega_{Tu} < |\omega_T| < \omega_{Ts}$. The instablity region for the retrograde orbit is

$$\Delta\omega_{Tu} = \omega_{Ts} - \omega_{Tu} = \sigma B = \frac{3\mu^{\frac{1}{2}}(I_{zz}-I_{xx})\sigma}{2a^{\frac{7}{2}}(1-e^2)^2} = \frac{3n(I_{yy}-I_{xx})}{2p^2}. \quad (3.94)$$

This indicates that a retrograde orbit in this situation is susceptible to an out-of-plane instability. Thus the results here correspond to the unstable and stable orbits analyses in the above two sections.

The stability condition for the retrograde orbit can also be obtained by following the above analysis procedure but instead defining $p_2 = \cot(i/2)\sin\Omega_R$, $q_2 = \cot(i/2)\cos\Omega_R$ and $\omega_T > 0$.

3.3.3 Dimensionless analysis and application

To give a more physically motivated application for our discussion we assume that the 2nd degree and order gravity coefficients are derived from a constant density, tri-axial ellipsoid shape. This assumption is not necessary, but provides a physical realization of our system. For definitions see Section 2.1.3

If we use $\mathrm{d}\theta = \omega_T \mathrm{d}t$ instead of $\mathrm{d}t$ in Equation 3.60-3.65, the averaged equations become dimensionless with

$$\tilde{B} = \frac{B}{\omega_T} = \frac{3\mu^{\frac{1}{2}}(I_{zz} - I_{xx})}{2a^{\frac{7}{2}}(1-e^2)^2\omega_T} \tag{3.95}$$

$$= \frac{3\mu^{\frac{1}{2}}}{a^{\frac{7}{2}}(1-e^2)^2\omega_T}\left(\frac{\alpha^2\epsilon_c^2}{10}\right) \tag{3.96}$$

$$= \frac{\sqrt{3\rho G}(1-\epsilon_b^2)^{1/4}(1-\epsilon_c^2)^{1/4}\epsilon_c^2\alpha^{\frac{7}{2}}}{5\omega_T(1-e^2)^2 a^{\frac{7}{2}}}, \tag{3.97}$$

where $\mu = (4/3)\pi\alpha\beta\gamma\rho G$, ρ is the density of the ellipsoid, G is the gravity constant. $\tilde{B}$ is a dimensionless variable which, in addition to σ, characterizes the averaged orbital motion of the particle in the second degree and order gravity field.

Now the retrograde orbit ($i = 180°$, $\omega_T > 0$) is unstable, when $1 < \tilde{B} < 1/(1-\sigma)$. The values of 1 and $1/(1-\sigma)$ of $\tilde{B}$ are also the critical conditions for the existence of the stable and the unstable frozen orbits, respectively(see Equation 3.76 and 3.85). When $\tilde{B} > 1$, the stable 1:1 orbit exists, and when $\tilde{B} > 1/(1-\sigma)$ the unstable 1:1 orbit exists. It can be seen that the value of $\tilde{B}$ is related with both the parameters of the central body and the S/C orbit. If we define "the minimum circular orbit" as the orbit when $a = \alpha, e = 0$, a new parameter can be found which is determined only by the central body's density, shape and rotation rate.

$$\tilde{B}^* = \sqrt{3\rho G}(1-\epsilon_b^2)^{1/4}(1-\epsilon_c^2)^{1/4}\epsilon_c^2 \Big/ (5\omega_T). \tag{3.98}$$

When $\tilde{B}^* > 1$, the stable 1:1 circular orbit can physically exist, and when $\tilde{B}^* >$

$1/(1-\sigma)$, the unstable 1:1 orbit physically exists(since $a > \alpha$ in general). Thus, the variable $\tilde{B}^*$ can be used to check if the resonant 1:1 orbits can exist for a particular asteroid which, in turn, will be a "measure" of how important the effects described here will be for any given asteroid.

The condition $\tilde{B}^* > 1$ can be restated as a condition on the density and rotation period of the asteroid which can be combined into one variable. When

$$\sqrt{\rho T^2} \;>\; 10\pi \Big/ \left[\sqrt{3G}(1-\sigma\epsilon_c^2)^{1/4}(1-\epsilon_c^2)^{1/4}\epsilon_c^2\right], \tag{3.99}$$

the minimum circular orbit exists and the effects described in this section are important. The right hand side of the above inequality is determined only by the shape of the asteroid which can be estimated from ground-based observation of the asteroid. The minimum value of the right-hand-side occurs when

$$\epsilon_c^2 \;=\; \left[5(1+\sigma) - \sqrt{25\sigma^2 - 46\sigma + 25}\right] \Big/ (12\sigma). \tag{3.100}$$

For example, when $\sigma = 1$ the minimum point is $\epsilon_c^2 = 2/3$, and leads to $\sqrt{\rho T^2} > 50.7$ $(\mathrm{g/cm^3})^{1/2}$ hr. Figure 3.8 shows the curves of Equation 3.99 for different values of σ. The overall pattern of the curves is similar.

The rotation rate and size of 748 asteroids have been analyzed [30], with about 10% of the asteroids being slow rotators for which the spin period is more than 20 hr. One of the largest known slow rotators is (253) Mathilde with diameter $D = 58$ km, $T = 418$ hr and density $\rho = 1.3$ g/cm^3. We can see that the slow rotation effects will play an important role in spacecraft motion about this body as $T \gg 50.7/\sqrt{\rho} = 44.7$ hr when $\sigma = 1$, $\epsilon_c^2 = 2/3$.

Finally we make a cursory check of our assumptions in performing the averaging of the potential. In terms of the period of the spacecraft orbit relative to the rotation period of the asteroid, we assumed that $T_{S/C} \ll T$, which corresponds to the

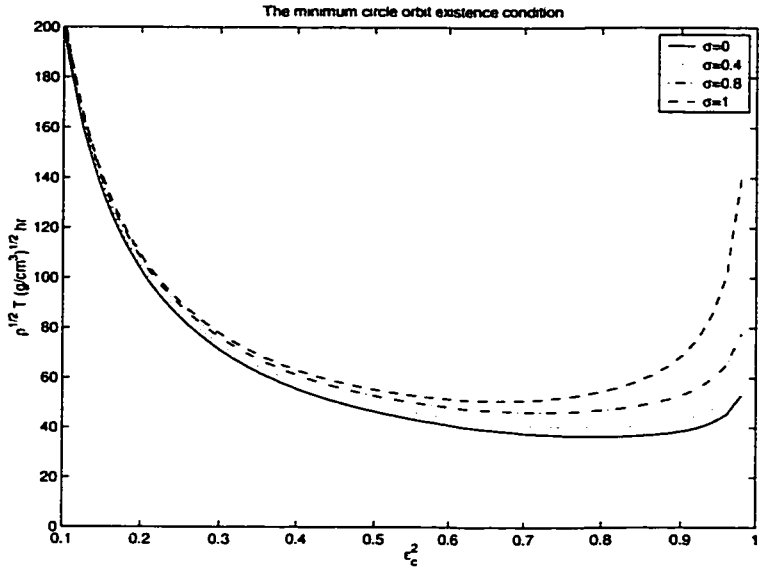

Figure 3.8: Plots of Equation 3.99 for different values of σ, note that the minimum $\sqrt{\rho}T$ exists and is a function of ϵ_c^2

inequality:

$$\frac{T_{S/C}}{T} = \frac{3(I_{zz}-I_{yy})}{2p^2} = \frac{3}{10}\left(\frac{\alpha}{p}\right)^2 \epsilon_c^2(1-\sigma) \ll 1. \tag{3.101}$$

By inspection we note that each of the terms in the equation is less than one, and hence their product will be less than one.

3.3.4 Libration and circulation motion

The results in this section give a global, qualitative description of orbital motion. The main result applies to the motion of the orbit plane, as it exhibits two very different modes as a function of initial conditions and parameters. In the librational mode the precession rate of the orbit plane is in a 1:1 resonance with the asteroid rotation rate. Thus, in the body-fixed frame the orbit normal is seen to librate about a fixed direction in this frame. Physically, the asteroid gravity field is dragging the orbit plane along with itself, something which can only occur for a slow enough asteroid rotation rate. A similar phenomenon was observed for orbital motion about

the slowly tumbling asteroid Toutatis [37].

When the orbit plane is in circulation mode its precession rate is not equal to the asteroid rotation rate. Thus, on average, the longitude of the ascending node will circulate around the asteroid. We see that there can still be significant nutation of the orbit plane in this case, although the nutation amplitude decreases as the magnitude of the body-relative precession rate increases.

We can also relate the orbit plane motion in the body-fixed frame to orbit plane precession in the inertially-fixed frame. Here we note that $\dot{\Omega} = \dot{\Omega}_R + \omega_T = -B\cos i\,(1 - \sigma\cos^2\Omega_R)$. Thus, we still have the result that the precession rate of the orbit plane is zero at an inclination of 90 degrees, but now, due to the nutation of the orbit plane, the orbit inclination will not remain fixed at 90 degrees and will instead oscillate about this value.

3.3.5 Reduction to quadratures

By using both the averaged Jacobi integral and the averaged Lagrange equations we can reduce this problem to quadratures and find a complete qualitative understanding of orbital motion. It is important to note that Equations 3.62, 3.63, and 3.69 only contain the two averaged orbital elements Ω_R and i. Thus, we can use Equation 3.69 to reduce either of Equations 3.62 or 3.63 into a form that can be reduced to quadratures. Applying this reduction to both equations yields:

$$\frac{\mathrm{d}i}{\mathrm{d}t} = \frac{B}{\sin i}\sqrt{\left[(\sigma-1)\sin^2 i + C + \frac{2\omega_T}{B}\cos i\right]\left[\sin^2 i - C - \frac{2\omega_T}{B}\cos i\right]}, \quad (3.102)$$

$$\frac{\mathrm{d}\Omega_R}{\mathrm{d}t} = -\frac{B}{2}\left[\frac{2\omega_T}{B} \pm \sqrt{(\frac{2\omega_T}{B})^2 + 4(1 - C - \sigma\cos^2\Omega_R)(1 - \sigma\cos^2\Omega_R)}\right]. \quad (3.103)$$

We note that either of these equations can be reduced to a quadrature of the

form:

$$t - t_o = \int_{i_o}^{i} 1/g(i)\, \mathrm{d}i, \tag{3.104}$$

$$t - t_o = \int_{\Omega_{Ro}}^{\Omega_R} 1/f(\Omega_R)\, \mathrm{d}\Omega_R. \tag{3.105}$$

Subsequent to evaluating these integrals, Equations 3.64 and 3.65 can also be reduced to a quadrature. This indicates that the averaged problem is completely integrable. The special case of $\omega_T = 0$ is considered in [40] (Also see in Section 3.2), and the quadrature indicated in Equation 3.105 was carried out explicitly, yielding closed form solutions for the mean orbital elements in terms of elliptic functions and integrals.

3.3.6 Similarity to the free rigid body motion

The orbital angular momentum vector in rotating coordinates has direction given by the components:

$$h_x = \sin i \sin \Omega_R, \tag{3.106}$$

$$h_y = -\sin i \cos \Omega_R, \tag{3.107}$$

$$h_z = \cos i. \tag{3.108}$$

The averaged dynamics of the angular momentum can be found using Equation 3.62 and 3.63 :

$$\frac{\mathrm{d}h_x}{\mathrm{d}t} = [B(1-\sigma)h_z + \omega_T]h_y, \tag{3.109}$$

$$\frac{\mathrm{d}h_y}{\mathrm{d}t} = -(Bh_z + \omega_T)h_x, \tag{3.110}$$

$$\frac{\mathrm{d}h_z}{\mathrm{d}t} = B\sigma h_x h_y. \tag{3.111}$$

There are six equilibra (See Figure 3.12), which correspond to the two unstable frozen orbits, the two stable frozen orbits, the direct orbit and the retrograde orbit which

were discussed in the above sections. The averaged angular momentum dynamics are quite similar to the free rigid body motion, especially when $\omega_T = 0$. This is why there are several phenomena in our problem which are quite similar to torque free rigid body motion. For example, consider a particle's orbit plane precessing around a principal axis of inertia I_1 of the central body. It's secular orbit stability condition is then similar to the stability condition for torque free rigid body motion. The equivalent stability condition for Equation 3.93 is

$$\left[\frac{3n}{2p^2}(I_1 - I_2) + \omega_T\right]\left[\frac{3n}{2p^2}(I_1 - I_3) + \omega_T\right] > 0, \tag{3.112}$$

where I_1 is the central body rotation axis, I_2, I_3 are the other two principal axes of inertia. It can be seen that there are some similarities between the stability conditions of torque free rigid body rotational motion and our problem of a particle moving around a rigid body, especially when $\omega_T = 0$. For rigid body motion, rotation is stable when the rigid body rotates about its largest or smallest moment of inertia. For our problem, the particle's motion is stable when it circles the axis of the largest or smallest moment of inertia of the central body. There are fundamental reasons for this similarity, as the two kinds of motions are both determined by the mass distribution of the central body which is described by the moments of inertia. This similarity can provide insight into stable and unstable orbits in the second degree and order gravity field.

3.4 When Central Body Rotates Rapidly: $n << \omega_T$

When the central body rotates swiftly or the spacecraft is far away the central body, $|(\omega_T - n)/n| \gg 1$. In this case an averaging condition also applies. Before we derive the averaged equations for rapidy rotating asteroids, we give a summary of

the slowly rotating case analyzed in Section 3.3, paying attention to the averaging condition. It is interesting to give a comparison of the slow and fast rotating cases.

3.4.1 Summary when $n \gg \omega_T$

When the central body rotates slowly or the spacecraft is near the central body,

$$\left|\frac{n-\omega_T}{\omega_T}\right| \gg 1. \tag{3.113}$$

Here we assume $n > 0$ when inclination $i < \pi/2$, and $n < 0$ when $i > \pi/2$. The mean anomaly M is easily transformed to the true anomaly f, which is a linear function of time in unperturbed motion, by the relation

$$\mathrm{d}M = \frac{r^2}{a^2(1-e^2)^{1/2}}\mathrm{d}f. \tag{3.114}$$

and

$$r = \frac{a(1-e^2)}{1+e\cos(\omega+f)}. \tag{3.115}$$

Using Equation 3.6, the averaged potential becomes

$$\bar{U}_2 = \frac{1}{2\pi}\int_0^{2\pi} U_2 \mathrm{d}M \tag{3.116}$$

$$= \frac{\mu}{2\bar{a}^3(1-\bar{e}^2)^{\frac{3}{2}}}\left[C_{20}\left(\frac{3}{2}\sin^2\bar{i}-1\right) + 3C_{22}\sin^2\bar{i}\cos 2(\bar{\Omega}-\omega_T t)\right], \tag{3.117}$$

where the over-bars indicate that the orbital elements are now mean orbit elements. In the remainder of this section we drop the over-bar notation, implicitly assuming that all orbit elements referenced from this point on, unless otherwise defined, are mean (or averaged) orbital elements.

If $\tau_1 = nt$,

$$\frac{\mathrm{d}(-)}{\mathrm{d}\tau_1} = \frac{\mathrm{d}(-)}{\mathrm{d}t}\frac{\mathrm{d}t}{\mathrm{d}\tau_1} = \frac{1}{n}\frac{\mathrm{d}(-)}{\mathrm{d}t}, \tag{3.118}$$

then the averaged Lagrange equations become,

$$\frac{\mathrm{d}i}{\mathrm{d}\tau_1} = \frac{3C_{22}}{a^2(1-e^2)^2}\sin i\,\sin 2(\Omega - \frac{\omega_T}{n}\tau_1), \tag{3.119}$$

$$\frac{\mathrm{d}\Omega}{\mathrm{d}\tau_1} = \frac{3}{2a^2(1-e^2)}\cos i\left[C_{20} + 2C_{22}\cos 2(\Omega - \frac{\omega_T}{n}\tau_1)\right], \tag{3.120}$$

$$\frac{\mathrm{d}\omega}{\mathrm{d}\tau_1} = -\frac{3C_{20}}{2a^2(1-e^2)^2}\left(2 - \frac{5}{2}\sin^2 i\right) + \frac{3C_{22}}{a^2(1-e^2)^2}\left(\frac{5}{2}\sin^2 i - 1\right)\cos 2(\Omega - \frac{\omega_T}{n}\tau_1). \tag{3.121}$$

If we assume $p = a(1-e^2)$, the condition for which the averaging method can apply is

$$\frac{|C_{20}|}{p^2} << 1, \tag{3.122}$$

$$\frac{|C_{22}|}{p^2} << 1, \tag{3.123}$$

$$\frac{\omega_T}{|n|} << 1. \tag{3.124}$$

3.4.2 When $n \ll \omega_T$

When the central body rotates fast or the spacecraft is far from the central body, the averaging condition becomes:

$$\left|\frac{\omega_T - n}{n}\right| \gg 1. \tag{3.125}$$

Again, we assume $n > 0$ when inclination $i < \pi/2$(direct orbit), and $n < 0$ when $i > \pi/2$(regrograde orbit).

The averaged potential becomes:

$$\bar{U}_2 = \frac{1}{2\pi}\int_0^{2\pi} U_2\,\mathrm{d}\tau_2 \tag{3.126}$$

$$= \frac{\mu C_{20}}{2\bar{a}^3(1-\bar{e}^2)^{\frac{3}{2}}}\left(\frac{3}{2}\sin^2\bar{i} - 1\right). \tag{3.127}$$

We see that the C_{22} perturbation disappears on average for the rapid rotation case

if we assume $\tau_2 = \omega_T t$,

$$\frac{\mathrm{d}i}{\mathrm{d}\tau_2} = 0, \tag{3.128}$$

$$\frac{\mathrm{d}\Omega}{\mathrm{d}\tau_2} = \frac{3nC_{20}}{2a^2(1-e^2)\omega_T}\cos i, \tag{3.129}$$

$$\frac{\mathrm{d}\omega}{\mathrm{d}\tau_2} = -\frac{3C_{20}n}{2a^2(1-e^2)^2\omega_T}\left(2-\frac{5}{2}\sin^2 i\right). \tag{3.130}$$

For this case, the averaging conditions are

$$\frac{|C_{20}|}{p^2} << 1, \tag{3.131}$$

$$\frac{|C_{22}|}{p^2} << 1, \tag{3.132}$$

$$\frac{|n|}{\omega_T} << 1. \tag{3.133}$$

3.4.3 Comparision

The classical averaged equations for satellite motion about the Earth under the perturbation of C_{20} are [32]:

$$\frac{\mathrm{d}i}{\mathrm{d}t} = 0, \tag{3.134}$$

$$\frac{\mathrm{d}\Omega}{\mathrm{d}t} = \frac{3C_{20}n}{2a^2(1-e^2)}\cos i, \tag{3.135}$$

$$\frac{\mathrm{d}\omega}{\mathrm{d}t} = -\frac{3C_{20}n}{2a^2(1-e^2)^2}\left(2-\frac{5}{2}\sin^2 i\right). \tag{3.136}$$

The form of these equations are similar to the Equations 3.128-3.130. But physically, they can considered to be a special case of Equation 3.119-3.121, which belongs to the category of a slowly rotating central body ($n \gg \omega_T$) with $C_{22} = 0$. For example, a well-known application of the Equation 3.134-3.136 is the design of a Sun-synchronous orbit whose period is about 1 to 2 hours, which is much less than the Earth rotation period(24 hours).

3.5 Numerical Calculations and Verifications

To complete this study we present a number of numerical integrations which give partial validation of the assumptions made and which verify that the predicted behavior of the orbit plane does indeed occur. Due to the nature of numerical computations we can, realistically, only check our assumptions at a few points, but that agreement for a "generically" chosen set of conditions in the interval under consideration provides confidence in the analysis. The numerical approach solves Equations 2.23-2.25 by direct numerical integration of accelerations and velocities in the body-fixed coordinate. The osculating orbital elements are computed at each time step by transforming the position and velocity vectors from the body-fixed to inertial coordinates.

First consider Figure 3.9 which shows the osculating orbit elements for a particular numerical solution when $\mu = 1.0, \omega_T = 3.733 \times 10^{-4}$ and $\sigma = 4/7$. From this we clearly see that the orbital elements a and e are constant on average as predicted from our averaging analysis. We see that the other elements have non-trivial motions and that the Jacobi integral is constant.

Next consider Figure 3.10. This figure compares a single orbit of Ω_R versus i as computed from the analytical theory in Section 3.2 for $\omega_T = 0$, with a numerical integration of a similar orbit; the two curves are superimposed. This case represents a solution where the orbit plane has a nutation amplitude of $\pm 45°$ about a polar orbit and has a precession of the same amplitude about $\Omega_R = 90°$. We see close agreement between the averaged and numerical solutions, clearly indicating that our averaging analysis captures the essential character of motion in this case.

Finally consider Figure 3.11 which shows the results of a number of numerical

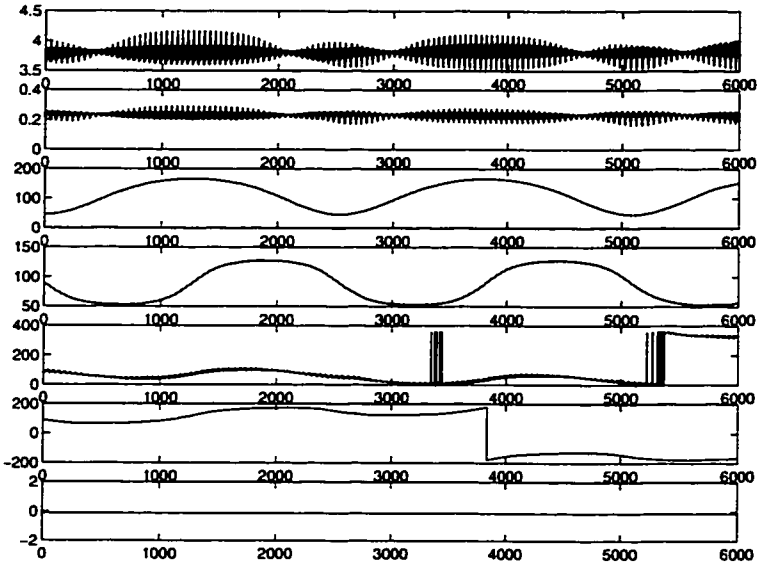

Figure 3.9: Numerically computed osculating orbital elements and Jacobi constant for a generic orbit. Shown in order from top to bottom are a, e, i, Ω_R, ω, Ω, J.

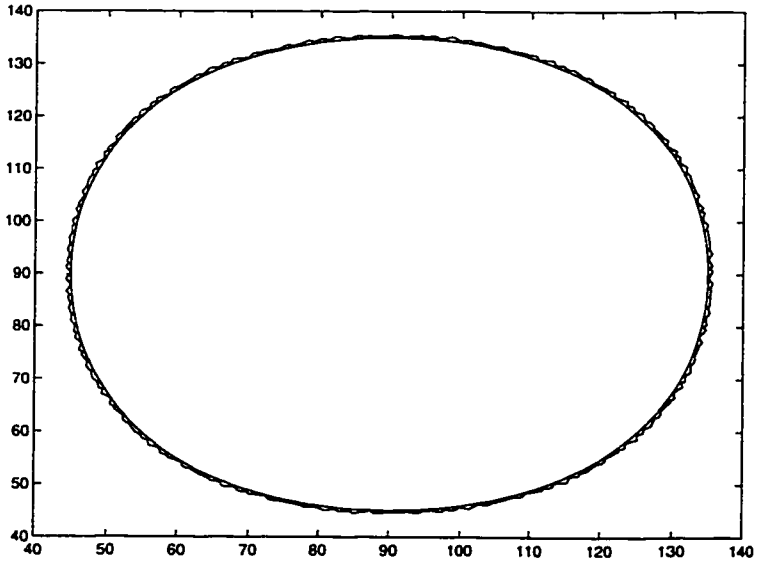

Figure 3.10: Quantitative comparison of the averaged analytical solution[40] for i and Ω_R and the numerical solution of these quantities for $\omega_T = 0$.

integrations plotted in the Ω_R–i space when $\mu = 1.0$, $\omega_T = 3.733 \times 10^{-4}$ and $\sigma = 4/7$ i.e. $C_{20} = -0.1$, $C_{22} = 0.02$. We note that this computation recreates the curves from our averaged analysis. Again, for this particular case, we see that the contours generated are qualitatively equivalent to those generated from the averaging theory. It is important to note that the contour lines in Figures 3.4-3.7 are not lines of constant Jacobi integral values in the unaveraged problem. This result validates our approach and shows that we can project the 5-dimensional surface of constant Jacobi values onto a 2-dimensional space and reduce the general problem of orbiting about a slowly rotating 2nd degree and order gravity field to a series of contour plots showing how the orbit plane precesses and nutates.

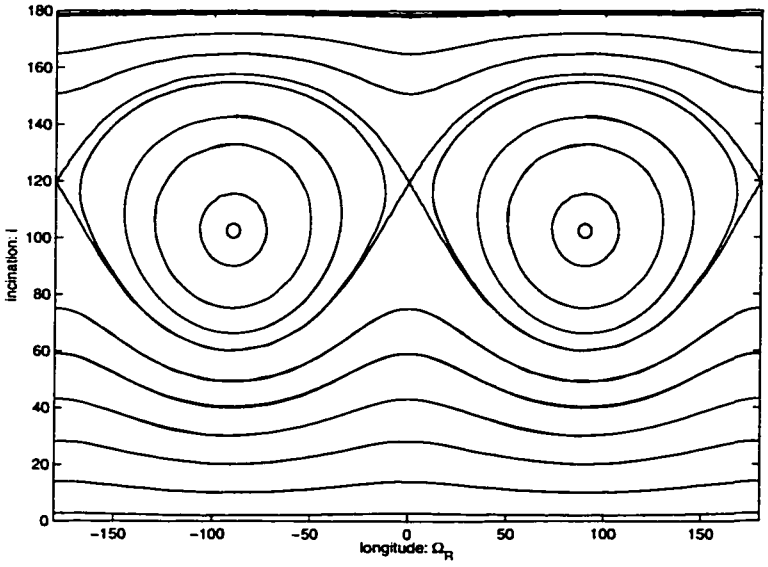

Figure 3.11: Numerical calculation of the contours of Ω_R and i for a range of different initial conditions.

Figure 3.12 shows the orbital angular momentum vector in 3-D space corresponding the Figure 3.11. We note that this computation uses the same initial conditions for Figure 3.11. We see the averaged Equation 3.109-3.111 completely describe the orbital angular momentum motion.

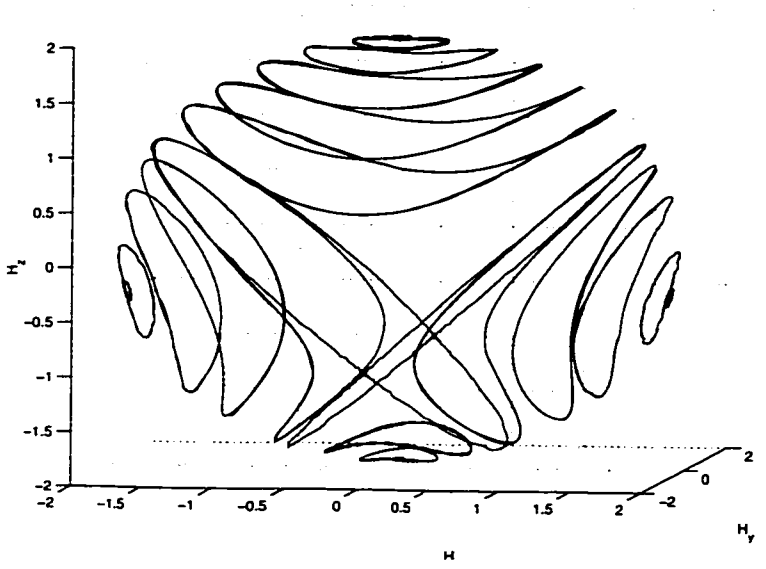

Figure 3.12: Numerical calculation of the angular momentum vector in 3-D space for a range of different initial conditions.

Particularly interesting are the "separatrices" between the libration and circulation cases – heteroclinic connections between the unstable frozen orbits for the mean elements in our averaged motion analysis. The orbit normal can cross these lines without violating any fundamental uniqueness properties of the full solution. Thus, it is possible for orbital motion in the real system to jump between circulation and libration, potentially defining a region of chaotic motion in terms of the orientation of the orbit plane.

CHAPTER IV

RESONANCES

In Chapter III, we discussed secular motion in a uniformly rotating second degree and order gravity field. In this chapter, we analyze the short-period motion which is closely related to resonances. The study of resonances can answer some of the size-shape stability problems posed in Section 2.3.3. Resonance in our system occurs due to the longitude dependence of the sectoral C_{22} and the commensurability between the orbital mean motion n and the asteroid rotation rate ω_T.

In this chapter, we use elliptic expansions to derive the Fourier expansions for the semi-major axis $a(t)$ and eccentricity $e(t)$ for nominal orbits in our system, i.e., the frequencies, amplitudes and phase angles of the Fourier expansion of $a(t), e(t)$ are estimated. Using the Fourier expansions, we can explain how the semi-major axis changes as it moves through the four quadrants of the rotating coordinate system. By averaging along a near resonant orbit, we can explain why the semi-major axis and eccentrity sometimes experience large fluctuations. Together with the resonant integrals given by Scheeres in [38], we can estimate a stability index for our size-shape stability analysis proposed in Chapter II. Furthermore, the Fourier expansions can also be used to analyze the periodic orbits discussed in Chapter V. Some numerical analyses and verifications are also given.

4.1 Elliptic Expansion

In this section we discuss the short period oscillation of the semi-major axis $a(t)$ and eccentricity $e(t)$ for a nominal orbit in a uniformly rotating second degree and order gravity field.

4.1.1 Some basic elliptic expansions

Some relations between true anomaly f, eccentric anomaly E, mean anomaly M, and radius r are given,

$$M = nt = E - e\sin E, \tag{4.1}$$

$$\tan\frac{f}{2} = \sqrt{\frac{1+e}{1-e}}\tan\frac{E}{2}, \tag{4.2}$$

$$\sin E = \frac{r\sin f}{a(1-e^2)^{1/2}}, \tag{4.3}$$

$$r = \frac{p}{1-e\cos f} = a(1-e\cos E), \tag{4.4}$$

$$r\sin f = a(1-e^2)^{1/2}\sin E, \tag{4.5}$$

$$r\cos f = a(\cos E - e). \tag{4.6}$$

Some basic elliptic expansions up to order two in the eccentricity are[43],[9]:

$$E = M + e\sin M + \frac{e^2}{2}\sin 2M + O(e^3), \tag{4.7}$$

$$f = M + 2e\sin M + \frac{5}{4}e^2\sin 2M + O(e^3), \tag{4.8}$$

$$r = a(1 - e\cos M + e^2\sin^2 M) + O(e^3), \tag{4.9}$$

$$\frac{\mu}{r} = \frac{\mu}{a}[1 + e\cos M + e^2\cos 2M] + O(e^3), \tag{4.10}$$

$$\frac{\mu}{r^3} = \frac{\mu}{a^3}\left[1 + 3e\cos M + 3e^2(3\cos^2 M - 1)\right] + O(e^3), \tag{4.11}$$

$$\sin E = \sin M + \frac{e}{2}\sin 2M + \frac{e^2}{8}(3\sin M - M) + O(e^3), \tag{4.12}$$

$$\cos E = -\frac{e}{2} + \cos M + \frac{e}{2}\cos 2M - \frac{3e^2}{8}(\cos M - \cos 3M) + O(e^3), \tag{4.13}$$

$$r\sin f = a[\sin M + \frac{e}{2}\sin 2M + \frac{e^2}{8}(3\sin 3M - 5\sin M)] + O(e^3), \tag{4.14}$$

$$r\cos f \;=\; a[\cos M + \frac{e}{2}(\cos 2M - 3) + \frac{3e^2}{8}(\cos 3M - \cos M)] + O(e^3). \quad (4.15)$$

We see that all the variables and equations can be expressed as explicit functions of the mean anormaly M.

4.1.2 Expansion of the potential

For a nominal orbit, its semi-major axis and eccentricity a_0 and e_0 are constant. A perturbed orbit is assumed to be oscillating about its nominal orbit.

For planar motion, the inclination $i = 0$ and, assuming its longitude of ascending node $\Omega = 0$ without loss of generality, then the longitude in body-fixed coordinates is $\lambda = f - \omega_T t + \omega$ and the gravity perturbation potential becomes (see Equation 3.6)

$$U_p \;=\; U_2 = \frac{\mu}{r^3}\left[-\frac{1}{2}C_{20} + 3C_{22}\cos 2(f - \omega_T t + \omega)\right]. \quad (4.16)$$

Using the basic elliptic expansions from the last section, the expansion of the gravity potential in inertial coordinates is

$$\begin{aligned} U_p = {} & \frac{\mu}{2a^3}\left[-C_{20} + 6C_{22}\cos(2M - 2\omega_T t + 2\omega)\right] \\ & -\frac{3\mu e}{2a^3}\Big[C_{20}\cos M + C_{22}\cos(M - 2\omega_T t + 2\omega) \\ & \qquad -7C_{22}\cos(3M - 2\omega_T t + 2\omega)\Big] \\ & -\frac{3\mu e^2}{4a^3}\Big[C_{20} + 3C_{20}\cos 2M + 10C_{22}\cos(2M - 2\omega_T t + 2\omega) \\ & \qquad -34C_{22}\cos(4M - 2\omega_T t + 2\omega)\Big] + O(e^3). \end{aligned} \quad (4.17)$$

Then the partial derivatives with respect to M and ω are

$$\begin{aligned} \frac{\partial U_p}{\partial M} = {} & -\frac{6\mu C_{22}}{a^3}\sin(2M - 2\omega_T t + 2\omega) \\ & +\frac{3\mu e}{2a^3}\Big[C_{20}\sin M + C_{22}\sin(M - 2\omega_T t + 2\omega) \end{aligned}$$

$$-21C_{22}\sin(3M-2\omega_T t+2\omega)\Big]$$
$$+\frac{3\mu e^2}{2a^3}\Big[3C_{20}\sin 2M+10C_{22}\sin(2M-2\omega_T t+2\omega)$$
$$-68C_{22}\sin(4M-2\omega_T t+2\omega)\Big]+O(e^3), \tag{4.18}$$

$$\frac{\partial U_p}{\partial \omega}=-\frac{6C_{22}\mu}{a^3}\sin(2M-2\omega_T t+2\omega)$$
$$+\frac{3C_{22}\mu e}{a^3}\Big[\sin(M-2\omega_T t+2\omega)-7\sin(3M-2\omega_T t+2\omega)\Big]$$
$$+\frac{3C_{22}\mu e^2}{a^3}\Big[5\sin(2M-2\omega_T t+2\omega)-17C_{22}\sin(4M-2\omega_T t+2\omega)\Big]$$
$$+O(e^3). \tag{4.19}$$

4.1.3 Expansion for $a(t), e(t)$

The perturbation of the semi-major axis using the Lagrange planetary equations are (Equation C.1)

$$\frac{da}{dt}=\frac{2}{na}\frac{\partial U_p}{\partial M} \tag{4.20}$$
$$=-\frac{12C_{22}n}{a}\sin(2M-2\omega_T t+2\omega)$$
$$+\frac{3ne}{a}\Big[C_{20}\sin M+C_{22}\sin(M-2\omega_T t+2\omega)$$
$$-21C_{22}\sin(3M-2\omega_T t+2\omega)\Big]$$
$$+\frac{3ne^2}{a}\Big[3C_{20}\sin 2M+10C_{22}\sin(2M-2\omega_T t+2\omega)$$
$$-68C_{22}\sin(4M-2\omega_T t+2\omega)\Big]+O(e^3). \tag{4.21}$$

If $e_0 \ll 1$ and n_0, a_0, $M=n_0 t$ correspond to the nominal orbit in inertial coordinates, then

$$a(t)=a_{00}+\frac{6n_0C_{22}}{a_0(n_0-\omega_T)}\cos(2n_0t-2\omega_T t+2\omega)$$
$$-\frac{3n_0e_0}{a_0}\Big[\frac{C_{20}}{n_0}\cos n_0t+\frac{C_{22}}{n_0-2\omega_T}\cos(n_0t-2\omega_T t+2\omega)$$

$$-\frac{21C_{22}}{3n_0-2\omega_T}\cos(3n_0t-2\omega_Tt+2\omega)\Big]$$
$$-\frac{3n_0e_0^2}{a_0}\Big[\frac{3C_{20}}{2n_0}\cos 2n_0t+\frac{5C_{22}}{n_0-\omega_T}\cos(2n_0t-2\omega_Tt+2\omega)$$
$$-\frac{34C_{22}}{2n_0-\omega_T}\cos(4n_0t-2\omega_Tt+2\omega)\Big]+O(e_0^3). \tag{4.22}$$

We can rewrite this equation as

$$a(t)=a_{00}+a_{01}\cos f_{01}t+a_{02}\cos f_{02}t+a_{12}\cos(f_{12}t+2\omega)+a_{11}\cos(f_{11}t+2\omega)$$
$$+a_{32}\cos(f_{32}t+2\omega)+a_{21}\cos(f_{21}t+2\omega)+O(e_0^3), \tag{4.23}$$

where the amplitudes and frequencies are

$$a_{00} = a_0, \quad (f_{00}=0), \tag{4.24}$$
$$a_{01} = -\frac{3C_{20}e_0}{a_0}, \quad f_{01}=n_0, \tag{4.25}$$
$$a_{02} = -\frac{9C_{20}e_0^2}{2a_0}, \quad f_{02}=2n_0 \tag{4.26}$$
$$a_{12} = -\frac{3C_{22}n_0e_0}{a_0(n_0-2\omega_T)}, \quad f_{12}=n_0-2\omega_T, \tag{4.27}$$
$$a_{11} = +\frac{3C_{22}n_0(2-5e_0^2)}{a_0(n_0-\omega_T)}, \quad f_{11}=2(n_0-\omega_T), \tag{4.28}$$
$$a_{32} = +\frac{63C_{22}n_0e_0}{a_0(3n_0-2\omega_T)}, \quad f_{32}=3n_0-2\omega_T, \tag{4.29}$$
$$a_{21} = +\frac{102C_{22}n_0e_0^2}{a_0(2n_0-\omega_T)}, \quad f_{21}=2(2n_0-\omega_T). \tag{4.30}$$

We see that the coefficients $a_{11}(e^0), a_{01}(e^1), a_{12}(e^1), a_{32}(e^1)$ dominate.

Similarly, we can also find the eccentricity perturbation from Equation C.2

$$\frac{de}{dt}=\frac{1-e^2}{na^2e}\frac{\partial U_p}{\partial M}-\frac{(1-e^2)^{1/2}}{na^2e}\frac{\partial U_p}{\partial \omega} \tag{4.31}$$
$$=\frac{3n}{2a^2}\Big[C_{20}\sin M-C_{22}\sin(M-2\omega_Tt+2\omega)$$
$$-7C_{22}\sin(3M-2\omega_Tt+2\omega)\Big]$$
$$+\frac{3ne}{2a^2}\Big[3C_{20}\sin 2M+2C_{22}\sin(2M-2\omega_Tt+2\omega)+$$
$$-34C_{22}\sin(4M-2\omega_Tt+2\omega)\Big]+O(e^2). \tag{4.32}$$

Then, similar to the expansion of $a(t)$, $e(t)$ becomes

$$\begin{aligned} e(t) = e_{00} + \frac{3n_0}{2a_0^2}\Big[& -\frac{C_{20}}{n_0}\cos n_0 t + \frac{C_{22}}{n_0 - 2\omega_T}\cos(n_0 t - 2\omega_T t + 2\omega) \\ & + \frac{7C_{22}}{3n_0 - 2\omega_T}\cos(3n_0 t - 2\omega_T t + 2\omega)\Big] \\ -\frac{3n_0 e_0}{4a_0^2}\Big[& \frac{3C_{20}}{n_0}\cos 2n_0 t + \frac{2C_{22}}{n_0 - \omega_T}\cos(2n_0 t - 2\omega_T t + 2\omega) + \\ & - \frac{34C_{22}}{2n_0 - \omega_T}\cos(4n_0 t - 2\omega_T t + 2\omega)\Big] + O(e^2). \end{aligned} \tag{4.33}$$

We can rewrite this equation as

$$\begin{aligned} e(t) = e_{00} + e_{01}\cos f_{01}t + e_{02}\cos f_{02}t + e_{12}\cos(f_{12}t + 2\omega) + e_{11}\cos(f_{11}t + 2\omega) \\ + e_{32}\cos(f_{32}t + 2\omega) + e_{21}\cos(f_{21}t + 2\omega) + O(e_0^2), \end{aligned} \tag{4.34}$$

where the amplitudes and frequencies are

$$e_{00} = e_0, \quad (f_{00} = 0), \tag{4.35}$$

$$e_{01} = -\frac{3C_{20}}{2a_0^2}, \quad f_{01} = n_0, \tag{4.36}$$

$$e_{02} = -\frac{9C_{20}e_0}{4a_0^2}, \quad f_{02} = 2n_0, \tag{4.37}$$

$$e_{12} = +\frac{3C_{22}n_0}{2a_0^2(n_0 - 2\omega_T)}, \quad f_{12} = n_0 - 2\omega_T, \tag{4.38}$$

$$e_{11} = -\frac{3C_{22}n_0 e_0}{2a_0^2(n_0 - \omega_T)}, \quad f_{11} = 2(n_0 - \omega_T), \tag{4.39}$$

$$e_{32} = +\frac{21C_{22}n_0}{2a_0^2(3n_0 - 2\omega_T)}, \quad f_{32} = 3n_0 - 2\omega_T, \tag{4.40}$$

$$e_{21} = +\frac{51C_{22}n_0 e_0}{2a_0^2(2n_0 - \omega_T)}, \quad f_{21} = 2(2n_0 - \omega_T). \tag{4.41}$$

We see that the coefficients which dominate are $e_{01}(e^0), e_{12}(e^0), e_{32}(e^0)$.

4.1.4 Conclusions and numerical verifications

We can use the analytical Equations 4.23 and 4.34 to explain and analyze many phenomena found in the numerical integrations of Equation 2.23-2.25.

Oscillation when e_0 is small

For a planar, near circular, nominal orbit when $i_0 = e_0 = 0$, the term $a_{11}\cos(f_{11}t)$ in Equation 4.23 dominates; that is, $|a_{11}| \gg |a_{ij}|(i \neq 1 or j \neq 1)$. This explains a basic fact about an orbiting particle moving through the four quadrants of an asteroid; as a function of longitude it experiences an alternating increase and decrease in its semi-major axis. For example, if a particle moves counter-clockwise in inertial coordinates(a direct orbit) and clockwise in body-fixed coordinates, i.e. $\omega_T > n_0 > 0$, in quadrants I and III of the body-fixed coordinate the semi-major axis decreases; in quadrants II and IV the semi-major axis increases. The four quadrants I,II,III,IV are shown in Figure 4.1.

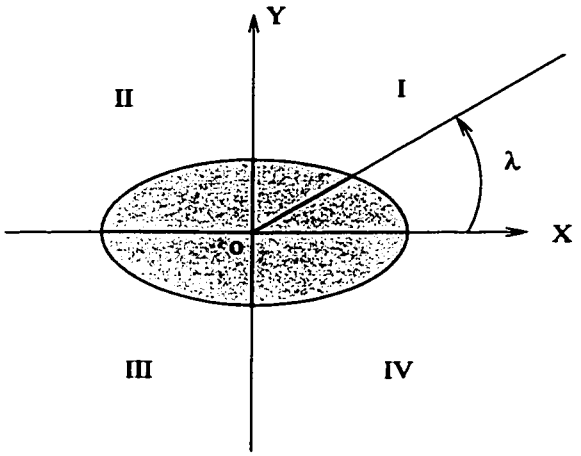

Figure 4.1: The four quadrants I,II,III,IV in body-fixed coordinates

In Figure 4.2, $a_0 = 1.53$, $e_0 \approx 0$, where in the figure $\lambda \approx (n_0 - \omega_T)t$ corresponds to the longitude in body fixed coordinate in Figure 2.1 and 3.1. And in this figure,

$$a(t) \approx a_{00} + a_{11}\cos f_{11}t, \tag{4.42}$$

$$\frac{da}{dt} \approx -\frac{12n_0C_{22}}{a_0}\sin 2(n_0 - \omega_T)t \equiv -\frac{12n_0C_{22}}{a_0}\sin 2\lambda. \tag{4.43}$$

So, this explains why the semi-major axis decreases when λ is in quadrant I ($0 <$

$\lambda < 90°$) and III($-180° < \lambda < -90°$), and semi-major axis increases when λ is in quadrant II($90° < \lambda < 180°$) and IV($-90° < \lambda < 0°$).

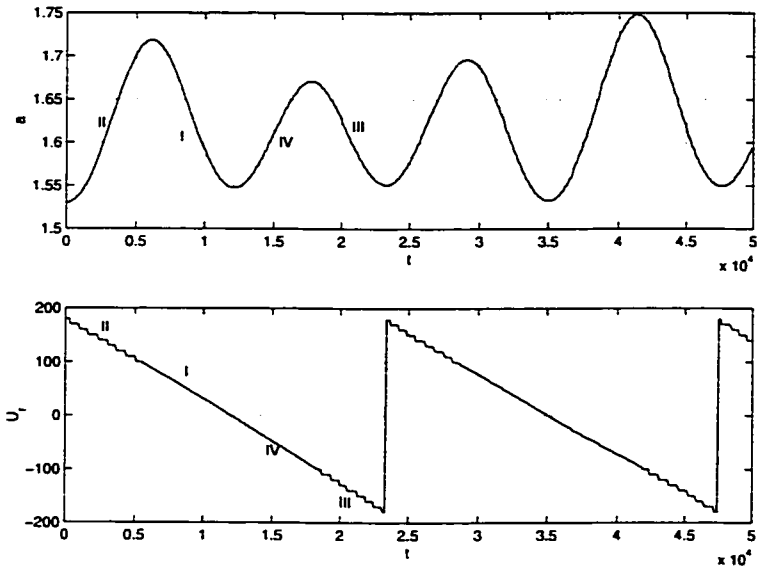

Figure 4.2: Relation between oscillating a(t) to the quadrants in the rotating coordinate when $\omega_T > n_0 > 0$, $U_r = \lambda$

If the particle moves clockwise in inertial coordinates(a retrograde orbit), i.e., $n_0 < 0$. in quadrant I and III of the body-fixed coordinates, the semi-major axis increases; in quadrant II and IV the semi-major axis decreases(See Figure 4.3). This can be explained by Equations 4.43 as well.

Oscillation frequencies f_{ij}

We denote the frequencies n_0 and $|n_0 - \omega_T|$ as "basic frequencies" which have clear physical meanings; n_0 is the mean motion in an inertial frame, and $|n_0 - \omega_T|$ is the mean motion in a body-fixed frame. Other frequencies in Equation 4.23, 4.34 are combinations of the above two.

By integrating Equations 2.23-2.25, we can evaluate the dynamic response of semi-major axis and eccentricity, $a(t)$ and $e(t)$, to the perturbations. Then by using

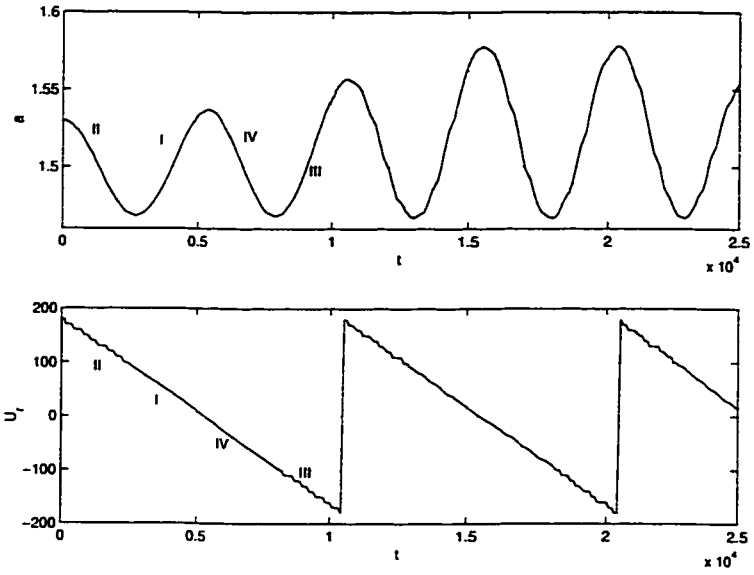

Figure 4.3: Relation between oscillating a(t) to quadrant in the rotating coordinate when $n_0 < 0$

numerical FFT, we can analyze $a(t)$ and $e(t)$ to verify the oscillation frequencies and amplitudes which appear in Equation 4.23 for $a(t)$ and Equation 4.34 for $e(t)$. See Figure 4.4 for a FFT analysis applied to $a(t)$ and Figure 4.5 for a FFT analysis applied to $e(t)$ for a near stable orbit with $a_0 = 1.53$, $e_0 \approx 0$.

When the central body rotates rapidly, $\omega_T >> n_0$, the dominating frequencies are $2(\omega_T - n_0), (2\omega_T - 3n_0), (2\omega_T - 4n_0), n_0, (2\omega_T - 5n_0)$, (see Figure 4.4); when the central body rotates slowly($\omega_T < n_0$), the dominating frequencies become n_0, $2(n_0 - \omega_T)$, $n_0 - 2\omega_T$. Note that when e_0 is large, the dominating frequencies may change. See Section 4.3.1.

Oscillation amplitudes a_{ij}, e_{ij}

We calculate the coefficients a_{ij} and e_{ij} in Figure 4.6 and 4.7 by using Equations 4.23 and 4.34. For different values of a_0, we find

$$\lim_{n_0 \to 2\omega_T} a_{12} \to \infty, \quad \lim_{n_0 \to 2\omega_T} e_{12} \to \infty, \tag{4.44}$$

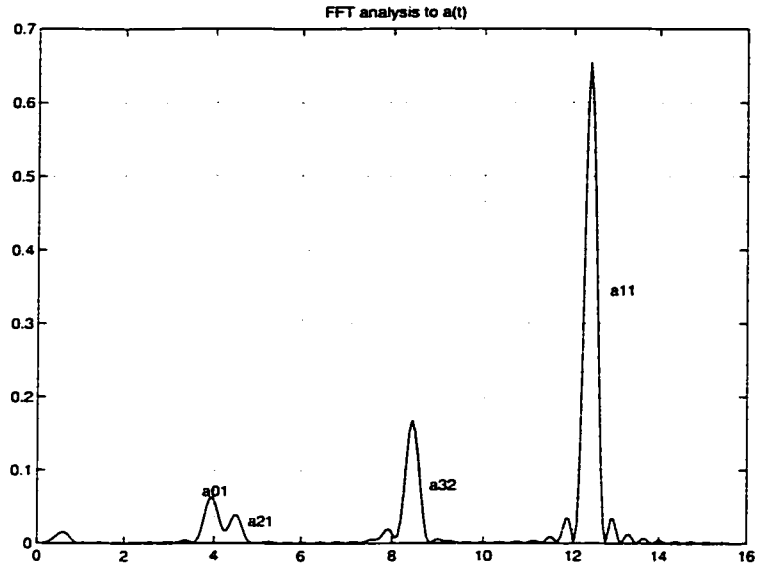

Figure 4.4: FFT analysis of oscillating $a(t)$

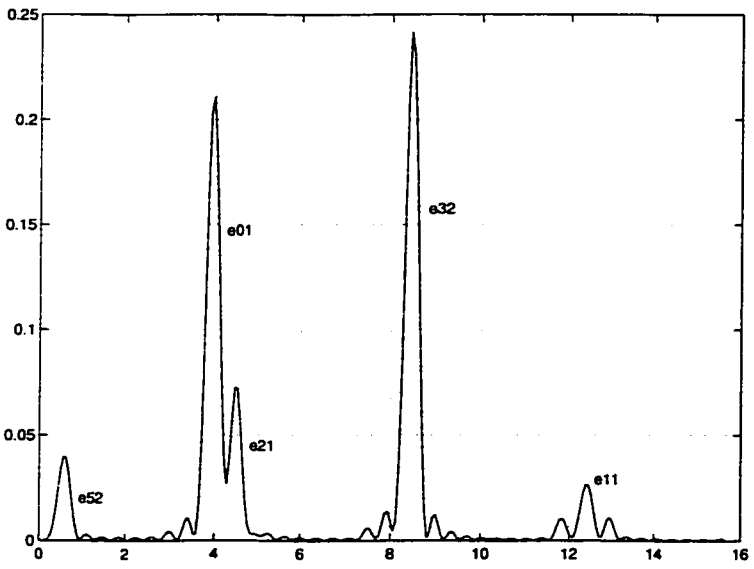

Figure 4.5: FFT analysis of oscillating $e(t)$

$$\lim_{n_0 \to \omega_T} a_{11} \to \infty, \quad \lim_{n_0 \to \omega_T} e_1 \to \infty, \tag{4.45}$$

$$\lim_{n_0 \to 2\omega_T/3} a_{32} \to \infty, \quad \lim_{n_0 \to 2\omega_T/3} e_{32} \to \infty, \tag{4.46}$$

$$\lim_{n_0 \to \omega_T/2} a_{21} \to \infty, \quad \lim_{n_0 \to \omega_T/2} e_{21} \to \infty. \tag{4.47}$$

Thus, in a neighborhood of these resonant orbits, oscillations about their nominal semi-major axis a_0 and eccentricity e_0 should be large in general.

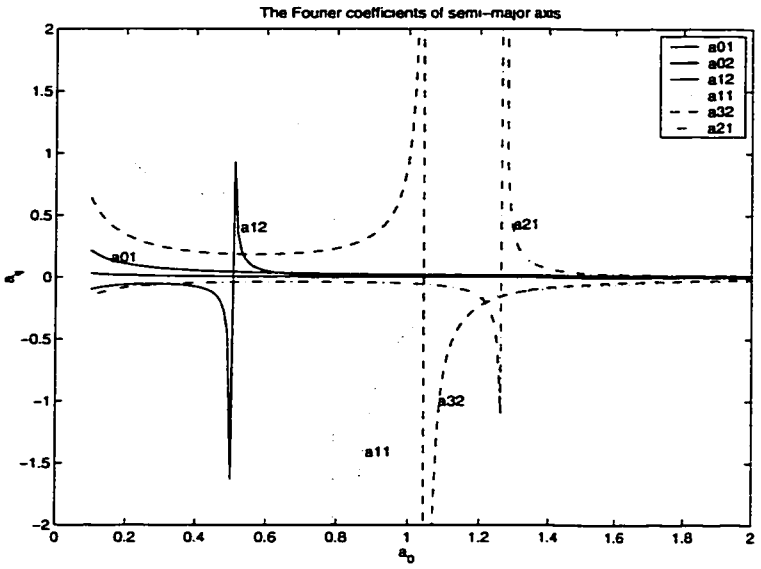

Figure 4.6: Some oscillation coefficients of $a(t)$ for different mean motions

Note that in Figure 4.6 and 4.7, when $a_0 > 1.4$, $|a_{11}| > |a_{32}| > |a_{01}| > |a_{21}|$ and $|e_{32}| > |e_{01}| > |e_{21}| > |e_{11}|$, which are compatible with the FFT analyses shown in Figures 4.4 and 4.5. For example when $a_0 = 1.53$, $e_0 = 0.038$, the oscillation coefficients calculated using the analytic Equations 4.23 and 4.34 are close to the numerical FFT comparations in Figure 4.4 and 4.5. See Table 4.1 where a_{ij} is normalized by a_{11}, and e_{ij} is normalized by e_{32}.

We note that all the data for the calculations in Figures 4.2-4.7 are from the asteroid Castalia parameters(see Appendix C.3).

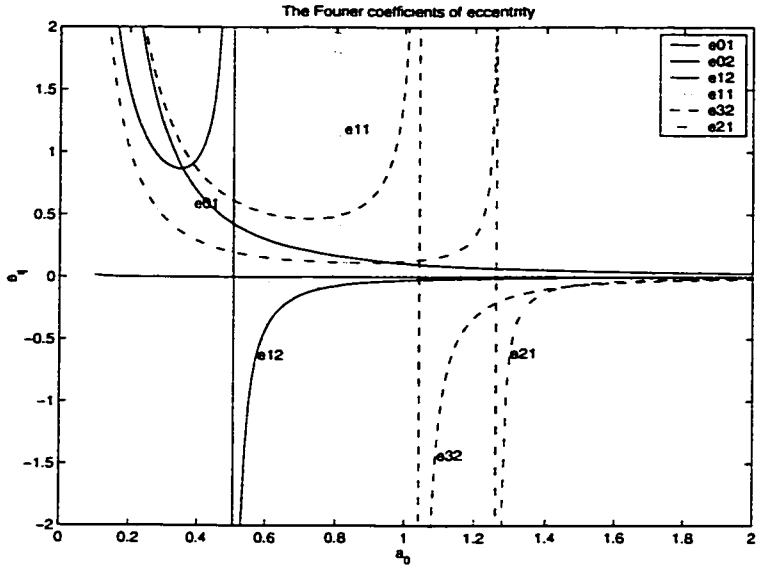

Figure 4.7: Some oscillation coefficients of $e(t)$ for different mean motions

ij	11	32	21	01	Method
$\lvert a_{ij}/a_{11}\rvert$	1.000	0.286	0.062	0.076	analytical
$\lvert a_{ij}/a_{11}\rvert$	1.000	0.268	0.058	0.083	FFT
$\lvert e_{ij}/e_{32}\rvert$	0.009	1.000	0.328	0.799	analytical
$\lvert e_{ij}/e_{32}\rvert$	0.010	1.000	0.324	0.875	FFT

Table 4.1: Comparisons between analytical and numerical calculations of the amplitudes

4.2 Averaging Along Resonant Orbits

In this section we study the secular changes(accumulated effect) of the perturbation in $a(t)$ and $e(t)$ for near resonant orbits. There are a number of near circular, resonant orbits in our system, such as $\omega_T/n \approx$ 1:2, 2:3, 1:1, 3:2, 1:2 etc, where $\epsilon_{ij} = in - j\omega_T$, $|\epsilon_{ij}| << \omega_T$, and i, j are integers. Here we assume that changes in M are much faster than changes in $\Omega, \omega, \epsilon_{ij}t, a, e, i$ and n.

In the following we will study a few typical near-resonant orbits whose averaged Lagrange equations for semi-major axis and eccentricity are derived and solutions obtained. We see that there exist secular transitions in $a(t)$ and $e(t)$ for some near resonant orbits.

4.2.1 1:2 resonant orbit

For ϵ_{12} a small number, where $\epsilon_{12}t = M - 2\omega_T t$, the averaged gravity potential for Equation 4.17 is

$$\bar{U}_p = \frac{1}{2\pi}\int_0^{2\pi} U_p \mathrm{d}M \tag{4.48}$$

$$= -\frac{\mu}{2\bar{a}^3}\left[C_{20}(1+\frac{3}{2}\bar{e}^2) + 3\bar{e}C_{22}\cos(2\bar{\Omega}+2\bar{\omega}+\epsilon_{12}t)\right] + O(\bar{e}^3). \tag{4.49}$$

The averaged semi-major axis and eccentricity Lagrange equations are

$$\frac{\mathrm{d}\bar{a}}{\mathrm{d}t} = \frac{3C_{22}\bar{n}\bar{e}}{\bar{a}}\sin(2\bar{\Omega}+2\bar{\omega}+\epsilon_{12}t) + O(\bar{e}^3), \tag{4.50}$$

$$\frac{\mathrm{d}\bar{e}}{\mathrm{d}t} = -\frac{3C_{22}\bar{n}}{2\bar{a}^2}\sin(2\bar{\Omega}+2\bar{\omega}+\epsilon_{12}t) + O(\bar{e}^2). \tag{4.51}$$

Hence, for near-resonant 1:2 orbits, the relation between $\bar{a}$ and $\bar{e}$ is

$$\frac{\mathrm{d}\bar{a}}{\mathrm{d}\bar{e}} = -2\bar{a}\bar{e} + O(\bar{e}^2), \tag{4.52}$$

$$\text{i.e.,}\quad \bar{a}\exp(\bar{e}^2) = \text{constant}. \tag{4.53}$$

Thus we see that when $\bar{a}$ decreases $\bar{e}$ increases, and hence radius of periapsis decreases potentially leading to a collision orbit. More importantly, it leads to a stronger interaction between the orbit and the asteroid, which destabilizes the motion. Integrate Equations 4.50 and 4.51 to find

$$\bar{a} = \bar{a}_{00} - \frac{3C_{22}\bar{n}_0\bar{e}_0}{\bar{a}_0\epsilon_{12}}\cos(2\bar{\Omega} + 2\bar{\omega} + \epsilon_{12}t) + O(\bar{e}^3), \tag{4.54}$$

$$\bar{e} = \bar{e}_{00} + \frac{3C_{22}\bar{n}_0}{2\bar{a}_0^2\epsilon_{12}}\cos(2\bar{\Omega} + 2\bar{\omega} + \epsilon_{12}t) + O(\bar{e}^2). \tag{4.55}$$

At this 1:2 resonant case, the averaging conditions are

$$\frac{|C_{22}|}{a^2} << 1, \tag{4.56}$$

$$\bar{e} << 1, \tag{4.57}$$

$$\frac{|\epsilon_{12}|}{\omega_T} << 1. \tag{4.58}$$

We see $\mathrm{d}\bar{a}/\mathrm{d}t \in O(\bar{e}^1)$, $\mathrm{d}\bar{e}/\mathrm{d}t \in O(\bar{e}^0)$. This means that even for $\bar{e} = 0$, the eccentricity will not be constant on average if $C_{22} \neq 0$, except for some special cases.

4.2.2 Some other resonant orbits

Following a similar procedure for the 1:2 resonant orbit, we analyze some other near resonant orbits.

1:1 resonant orbit

Similarly, if $\epsilon_{11}t = 2M - 2\omega_T t$, the averaged semi-major axis and eccentricity of the Lagrange equation for 1:1 resonant orbits are

$$\frac{\mathrm{d}\bar{a}}{\mathrm{d}t} = -\frac{6C_{22}\bar{n}}{\bar{a}}(2 - 5\bar{e}^2)\sin(2\bar{\Omega} + 2\bar{\omega} + \epsilon_{11}t) + O(\bar{e}^3), \tag{4.59}$$

$$\frac{\mathrm{d}\bar{e}}{\mathrm{d}t} = \frac{3C_{22}\bar{n}\bar{e}}{\bar{a}^2}\sin(2\bar{\Omega} + 2\bar{\omega} + \epsilon_{11}t) + O(\bar{e}^2). \tag{4.60}$$

So for near resonant, 1:1 orbits, the relation between $\bar{a}$ and $\bar{e}$ is

$$\frac{\mathrm{d}\bar{a}}{\mathrm{d}\bar{e}} = -\frac{4\bar{a}}{\bar{e}} + O(\bar{e}^2), \tag{4.61}$$

$$\text{i.e.,} \quad \bar{a}\bar{e}^4 = \text{constant.} \tag{4.62}$$

We see that $\mathrm{d}\bar{a}/\mathrm{d}t \in O(\bar{e}^0)$, $\mathrm{d}\bar{e}/\mathrm{d}t \in O(\bar{e}^1)$. This means that, even if $\bar{e} = 0$, the semi-major axis can't stay constant on average if $C_{22} \neq 0$. Similar to the 1:2 near resonant orbit, $\bar{a}$ decreases when $\bar{e}$ increases, which could also lead to collision orbits.

3:2 resonant orbit

If $\epsilon_{32}t = 3M - 2\omega_T t$, the averaged semi-major axis and eccentricity of the Lagrange equation are

$$\frac{\mathrm{d}\bar{a}}{\mathrm{d}t} = -\frac{63C_{22}\bar{n}\bar{e}}{\bar{a}}\sin(2\bar{\Omega} + 2\bar{\omega} + \epsilon_{32}t) + O(\bar{e}^3), \tag{4.63}$$

$$\frac{\mathrm{d}\bar{e}}{\mathrm{d}t} = -\frac{21C_{22}\bar{n}}{2\bar{a}^2}\sin(2\bar{\Omega} + 2\bar{\omega} + \epsilon_{32}t) + O(\bar{e}^2). \tag{4.64}$$

So for near resonant 3:2 orbits, the relation between $\bar{a}$ and $\bar{e}$ is

$$\frac{\mathrm{d}\bar{a}}{\mathrm{d}\bar{e}} = 6\bar{a}^2\bar{e} + O(\bar{e}^2), \tag{4.65}$$

$$\text{i.e.,} \quad \frac{1}{\bar{a}} + 3\bar{e}^2 = \text{constant.} \tag{4.66}$$

We see that $\mathrm{d}\bar{a}/\mathrm{d}t \in O(\bar{e}^1)$, $\mathrm{d}\bar{e}/\mathrm{d}t \in O(\bar{e}^0)$. Thus even if $\bar{e} = 0$, eccentricity can't keep constant on average if $C_{22} \neq 0$. In this situation, $\bar{a}$ increases when $\bar{e}$ increases, potentially leading to an escape orbit.

2:1 resonant orbit

If $\epsilon_{21}t = 4M - 2\omega_T t$, the averaged semi-major axis and eccentricity of Lagrange equation are

$$\frac{\mathrm{d}\bar{a}}{\mathrm{d}t} = -\frac{204C_{22}\bar{n}\bar{e}^2}{\bar{a}}\sin(2\bar{\Omega} + 2\bar{\omega} + \epsilon_{32}t) + O(\bar{e}^3), \tag{4.67}$$

$$\frac{\mathrm{d}\bar{e}}{\mathrm{d}t} = -\frac{51C_{22}\bar{n}\bar{e}}{\bar{a}^2}\sin(2\bar{\Omega} + 2\bar{\omega} + 2\epsilon_{32}t) + O(\bar{e}^2). \tag{4.68}$$

So for near resonant 2:1 orbits, the relation between $\bar{a}$ and $\bar{e}$ is

$$\frac{d\bar{a}}{d\bar{e}} = 4\bar{a}\bar{e} + O(\bar{e}^2), \tag{4.69}$$

$$\text{i.e.,} \quad \frac{\bar{a}}{\exp(2\bar{e}^2)} = \text{constant} \tag{4.70}$$

We see that $d\bar{a}/dt \in O(\bar{e}^2)$, $d\bar{e}/dt \in O(\bar{e}^1)$. This means that when $\bar{e} = 0$, both the semi-major axis and eccentricity can be constant on average, even if $C_{22} \neq 0$. Now, $\bar{a}$ increases when $\bar{e}$ increases, so this could also be a potential escape orbit.

2:3, 5:2, 3:1 resonant orbit

For other near circular resonant orbits, such as 2:3, 5:2, 3:1, the C_{22} perturbation disappears. The averaged gravity potential in the vicinity of these resonance becomes

$$\bar{U}_p = -\frac{\mu C_{20}}{2\bar{a}^3}(1 + \frac{3}{2}\bar{e}^2) + O(e^3). \tag{4.71}$$

Just as in the rapid rotation case, only the C_{20} perturbation is left. So for near resonant 2:3 orbits, their secular semi-major axis $\bar{a}_{23} = 0$ and secular eccentricity $\bar{e}_{23} = 0$ also. The same results exist for 5:2, 3:1 resonant orbits whose secular $\bar{a}, \bar{e} \in O(\bar{e}^k), k \geq 2$.

4.2.3 Analyses

For a near circular, resonant orbit, the relation between a and e have no relation on its orbital orientation i, Ω, ω, or even on the gravity coefficient C_{22}, that is

$$\frac{d\bar{a}}{d\bar{e}} = R_{ij}(\bar{a}, \bar{e}), \tag{4.72}$$

where $i : j$=1:2, 1:1, 3:2, 2:1. This analysis explains why $\bar{a}$ and $\bar{e}$ sometimes increase or decrease in step. For a collision orbit, a decreases as e increases; for an escape orbit, a increases as e increases.

One application of the averaged resonant equations is to analyze the size-shape stability of near circular resonant orbits and compare them with Figure 2.5. At the resonant orbits of 1:2, 1:1, 3:2 , we found transitions from stable to unstable orbits. Whereas at the resonant orbits 2:3, 2:1 5:2, there were no such stability transitions. This implies that near circular 1:2, 1:1, 3:2 resonant orbits are not stable, and that the 2:3, 2:1, 5:2 resonant orbits could be stable. More discussions of this are given in Section 4.3.2.

We note here, in the near resonant orbit analysis (different from the slow and fast rotation cases in Chapter III), we focused the discussion on the size and shape of the perturbed orbit, i.e. a, e, and not the orientation, i.e. i, Ω, ω. For the slowly and rapidly rotating problem, the shape and size of the orbit were invariant on average, i.e. size-shape stable. Only for size-shape stable orbits does the study of orbital orientation changes become meaningful.

4.3 Resonance and Size-shape Stability

Similar to the procedure in Section 4.1, we use a computer to realize high order elliptic expansions, up to order seven in ellipticity, for planar orbits. Mathematica 4.0 [47] was applied to perform the derivations. See the results in Appendix B.1.

4.3.1 Summary

The dynamic responses of the semi-major axis and eccentricity, more general than Equation 4.23 and 4.34, are (See Appendix B.1.2)

$$a(t) = \sum_{i=0,j=0}^{\infty,\infty} a_{ij} \cos(f_{ij}t + \phi_{ij}^{a}), \tag{4.73}$$

$$e(t) = \sum_{i=0,j=0}^{\infty,\infty} e_{ij} \cos(f_{ij}t + \phi_{ij}^{e}), \tag{4.74}$$

i	j	$\bar{a}_{ij}$	$\bar{e}_{ij}$	a_{ij}	e_{ij}	f_{ij}
0	0	-	-	a_0	e_0	0
0	1	-	-	$-\frac{3C_{20}e_0}{a_0}$	$-\frac{3C_{20}}{2a_0^2}$	n_0
0	2	-	-	$-\frac{9C_{20}e_0^2}{2a_0}$	$-\frac{9C_{20}e_0}{4a_0^2}$	$2n_0$
1	2	$\in O(\bar{e}^1)$	$\in O(\bar{e}^0)$	$-\frac{3C_{22}n_0e_0}{a_0(n_0-2\omega_T)}$	$\frac{3C_{22}n_0}{2a_0^2(n_0-2\omega_T)}$	$n_0-2\omega_T$
2	3	$\in O(\bar{e}^\infty)$	$\in O(\bar{e}^\infty)$	0	0	$2n_0-3\omega_T$
2	2	$\in O(\bar{e}^0)$	$\in O(\bar{e}^1)$	$\frac{3n_0C_{22}(2-5e_0^2)}{a_0(n_0-\omega_T)}$	$-\frac{3C_{22}n_0e_0}{2a_0^2(n_0-\omega_T)}$	$2(n_0-\omega_T)$
3	2	$\in O(\bar{e}^1)$	$\in O(\bar{e}^0)$	$\frac{63C_{22}n_0e_0}{a_0(3n_0-2\omega_T)}$	$\frac{21C_{22}n_0}{2a_0^2(3n_0-2\omega_T)}$	$3n_0-2\omega_T$
4	2	$\in O(\bar{e}^2)$	$\in O(\bar{e}^1)$	$\frac{102C_{22}n_0e_0^2}{a_0(2n_0-\omega_T)}$	$\frac{51C_{22}n_0e_0}{2a_0^2(2n_0-\omega_T)}$	$2(2n_0-\omega_T)$
5	2	$\in O(\bar{e}^3)$	$\in O(\bar{e}^2)$	$\frac{4225C_{22}n_0e_0^3}{8a_0(5n_0-2\omega_T)}$	$\frac{2535C_{22}n_0e_0^2}{16a_0^2(5n_0-2\omega_T)}$	$5n_0-2\omega_T$
6	2	$\in O(\bar{e}^4)$	$\in O(\bar{e}^3)$	$\frac{4797C_{22}n_0e_0^4}{8a_0(3n_0-\omega_T)}$	$\frac{1599C_{22}n_0e_0^3}{8a_0^2(3n_0-\omega_T)}$	$2(3n_0-\omega_T)$
$\vdots$	$\vdots$	$\vdots$	$\vdots$	$\vdots$	$\vdots$	$\vdots$

Table 4.2: Amplitudes and frequencies of elliptic expansion of $a(t), e(t)$

where a_{00}, and e_{00} are the nominal semi-major axis and eccentricity without perturbation, $a_{0j}, e_{0j}, (j \neq 0)$ are amplitudes of the oscillation with the frequency of the mean motion and its multiples in inertial coordinate, and $a_{ij}, e_{ij}, (i \neq 0, j = 2)$ are the oscillation amplitude with the frequency of $in_0 - 2\omega_T$. See Table 4.2.

Note, for convenience, we redefine $f_{00} = 0$, $a_{11} \equiv a_{22}$, $a_{21} \equiv a_{42}$,$a_{31} \equiv a_{62}$, $e_{11} \equiv e_{22}$, $e_{21} \equiv e_{42}$, $e_{31} \equiv e_{62}$, etc. The relations between the coefficients and the nominal orbit in general form are

$$a_{ij} = a_{ij}(a_0, e_0, C_{20}, C_{22}, \omega_T, \mu), \tag{4.75}$$

$$e_{ij} = e_{ij}(a_0, e_0, C_{20}, C_{22}, \omega_T, \mu), \tag{4.76}$$

$$\phi^a_{ij} = \phi^a_{ij}(\Omega,\omega), \tag{4.77}$$

$$\phi^e_{ij} = \phi^e_{ij}(\Omega,\omega). \tag{4.78}$$

We see ϕ^a_{ij}, ϕ^e_{ij} are only functions of the orientation of the nominal orbit. For Equation 4.23 and 4.34, $\phi^a_{ij} = \phi^e_{ij} = 2\omega$ as we assume $\Omega = 0$, actually they equal $2\Omega + 2\omega$ in the two equations.

For high eccentricity nominal orbits, a_{ij}, e_{ij} are functions of eccentricity. Here we list some of the coefficients taken from Appendix B.1,

$$a_{01} = \frac{C_{20}}{a_0}\Big[-3e_0 - \frac{27}{8}e_0^3 - \frac{261}{64}e_0^5 - \frac{100163}{21504}e_0^7\Big], \tag{4.79}$$

$$a_{02} = \frac{C_{20}}{a_0}\Big[-\frac{9}{2}e_0^2 - \frac{7}{2}e_0^4 - \frac{141}{32}e_0^6\Big], \tag{4.80}$$

$$a_{12} = \frac{C_{22}n_0}{a_0(n_0-2\omega_T)}\Big[-3e_0 - \frac{3}{8}e_0^3 - \frac{5}{64}e_0^5 - \frac{1001}{21504}e_0^7\Big], \tag{4.81}$$

$$a_{22} \equiv a_{11} = \frac{C_{22}n_0}{a_0(n_0-\omega_T)}\Big[6 - 15e_0^2 + \frac{39}{8}e_0^4 - \frac{35}{48}e_0^6\Big], \tag{4.82}$$

$$a_{32} = \frac{C_{22}n_0}{a_0(3n_0-2\omega_T)}\Big[63e_0 - \frac{1107}{8}e_0^3 + \frac{4401}{64}e_0^5 - \frac{15867}{1024}e_0^7\Big], \tag{4.83}$$

$$a_{42} \equiv a_{21} = \frac{C_{22}n_0}{a_0(2n_0-\omega_T)}\Big[102e_0^2 - 230e_0^4 + \frac{601}{4}e_0^6\Big], \tag{4.84}$$

$$e_{01} = \frac{C_{20}}{a_0^2}\Big[-\frac{3}{2} - \frac{3}{16}e_0^2 - \frac{45}{128}e_0^4 - \frac{1781}{6144}e_0^6\Big], \tag{4.85}$$

$$e_{02} = \frac{C_{22}}{a_0^2}\Big[-\frac{9}{4}e_0 + \frac{1}{2}e_0^3 - \frac{29}{64}e_0^5\Big], \tag{4.86}$$

$$e_{12} = \frac{C_{22}n_0}{a_0^2(n_0-2\omega_T)}\Big[\frac{3}{2} - \frac{3}{16}e_0^2 - \frac{43}{128}e_0^4 - \frac{721}{6144}e_0^6\Big], \tag{4.87}$$

$$e_{22} \equiv e_{11} = \frac{C_{22}n_0}{a_0^2(n_0-\omega_T)}\Big[-\frac{3}{2}e_0 + \frac{33}{8}e_0^3 - \frac{63}{32}e_0^5\Big], \tag{4.88}$$

$$e_{32} = \frac{C_{22}n_0}{a_0^2(3n_0-2\omega_T)}\Big[\frac{21}{2} - \frac{705}{16}e_0^2 + \frac{7707}{128}e_0^4 - \frac{61353}{2048}e_0^6\Big], \tag{4.89}$$

$$e_{42} \equiv e_{21} = \frac{C_{22}n_0}{a_0^2(2n_0-\omega_T)}\Big[\frac{51}{2}e_0 - \frac{383}{4}e_0^3 + 127e_0^5\Big]. \tag{4.90}$$

Using the data for asteroid Castalia and assuming $a_0 = 1.53$, we plot these coefficients as a function of eccentricity in Figure 4.8. We see that when eccentricity is small, a_{11} dominates, but when eccentricity is large, a_{21} is dominates. In Figure

4.9 when eccentricity is small e_{01}, e_{32} dominate, but when eccentricity is large e_{21} dominates. Thus, we expect some of the resonance conditions to become modified for high eccentric orbits.

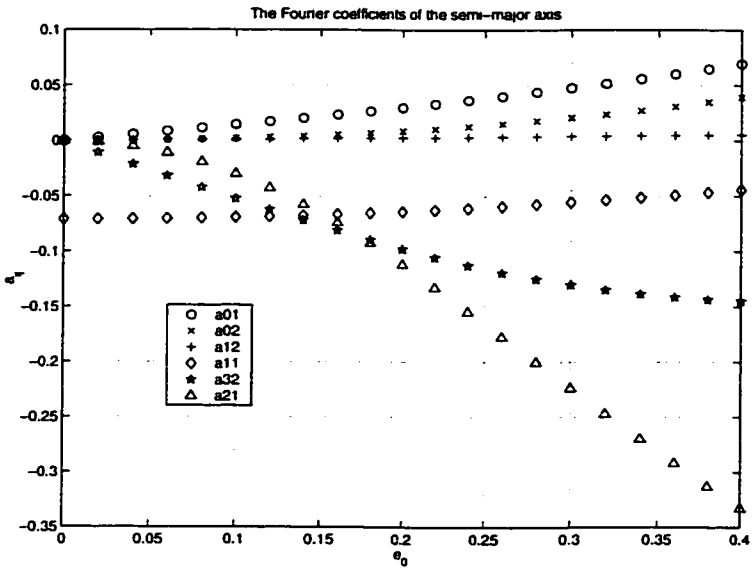

Figure 4.8: Some oscillation coefficients of $a(t)$ for different eccentricities

4.3.2 Size-shape stability

As stated in Chapter II, when the changes of semi-major axis and eccentricity are large enough within one nominal orbit, this orbit can be considered to be size-shape unstable. The averaging analysis for resonant orbits in Section 4.2 show that some near resonant orbits are expected to experience large changes in semi-major axis and eccentricity, giving an analytic explanation for the "jumping" phenomena presented in Figure 2.5.

Let's review that figure again. The critical line was the boundary of stable near circular orbits(semi-major axis constant on average) with a minimum a_0 at a fixed central body rotation rate ω_T. We plot this boundary line in the plane a_0 vs. ω_T computed using numerical integrations. The threshold for a "size-shape unstable"

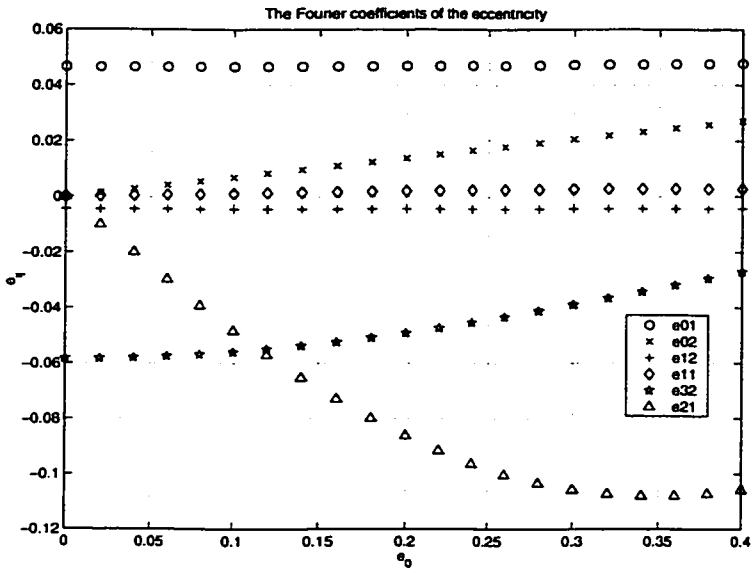

Figure 4.9: Some oscillation coefficients of $e(t)$ for different eccentricities

classification is, if for a long enough time evolution the eccentricity $e(t) < e_{max}$, say $e_{max} = 0.4$, we assume the orbit is size-shape stable. Using this criterion we see that the jumping phenomena only happens at the resonant nominal orbits. We see the large jumps at 1:2 and 3:2 resonant orbits, which is because $\bar{e} \in O(e^0)$.

Also from the Figure 2.5, we see that unstable transition occurs at resonances with such secular effects. For example, $\bar{a}_{ij} \in O(\bar{e}^0)$ or $\bar{e}_{ij} \in O(\bar{e}^0)$ when $i : j$ = 1:2, 2:2, 3:2, and there are big jumps for these resonant points at the critical line (see Figure 2.5). But for near resonant orbits $i : j$=4:2,5:2,6:2, $\bar{a}_{ij} \in O(\bar{e}^k)$ or $\bar{e}_{ij} \in O(\bar{e}^k)$ where $k \geq 2$, we see small jumps in the figure as all the orbits represented in the figure are near circular. And no transitions occur at these resonances without secular effect. For example, at the resonant orbit $i : j$=2:3, there is no jumping in the figure as, $\bar{a}_{ij} = 0$, $\bar{e}_{ij} = 0$.

Therefore, we can predict the onset of "general instability" with this analysis.

4.3.3 Resonance and Chaos

There are many dynamic systems which have similar resonant phenomena. Such resonant orbits often lead to chaotic motion. For a chaotic orbit, if there is a small deviation from a nominal orbit, the subsequent evolution transforms to a completely different orbit after a certain time. There are many kinds of chaotic orbits [33]. "Size-shape unstable" orbits can be considered as a kind of chaotic orbit that results from resonance.

Spin-orbits[8] [5] are normally stable if the planet's rotation and revolution rate are in some resonance; for example, Mercury (in a resonance 3:2) and the Moon (in a resonance 1:1). Another well known problem which is closely related to resonance is the motion of asteroids in the Solar system (See papers[12] [28]). These resonance arise because of the commensurability between the mean motion of the asteroid and the mean motion of Jupiter or other planets.

For our problem, resonance results from the commensurability between the central body's rotation(ω_T) and the mean motion(n_0) of a spacecraft. The resonant orbits are either unstable, or stable, as a predictable function of their resonance. Our approach provides a new attempt to study resonant motions by directly estimating the oscillation frequencies, amplitudes and phase angles of the semi-major axis and eccentricity. An improved understanding of this aspect of our research could help in the understanding of other resonance problems, such as the asteroid motion in the Solar system.

4.4 The Resonant Integral Analyses

The elliptic expansion method presented in this chapter has some applications which predict our numerical results, but it has some limitations also. It only works

well for small-eccentrity, planar orbits. For the analysis of high eccentricity or three dimensional orbits, we introduce a resonant integral analysis defined in [38].

4.4.1 Estimation of the stability index

. In chapter II, we gave some discussion about the size-shape stability for a spacecraft motion in a rotating second degree and order gravity field. One fact states that if the oscillation of semi-major axis $a(t)$ and eccentricity $e(t)$ are small enough the nominal orbit is size-shape stable, i.e, the orbit's $a(t)$ and $e(t)$ are constant on average. The changes in semi-major axis or eccentrity over one nominal orbit provides *a stability index* for the nominal orbit. If this change is too large, the nominal orbit is size-shape unstable. One application of the elliptic expansions in this chapter is to evaluate this stability index. By Equation 4.23 and 4.34, the semi-major axis and eccentrity changes over one nominal orbit are

$$\begin{aligned}
\Delta a(T) &= a(\frac{2\pi}{n_0}) - a(0), \\
&= \frac{C_{22}}{a_0}\Big[\frac{3e_0}{1-\frac{2\omega_T}{n_0}} - \frac{3(2-5e_0^2)}{1-\frac{\omega_T}{n_0}} - \frac{63e_0}{3-\frac{2\omega_T}{n_0}} \\
&\qquad -\frac{102e_0^2}{2-\frac{\omega_T}{n_0}}\Big](1-\cos\frac{4\pi\omega_T}{n_0}), \qquad (4.91) \\
\Delta e(T) &= e(\frac{2\pi}{n_0}) - e(0), \\
&= \frac{C_{22}}{a_0^2}\Big[-\frac{3}{2(1-\frac{2\omega_T}{n_0})} + \frac{3e_0}{2(1-\frac{\omega_T}{n_0})} - \frac{21}{2(3-\frac{2\omega_T}{n_0})} \\
&\qquad -\frac{51e_0}{2(2-\frac{\omega_T}{n_0})}\Big](1-\cos\frac{4\pi\omega_T}{n_0}). \qquad (4.92)
\end{aligned}$$

We see that $\Delta a(T)$ and $\Delta e(T)$ have no relation with C_{20}, which only results in bounded oscillations, and has a close relation with the ratio ω_T/n_0. When $\omega_T >> |n_0|$ (i.e., the central body rotates rapidly) or $\omega_T << |n_0|$ (i.e, the central body rotates slowly), $\Delta a(T)$ and $\Delta e(T)$ are small, which are precisely the averaging conditions assumed in Chapter III, and also the size-shape stability condition in Chapter II. All

theses results are compatible with the analysis in [38]. Actually Equation 4.91 and 4.92 are definite version of the general results of the integral analysis from that the paper, for the case of planar, small-eccentrity orbits. We plot $\Delta a(T)/a_0$, $\Delta e(T)$ by Equation 4.91 and 4.92 as a function of ω_T/n_0 in Figure 4.10. We see that besides the above conclusions, the stability indices, $\Delta a(T)/a_0 = 0$, $\Delta e(T) = 0$ at resonant points. This justifies the existence of resonant periodic orbits.

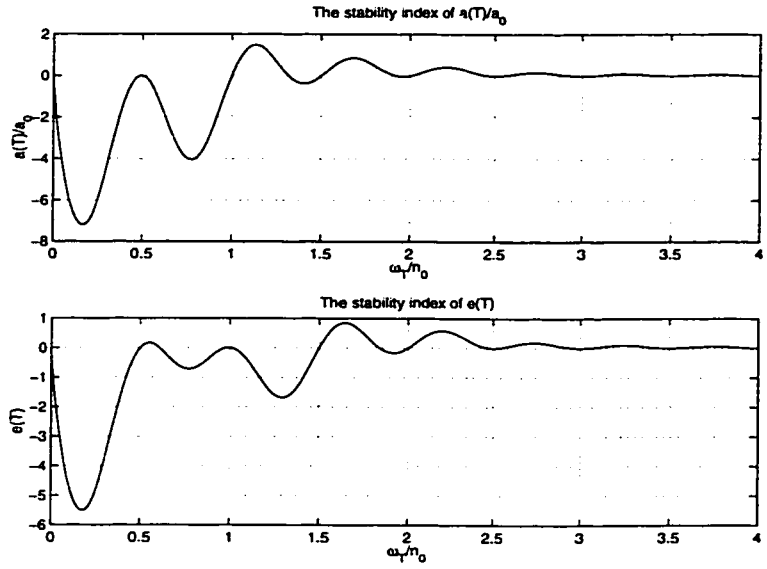

Figure 4.10: The stability index as functions as relative velocity

In the Appendix B.2, we show that the elliptic expansion method in this chapter doesn't work well for three dimensional orbits. If we want to estimate the stability indices for three dimensional orbits, we can use the variation of energy and angular momentum over one nominal orbit, $(\Delta C, \Delta G)$, to estimate our stability indices, $\Delta a(T), \Delta e(T)$. In [38], the changes of the energy $C = -\mu/(2a)$ and angular momentum magnitude $G = \sqrt{\mu a(1-e^2)}$ for a nominal orbit are calculated systematically by introducing "resonant integrals". Their relation to $\Delta a(T)$ and $\Delta e(T)$ in Equation

4.91 and 4.92 are

$$\Delta C = \frac{\mu}{2a_0}\Delta a(T), \tag{4.93}$$

$$\Delta G = \frac{1}{2}\sqrt{\frac{\mu(1-e_0^2)}{a_0}}\Delta a(T) + \sqrt{\frac{\mu a_0}{1-e_0^2}}e_0\Delta e(T). \tag{4.94}$$

We see that $(\Delta C, \Delta G)$ and $(\Delta a(T), \Delta e(T))$ are mutually interchangeable. So for high eccentricity planar nominal orbits or three dimension nominal orbits, we can use $(\Delta C, \Delta G)$, as in [38], to calculate $\Delta a(T), \Delta e(T)$ here.

4.4.2 Expansion in three dimension

For a general three dimensional nominal orbit where $e_0 \neq 0$, $i_0 \neq 0$, we can include inclination and longitude of ascending node in the gravity perturbation expansion. The equations, however, are very long and messy (see Appendix B.2). We see that a_{ij}, e_{ij} have a relation not only with $a_0, e_0, C_{20}, C_{22}, \omega_T, \mu$, but also with the inclination of its nominal orbit i_0. (see Equations 4.75 and 4.76)

Another method to estimate the coefficients a_{ij}, e_{ij} in Equations 4.73 and 4.74 for a 3-D orbit is to use the integrals defined in [38]. The integrals can be modified for a nominal orbit

$$I_m^n(e,q,i,j) = \frac{2f_{ij}}{\pi}\int_0^{\pi/f_{ij}}(1+e_0\cos f_0)^n\cos(mf_0 - 2\omega_T t)\sin(f_{ij}t)\mathrm{d}f, \tag{4.95}$$

where $f_{ij} = in_0 - j\omega_T$. The modification is justified by Fourier expansion:

$$a_{ij} = \frac{2f_{ij}}{\pi}\int_0^{\frac{\pi}{f_{ij}}} a(t)\cos(f_{ij}t)\mathrm{d}f \tag{4.96}$$

For the new integration, not only the integrated functions but also the beginning and ending integration times are also modified. For example, the integration time of the integral $I_m^n(e,q,1,1)$ should be from 0 to t_f , especially when e_0 is small, where

$$t_f = \frac{\pi}{2(\omega_T - n_0)}.$$

CHAPTER V

PERIODIC ORBITS

The study of periodic orbits about an uniformly rotating second degree and order gravity field can help us to understand the nature of orbital dynamics around asteroids in general. Practically, the study gives insight that can be used for planning orbital motion. Stable periodic orbits can be used directly for missions and even unstable periodic orbits, if stabilized, can be used to realize safe close proximity orbital missions. Scheeres in[36],[37],[39] calculated and analyzed some families of periodic orbits for a number of specific asteroids. This chapter studies periodic orbits around asteroids in general by modeling the asteroid perturbation potential with the most significant gravity coefficients, C_{20} and C_{22}. Stability analysis of these orbits is performed using Floquet's theorem.

First, we analyze the four equilibra in the rotating second degree and order gravity field. Two of equilibra are always unstable; the other two can be stable or unstable, depending on the central body rotation rate ω_T, the two gravity coefficients, C_{20} and C_{22}.

Next we compute families of periodic orbits. In our searching procedure, we remove the two unity eigenvalues from the state transition matrix (STM) to find a robust, non-singular linear map to solve for the periodic orbits. The algorithm

converges well, especially for stable periodic orbits. As we give the initial variations a Jacobi constraint, the procedure automatically searches for a periodic orbit at a fixed energy level.

By calculating the STM for the periodic orbit, we find the characteristic multipliers which are the stability indices for the periodic orbit. These are used to test the stability of the periodic orbits.

Then, by using a relatively automatic searching procedure for the periodic orbits, we find five basic families of periodic orbits and discuss their existence and stability at different central body rotation rates. We call these five basic families the near direct, far direct, 1:1 resonant, 1:2 resonant and retrograde periodic orbits. There are also other "special" periodic orbits which lie between these basic periodic orbit families.

Some of the periodic orbits we find here are similar to the periodic orbits of the restricted three body problem, which are comprehensively discussed in [42]. More recently, Hénon in [19] gives a systematic study of a limiting case of restricted three body problem when the main mass ratio approches zero. Fundamentally speaking, our problem is also one of the different limiting cases of the three body problems when the distance between the two main bodies becomes small while the rotation rate remains constant.

5.1 State Transition Matrix

To analyze the stability of equilibra and calculate the state transition matrix, we need to know the second order partial derivatives of the gravity potential. They are computed in the subsequent sections.

5.1.1 Derivatives of gravity potential

The effective potential function in Cartesian coordinates (Equation 2.40) is

$$U_e = \frac{1}{2}\omega_T^2(x^2+y^2) + \frac{\mu}{r} - \frac{\mu C_{20}(x^2+y^2-2z^2)}{2r^5} + \frac{3\mu C_{22}(x^2-y^2)}{r^5}. \tag{5.1}$$

First order partial derivatives of the potential are

$$\begin{aligned} U_x &= \omega_T^2 x - \frac{\mu x}{r^3} - \frac{\mu C_{20} x}{r^5} + \frac{5\mu C_{20} x(x^2+y^2-2z^2)}{2r^7} \\ &\quad + \frac{6\mu C_{22} x}{r^5} - \frac{15\mu C_{22} x(x^2-y^2)}{r^7}, \end{aligned} \tag{5.2}$$

$$\begin{aligned} U_y &= \omega_T^2 y - \frac{\mu y}{r^3} - \frac{\mu C_{20} y}{r^5} + \frac{5\mu C_{20} y(x^2+y^2-2z^2)}{2r^7}, \\ &\quad - \frac{6\mu C_{22} y}{r^5} - \frac{15\mu C_{22} y(x^2-y^2)}{r^7} \end{aligned} \tag{5.3}$$

$$U_z = -\frac{\mu z}{r^3} + \frac{2\mu C_{20} z}{r^5} + \frac{5\mu C_{20} z(x^2+y^2-2z^2)}{2r^7} - \frac{15\mu C_{22} z(x^2-y^2)}{r^7}. \tag{5.4}$$

Second order partial derivatives of the potential are

$$\begin{aligned} U_{xx} &= \omega_T^2 - \frac{\mu}{r^3} + \frac{3\mu x^2}{r^5} \\ &\quad - \frac{\mu C_{20}}{r^5} + \frac{5\mu C_{20}(5x^2+y^2-2z^2)}{2r^7} - \frac{35\mu C_{20} x^2(x^2+y^2-2z^2)}{2r^9} \\ &\quad + \frac{6\mu C_{22}}{r^5} - \frac{15\mu C_{22}(5x^2-y^2)}{r^7} + \frac{105\mu C_{22} x^2(x^2-y^2)}{r^9}, \end{aligned} \tag{5.5}$$

$$\begin{aligned} U_{xy} &= \frac{3\mu xy}{r^5} + \frac{10\mu C_{20} xy}{r^7} - \frac{35\mu C_{20} xy(x^2+y^2-2z^2)}{2r^9} \\ &\quad + \frac{105\mu C_{22} xy(x^2-y^2)}{r^9}, \end{aligned} \tag{5.6}$$

$$\begin{aligned} U_{xz} &= \frac{3\mu xz}{r^5} - \frac{5\mu C_{20} xz}{r^7} - \frac{35\mu C_{20} xz(x^2+y^2-2z^2)}{2r^9} \\ &\quad - \frac{30\mu C_{22} xz}{r^7} + \frac{105\mu C_{22} xz(x^2-y^2)}{r^9}, \end{aligned} \tag{5.7}$$

$$U_{yx} = U_{xy}, \tag{5.8}$$

$$\begin{aligned} U_{yy} &= \omega_T^2 - \frac{\mu}{r^3} + \frac{3\mu y^2}{r^5} \\ &\quad - \frac{\mu C_{20}}{r^5} + \frac{5\mu C_{20}(x^2+5y^2-2z^2)}{2r^7} - \frac{35\mu C_{20} y^2(x^2+y^2-2z^2)}{2r^9} \\ &\quad - \frac{6\mu C_{22}}{r^5} - \frac{15\mu C_{22}(x^2-5y^2)}{r^7} + \frac{105\mu C_{22} y^2(x^2-y^2)}{r^9}, \end{aligned} \tag{5.9}$$

$$
\begin{aligned}
U_{yz} &= \frac{3\mu yz}{r^5} - \frac{5\mu C_{20} yz}{r^7} - \frac{35\mu C_{20} yz(x^2+y^2-2z^2)}{2r^9} \\
&\quad + \frac{30\mu C_{22} yz}{r^7} + \frac{105\mu C_{22} yz(x^2-y^2)}{r^9}, \qquad (5.10)
\end{aligned}
$$

$$
U_{zx} = U_{xz}, \qquad (5.11)
$$

$$
U_{zy} = U_{yz}, \qquad (5.12)
$$

$$
\begin{aligned}
U_{zz} &= -\frac{\mu}{r^3} + \frac{3\mu z^2}{r^5} \\
&\quad + \frac{2\mu C_{20}}{r^5} + \frac{5\mu C_{20}(x^2+y^2-10z^2)}{2r^7} - \frac{35\mu C_{20} z^2(x^2+y^2-2z^2)}{2r^9} \\
&\quad - \frac{15\mu C_{22}(x^2-y^2)}{r^7} + \frac{105\mu C_{22} z^2(x^2-y^2)}{r^9}. \qquad (5.13)
\end{aligned}
$$

5.1.2 Definition of STM

Assume the system

$$
\dot{\mathbf{x}} = \mathbf{f}(\mathbf{x}), \qquad \text{for } \mathbf{x} \in \mathbf{R^n}, \qquad (5.14)
$$

has a periodic orbit Γ of period T. $\Gamma : \mathbf{x} = \gamma(\mathbf{t})$, $0 \leq t \leq T$, $\gamma(t+T) = \gamma(t)$. The linearization of Equation 5.14 about its periodic orbit Γ is

$$
\delta\dot{\mathbf{x}} = A(t)\,\delta\mathbf{x}, \qquad (5.15)
$$

where $A(t) = \partial\mathbf{f}(\gamma(\mathbf{t}))/\partial\mathbf{x}$. The state transition matrix for Equation 5.15 is a non-singular matrix $\Phi(t)$ which satisfies the matrix differential equation

$$
\dot{\Phi} = A(t)\Phi. \qquad (5.16)
$$

For Equation 2.23-2.25, the periodic matrix is

$$A(t) = \begin{bmatrix} 0 & 0 & 0 & 1 & 0 & 0 \\ 0 & 0 & 0 & 0 & 1 & 0 \\ 0 & 0 & 0 & 0 & 0 & 1 \\ U_{xx} & U_{xy} & U_{xz} & 0 & 2\omega_T & 0 \\ U_{yx} & U_{yy} & U_{yz} & -2\omega_T & 0 & 0 \\ U_{zx} & U_{zy} & U_{zz} & 0 & 0 & 0 \end{bmatrix}. \tag{5.17}$$

For planar motion($z = 0$), we see that $U_{xz} = U_{yz} = U_{zx} = U_{zy} = 0$. Thus $A(t)$ can be transformed to the similar matrix

$$A(t) \sim \begin{bmatrix} A_r(t) & 0 & 0 \\ 0 & 0 & 1 \\ 0 & U_{zz} & 0 \end{bmatrix}, \tag{5.18}$$

by linear transformation, where

$$A_r(t) = \begin{bmatrix} 0 & 0 & 1 & 0 \\ 0 & 0 & 0 & 1 \\ U_{xx} & U_{xy} & 0 & 2\omega_T \\ U_{yx} & U_{yy} & -2\omega_T & 0 \end{bmatrix}. \tag{5.19}$$

By choosing $\Phi(0) = I$ and numerically integrating $\dot{\Phi} = A(t)\Phi$, we find the state transition matrix $\Phi(t)$.

5.2 Equilibra

Fundamentally speaking, the equilibra are special kinds of periodic orbits whose period $T = 0$. By analyzing the eigenvalues of A_r at the equilibra, we can also understand the stability and existence of their nearby periodic orbits. Similar to

the results for an ellipsoidal central body as described in [35], it can be shown that the equilibra that lie on the x-axis always have an unstable saddle manifold and a center manifold. The equilibra that lie on the y-axis are stable when the central body rotates slowly; in such case, there are two center manifolds. These equilibra become unstable when the central body rotates fast enough; in such case, there are one stable spiral manifold and one unstable spiral manifold.

5.2.1 Equilibrium conditions

A synchronous orbit in inertial space corresponds to an equilibrium in the body-fixed frame. Such orbits exist if the condition $U_x = U_y = U_z = 0$ are satisfied. From Equation 5.4 we see that $z = 0$ always satisfies $U_z = 0$. From Equations 5.2-5.3, we can see that there are two kinds of equilibria: those that lie on the x-axis($y = 0$), and those that lie on the y-axis($x = 0$). See Figure 5.1

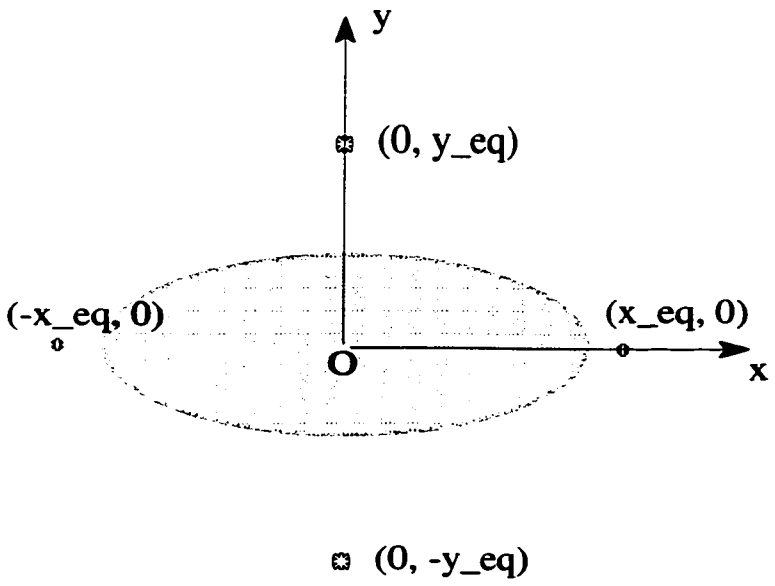

Figure 5.1: The four equilibra in the rotating body-fixed coordinate

At an equilibrium $(x_{eq}, 0, 0)$ the condition is

$$|x_{eq}|^5 - \frac{\mu}{\omega_T^2}(x_{eq}^2 - \frac{3}{2}C_{20} + 9C_{22}) = 0, \tag{5.20}$$

and the corresponding partial derivatives of the gravity potential on the x-axis are

$$U_{xx} = \omega_T^2 + \frac{2\mu}{|x|^3}(1 - \frac{3}{x^2}(C_{20} - 6C_{22})), \tag{5.21}$$

$$U_{yy} = \omega_T^2 - \frac{\mu}{|x|^3}(1 - \frac{3}{x^2}(\frac{1}{2}C_{20} - 7C_{22})), \tag{5.22}$$

$$U_{xy} = U_{yx} = 0. \tag{5.23}$$

At an equilibrium $(0, y_{eq}, 0)$ the condition is

$$|y_{eq}|^5 - \frac{\mu}{\omega_T^2}(y_{eq}^2 - \frac{3}{2}C_{20} - 9C_{22}) = 0, \tag{5.24}$$

and the corresponding partial derivatives of the gravity potential on the y-axis are

$$U_{xx} = \omega_T^2 - \frac{\mu}{|y|^3}(1 - \frac{3}{y^2}(\frac{1}{2}C_{20} + 7C_{22})), \tag{5.25}$$

$$U_{yy} = \omega_T^2 + \frac{2\mu}{|y|^3}(1 - \frac{3}{y^2}(C_{20} + 6C_{22})), \tag{5.26}$$

$$U_{xy} = U_{yx} = 0. \tag{5.27}$$

The radius of a synchronous orbit when $C_{20} = C_{22} = 0$ is

$$r_s = (\frac{\mu}{\omega_T^2})^{\frac{1}{3}}. \tag{5.28}$$

Generally, the central body's main attraction force is much larger than its irregular shape perturbation force, meaning that

$$\frac{|C_{20}|}{r_s^2} \ll 1, \quad \frac{|C_{22}|}{r_s^2} \ll 1. \tag{5.29}$$

By solving the implicit Equations 5.20 and 5.24 using analytic continuation starting from $x_{eq} = r_s + \epsilon_x, y_{eq} = r_s + \epsilon_y$, we have

$$|x_{eq}| \simeq r_s + (-\frac{1}{2}C_{20} + 3C_{22})/r_s, \tag{5.30}$$

$$|y_{eq}| \simeq r_s + (-\frac{1}{2}C_{20} - 3C_{22})/r_s. \tag{5.31}$$

5.2.2 Stability analysis

The eigenvalues of the system are computed from the linearized Equations 2.23-2.24 at the equilibria. The characteristic polynominal is

$$\begin{vmatrix} \lambda & 0 & -1 & 0 \\ 0 & \lambda & 0 & -1 \\ -U_{xx} & -U_{xy} & \lambda & -2\omega_T \\ -U_{yx} & -U_{yy} & 2\omega_T & \lambda \end{vmatrix} = \lambda^4 + b\lambda^2 + c, \tag{5.32}$$

where

$$b = 4\omega_T^2 - U_{xx} - U_{yy}, \quad c = U_{xx}U_{yy} - U_{xy}^2$$

. The stability condition for Equation 5.32 is $\lambda^2 < 0$, i.e., $b > 0, c > 0, b^2 - 4c > 0$.

For an equilibrium $(x_{eq}, 0, 0)$, using Equation 5.20 it is easy to show that

$$c = \frac{-90\omega_T^4 C_{22}(x_{eq}^2 - \frac{5}{2}C_{20} + 15C_{22})}{(x_{eq}^2 - \frac{3}{2}C_{20} + 9C_{22})^2}. \tag{5.33}$$

Since $C_{20} < 0, C_{22} > 0$, it can be seen that $c < 0$, so this equilibrium is always unstable.

For an equilibrium $(0, y_{eq}, 0)$

$$b = \frac{\omega_T^2(y_{eq}^2 + \frac{3}{2}C_{20} - 3C_{22})}{y_{eq}^2 - \frac{3}{2}C_{20} - 9C_{22}}, \tag{5.34}$$

$$c = \frac{36\omega_T^4 C_{22}(y_{eq}^2 - \frac{5}{2}C_{20} - 15C_{22})}{(y_{eq}^2 - \frac{3}{2}C_{20} - 9C_{22})^2}. \tag{5.35}$$

The condition for $\Delta = b^2 - 4c > 0$ is equivalent to

$$r_s^2 + C_{20} - 162C_{22} > 0. \tag{5.36}$$

Using Equation 5.34, 5.35, 5.31, it is easy to show that Condition 5.36 inplies that $b > 0, c > 0$. So Equation 5.36 can be used as a criterion to determine the stability

variable	unit	Earth	4769 Castalia
M	kg	5.9737×10^{24}	1.4091×10^{12}
μ	km^3/sec	3.98601×10^5	9.40×10^{-8}
C_{20}	km^2	-4.4040×10^4	-7.275×10^{-2}
C_{22}	km^2	7.38297×10^1	2.984×10^{-2}
ω_T	1/sec	7.2722×10^{-5}	4.2883×10^{-4}
$r_s = (\frac{\mu}{\omega_T^2})^{\frac{1}{3}}$	km	4.2241×10^4	7.996×10^{-1}
$\Delta = b^2 - 4c$	$1/sec^4$	$2.7964 \times 10^{-17} > 0$	$-2.7063 \times 10^{-13} < 0$
$r_s^2 + C_{20} - 162C_{22}$	km^2	$1.7843 \times 10^9 > 0$	$-4.2674 < 0$

Table 5.1: The equilibra of Earth and asteroid Castalia

of the synchronous orbit. We see that when the central body rotates fast enough, or C_{22} is large enough, the above equation in not satisfied. For the Earth, with C_{22} small and r_s large, the equilibrium $(0, y_{eq}, 0)$ is stable, as is well known [23].

5.2.3 Examples

For the Earth, with C_{22} small and r_s large, perturbed variations from an equilibrium $(0, y_{eq}, 0)$ are the superposition of two stable harmonic oscillations. This same conclusion can be found in [26]. For the asteroid 4769 Castalia, with C_{22} large and r_s small, variations near an equilibrium $(0, y_{eq}, 0)$ are the superposition of two hyperbolic spirals, one stable and one unstable. This conclusion appears in [36].

Data for the Earth and asteroid 4769 Castalia are shown in Table 5.1 .

5.3 Searching for Periodic Orbits

Scheeres in [39] gives a general procedure to find periodic orbits nearby a given periodic orbit with a slightly different energy. Here we follow the same idea. We reduce the state transition matrix (STM) from a 6×6 to a 4×4 matrix by removing the two unity eigenvalue associated with a periodic orbit in a time invariant system. For our system we can reduce our 4×4 STM $\Phi(T)$ into a 2×2 matrix $\Phi_{rr}(T)$. By giving a constraint on the initial value variation which keeps the Jacobi integral constant, we find an automatic approach to compute periodic orbits.

The approach to calculate periodic orbits is an application of the Poincaré map. The Poincaré surface we use here is $y_0 = 0$, $\dot{y}_0 \neq 0$, $y(T) = 0$ i.e., initial point is $(x_0, 0)$, first return is $(x_1, 0)$. See Figure 5.2. The computation of these orbits requires a precision integration routine and a set of programs which allow one to force the end-points of an orbit to coincide.

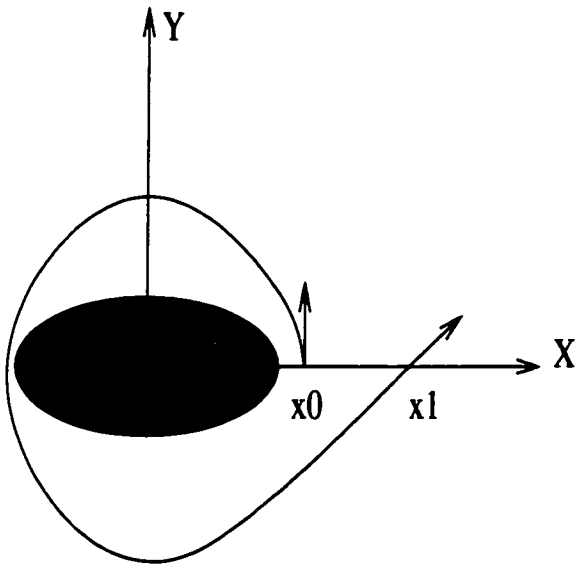

Figure 5.2: The Poincaré surface and the first return.

5.3.1 STM dimension reduction

At the initial condition $y_0 = 0$, $\delta y_0 = 0$, and at the first return to the Poincaré surface $y(T) = 0$, $\delta y(T + \delta T) = 0$. The system is expressed as

$$\begin{bmatrix} \delta x(T+\delta T) \\ \delta y(T+\delta T) \\ \delta \dot{x}(T+\delta T) \\ \delta \dot{y}(T+\delta T) \end{bmatrix} = \Phi(T) \begin{bmatrix} \delta x_0 \\ \delta y_0 \\ \delta \dot{x}_0 \\ \delta \dot{y}_0 \end{bmatrix} + \begin{bmatrix} \dot{x}(T) \\ \dot{y}(T) \\ \ddot{x}(T) \\ \ddot{y}(T) \end{bmatrix} \delta T. \tag{5.37}$$

The condition $\delta y(T + \delta T) = 0$ allows us to solve for δT necessary to stay on the Poincaré surface ($y = 0$). This result is

$$\delta T = -\frac{1}{\dot{y}(T)} \left[\phi_{21}(T)\delta x_0 + \phi_{23}(T)\delta \dot{x}_0 + \phi_{24}(T)\delta \dot{y}_0 \right]. \tag{5.38}$$

Introducing this variation allows us to obtain the reduced equation

$$\begin{bmatrix} \delta x(T+\delta T) \\ \delta \dot{x}(T+\delta T) \\ \delta \dot{y}(T+\delta T) \end{bmatrix} = \begin{bmatrix} \phi_{r11}(T) & \phi_{r12}(T) & \phi_{r13}(T) \\ \phi_{r21}(T) & \phi_{r22}(T) & \phi_{r23}(T) \\ \phi_{r31}(T) & \phi_{r32}(T) & \phi_{r33}(T) \end{bmatrix} \begin{bmatrix} \delta x_0 \\ \delta \dot{x}_0 \\ \delta \dot{y}_0 \end{bmatrix}, \tag{5.39}$$

where

$$\phi_{r11}(T) = \phi_{11}(T) - \frac{\dot{x}(T)}{\dot{y}(T)}\phi_{21}(T), \tag{5.40}$$

$$\phi_{r12}(T) = \phi_{13}(T) - \frac{\dot{x}(T)}{\dot{y}(T)}\phi_{23}(T), \tag{5.41}$$

$$\phi_{r13}(T) = \phi_{14}(T) - \frac{\dot{x}(T)}{\dot{y}(T)}\phi_{24}(T), \tag{5.42}$$

$$\phi_{r21}(T) = \phi_{31}(T) - \frac{\ddot{x}(T)}{\dot{y}(T)}\phi_{21}(T), \tag{5.43}$$

$$\phi_{r22}(T) = \phi_{33}(T) - \frac{\ddot{x}(T)}{\dot{y}(T)}\phi_{23}(T), \tag{5.44}$$

$$\phi_{r23}(T) = \phi_{34}(T) - \frac{\ddot{x}(T)}{\dot{y}(T)}\phi_{24}(T), \tag{5.45}$$

$$\phi_{r31}(T) = \phi_{41}(T) - \frac{\ddot{y}(T)}{\dot{y}(T)}\phi_{21}(T), \tag{5.46}$$

$$\phi_{r32}(T) = \phi_{43}(T) - \frac{\ddot{y}(T)}{\dot{y}(T)}\phi_{23}(T), \tag{5.47}$$

$$\phi_{r33}(T) = \phi_{44}(T) - \frac{\ddot{y}(T)}{\dot{y}(T)}\phi_{24}(T). \tag{5.48}$$

The Jacobi integral is restated as

$$J = \frac{1}{2}(\dot{x}^2 + \dot{y}^2 + \dot{z}^2) - \frac{1}{2}\omega_T^2(x^2 + y^2) - \frac{\mu}{r} - U_2 \tag{5.49}$$

For a fixed value of J, $\delta J = 0$, or

$$\frac{\partial J}{\partial x}\delta x + \frac{\partial J}{\partial y}\delta y + \frac{\partial J}{\partial \dot{x}}\delta \dot{x} + \frac{\partial J}{\partial \dot{y}}\delta \dot{y} = 0. \tag{5.50}$$

On the Poincaré surface $\delta y = 0$, $\frac{\partial J}{\partial \dot{y}} = \dot{y} \neq 0$, allowing us to solve for $\delta \dot{y}$ as

$$\delta \dot{y} = -\frac{1}{\frac{\partial J}{\partial \dot{y}}}\left(\frac{\partial J}{\partial x}\delta x + \frac{\partial J}{\partial \dot{x}}\delta \dot{x}\right). \tag{5.51}$$

Evaluated at the initial conditions we find

$$\frac{\partial J}{\partial x_0} = -\omega_T^2 x_0 + \frac{\mu}{x_0^2} - \frac{3\mu C_{20}}{2x_0^4} + \frac{9\mu C_{22}}{x_0^4}, \tag{5.52}$$

$$\frac{\partial J}{\partial \dot{x}_0} = \dot{x}_0, \tag{5.53}$$

$$\frac{\partial J}{\partial \dot{y}_0} = \dot{y}_0. \tag{5.54}$$

We find the necessary variation in $\dot{y}_0$ that keeps J constant

$$\delta \dot{y}_0 = -\frac{1}{\dot{y}_0}\left(\frac{\partial J}{\partial x_0}\delta x_0 + \dot{x}_0 \delta \dot{x}_0\right). \tag{5.55}$$

This allows a final reduction, equivalent to removing the two unity eigenvalues from the original 4×4 STM,

$$\begin{bmatrix} \delta x(T+\delta T) \\ \delta \dot{x}(T+\delta T) \end{bmatrix} = \begin{bmatrix} \phi_{rr11}(T) & \phi_{rr12}(T) \\ \phi_{rr21}(T) & \phi_{rr22}(T) \end{bmatrix} \begin{bmatrix} \delta x_0 \\ \delta \dot{x}_0 \end{bmatrix} \tag{5.56}$$

$$\equiv \Phi_{rr}(T) \begin{bmatrix} \delta x_0 \\ \delta \dot{x}_0 \end{bmatrix}, \tag{5.57}$$

where

$$\phi_{rr11}(T) = \phi_{r11}(T) - \frac{\frac{\partial J}{\partial x_0}}{\dot{y}_0}\phi_{r13}(T), \tag{5.58}$$

$$\phi_{rr12}(T) = \phi_{r12}(T) - \frac{\dot{x}_0}{\dot{y}_0}\phi_{r13}(T), \tag{5.59}$$

$$\phi_{rr21}(T) = \phi_{r21}(T) - \frac{\frac{\partial J}{\partial x_0}}{\dot{y}_0}\phi_{r23}(T), \tag{5.60}$$

$$\phi_{rr22}(T) = \phi_{r22}(T) - \frac{\dot{x}_0}{\dot{y}_0}\phi_{r23}(T). \tag{5.61}$$

For periodic orbits, there are some special properties of the reduced order map $\Phi_{rr}(T)$. First, $\phi_{r11}\phi_{r22} - \phi_{r12}\phi_{r21} = 1$ due to volume conservation property in phase space. Second, if a periodic orbit has $\dot{x}_0 = 0$, then $\phi_{r11} = \phi_{r22}$ due to symmetry of the orbit about the x-axis. Similar discussion can be found in [18] for the three body problem.

5.3.2 Search procedure

If the initial condition is $(x_0, \dot{x}_0)$, and its first return is $(x_1, \dot{x}_1)$ (see Figure 5.2), we wish to choose the correction $\delta x_0, \delta \dot{x}_0$ to drive

$$\begin{bmatrix} x_1 + \delta x_1 \\ \dot{x}_1 + \delta \dot{x}_1 \end{bmatrix} \rightarrow \begin{bmatrix} x_0 + \delta x_0 \\ \dot{x}_0 + \delta \dot{x}_0 \end{bmatrix}. \tag{5.62}$$

To do this we solve for the correction that makes this occur for our linear system

$$\begin{bmatrix} x_1 - x_0 \\ \dot{x}_1 - \dot{x}_0 \end{bmatrix} = \begin{bmatrix} \delta x_0 \\ \delta \dot{x}_0 \end{bmatrix} - \begin{bmatrix} \delta x_1 \\ \delta \dot{x}_1 \end{bmatrix} \tag{5.63}$$

$$= \begin{bmatrix} \delta x_0 \\ \delta \dot{x}_0 \end{bmatrix} - \Phi_{rr}(T) \begin{bmatrix} \delta x_0 \\ \delta \dot{x}_0 \end{bmatrix} \tag{5.64}$$

$$= [I - \Phi_{rr}(T)] \begin{bmatrix} \delta x_0 \\ \delta \dot{x}_0 \end{bmatrix}. \tag{5.65}$$

Then the new initial condition can be

$$\begin{bmatrix} x_{0n} \\ \dot{x}_{0n} \end{bmatrix} = \begin{bmatrix} x_0 \\ \dot{x}_0 \end{bmatrix} + [I - \Phi_{rr}(T)]^{-1} \begin{bmatrix} x_1 - x_0 \\ \dot{x}_1 - \dot{x}_0 \end{bmatrix}. \tag{5.66}$$

Since the unity eigenvalues have been removed, $I - \Phi_{rr}$ is invertible in general. By imposing Jacobi integral invariant with the initial condition variation, using Equation 5.49, we have $\dot{y}_{0n}$ by the following relationship when $x_0 > 0$

$$\dot{y}_{0n} = \pm\sqrt{2\left(J - \frac{1}{2}\dot{x}_{0n}^2 + \frac{1}{2}\omega_T^2 x_{0n}^2 + \frac{\mu}{x_{0n}} - \frac{\mu}{2x_{0n}^3}C_{20} + \frac{3\mu}{x_{0n}^3}C_{22}\right)}. \tag{5.67}$$

Thus, Equation 5.50 holds, which means that

$$J(x_{0n}, y_{0n} = 0, \dot{x}_{0n}, \dot{y}_{0n}) \;\; = \;\; J(x_0, y_0 = 0, \dot{x}_0, \dot{y}_0). \tag{5.68}$$

There exist some relations between the properties of the periodic orbit and the algorithm. If in the first return $(x_1, \dot{x}_1)$ is too far from $(x_0, \dot{x}_0)$, the searching program diverges, and a periodic orbit does not exist near $(x_0, \dot{x}_0)$ for the given Jacobi integral. If $\det|I - \Phi_{rr}(T)| \approx 0$, the periodic orbit is at a critical point and may be transitioning from a stable to an unstable orbit, and at this point the searching program usually fails. We use these properties to modify our searching program by adding some limitations on the searching step size and recursive counting number, which makes our program more "automatic".

5.4 Stability Analysis

Figure 5.3 shows two examples of periodic orbits, one is stable, the other is unstable. Given a periodic orbit, we can use the Floquet's Theorem to determine its stability by calculating its state transition matrix $\Phi(t)$ and its characteristic multipliers. If all its characteristic multipliers $|e^{\lambda_j T}| \leq 1$, the periodic orbit is stable.

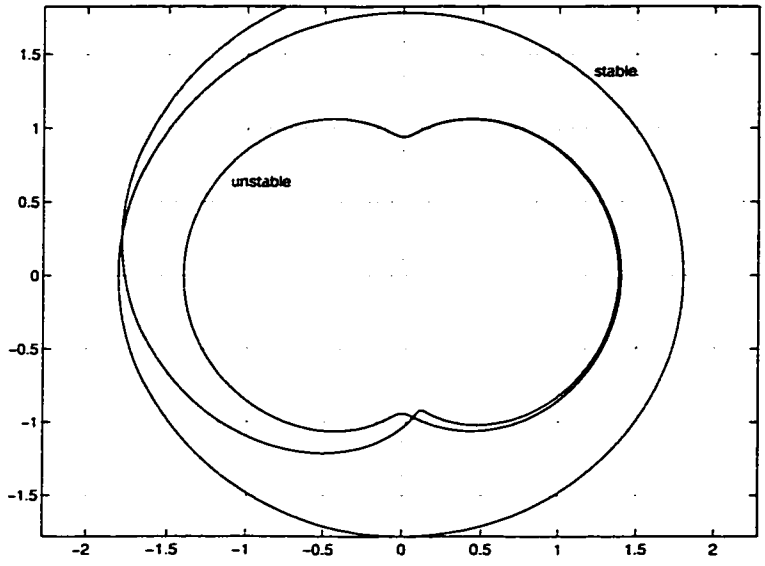

Figure 5.3: A stable and an unstable periodic orbits

5.4.1 Characteristic Multipliers

For a periodic matrix $A(t)$, we have the following result known as *Floquet's Theorem* (see [29]). If $A(t)$ is a continuous, T-periodic matrix, then for all $t \in \mathbf{R}$ any state transition matrix solution for Equation 5.15 can be written in the form

$$\Phi(t) = Q(t)e^{Bt}, \tag{5.69}$$

where $Q(t)$ is a nonsingular, differentiable, T-periodic matrix and B is a constant matrix. Furthermore, if $\Phi(0) = I$, then $Q(0) = I$. The eigenvalues of e^{BT} are given by $e^{\lambda_j T}$ where $\lambda_j, j = 1, ..., n$, are eigenvalues of the matrix B.

The eigenvalues of B, λ_j, are called *characteristic exponents* of the periodic orbit $\gamma(t)$ and the eigenvalues of e^{BT}, $e^{\lambda_j T}$, are called *characteristic multipliers* of $\gamma(t)$.

It can be shown that one of the characteristic exponents of the periodic orbit $\gamma(t)$ is always zero, i.e. one of the characteristic multipliers is always 1. But for Hamiltonian systems there exist two unity multipliers since if η is an eigenvalue of $\Phi(t)$ for a Hamiltonian system, its inverse η^{-1}, its complex conjugate $\bar{\eta}$, and its

inverse complex conjugate $\bar{\eta}^{-1}$ are also its eigenvalues. See the root locus of $\Phi(t)$ in Figure 5.4 for a stable periodic orbit ($x_0 = 1.6$).

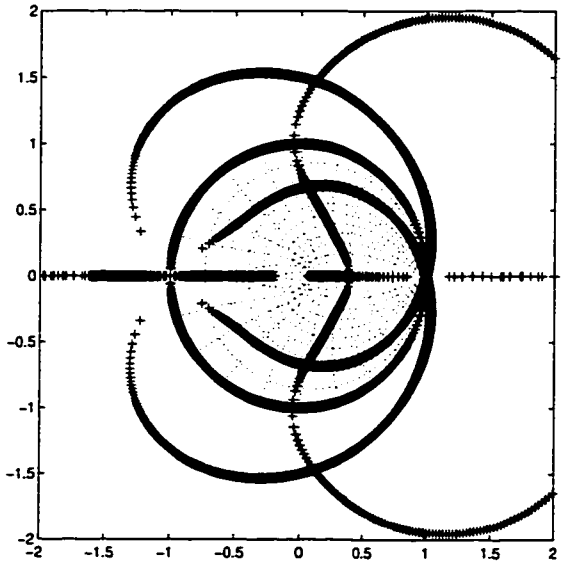

Figure 5.4: Root locus of $\Phi(t)$ for a stable periodic orbit

The product of all the characteristic multipliers are

$$\prod_{i=1}^{6} e^{\lambda_i T} = e^{(\sum_{i=1}^{6} \lambda_i)T} = |\Phi(T)| = e^{\int_0^T tr(A(q))dq} = e^0 = 1. \tag{5.70}$$

Thus, two characteristic multipliers of the periodic orbit are one, since the dynamics of our problem is Hamiltonian.

At the orbit period T, $Q(T) = I$, $e^{BT} = \Phi(T)$ whose eigenvalues are the characteristic multiplies of the periodic orbits according to the Floquet's theorem. The calculated characteristic multipliers $e^{\lambda_i T}$ of the periodic orbits in Figure 5.5 are shown in Table 5.2.

The two unity eigenvalues of the STM indicate the periodicity of the orbit, while the other two are just the index of the stability of the periodic orbit. In the example given in Figure 5.5 see that only the near circular periodic orbits are stable, and all the other periodic orbits are unstable.

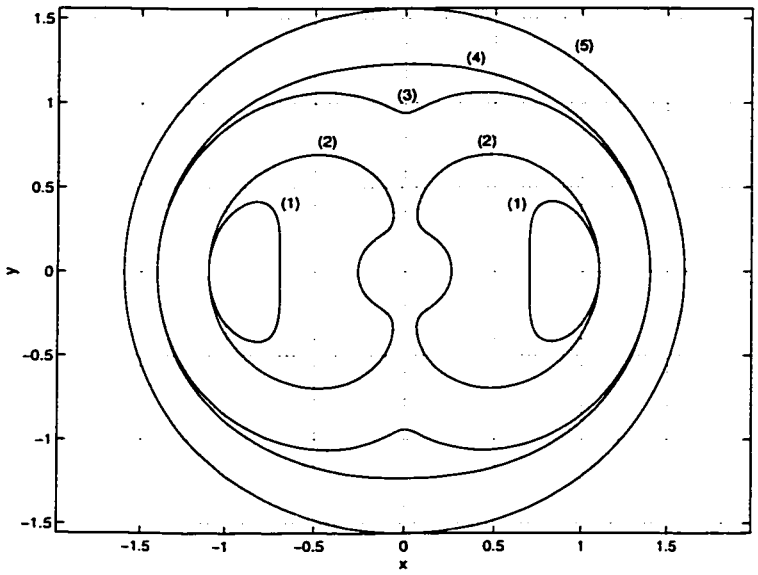

Figure 5.5: Some examples of periodic orbits when the initial value of x_0 ranging from 1.1 to 1.6, y_0=0, and $\dot{x}_0$=0 for asteroid 4769 Castalia.

orbit description	x_0	λ_1	λ_2	λ_3	λ_4
(1) small lobe	1.1	90.50	0.0110	1.0	1.0
(2) large lobe	1.1	126.6	0.0079	1.0	1.0
(3) double lobes	1.4	1275	0.00078	1.0	1.0
(4) near ellipse	1.4	42.46	0.0236	1.0	1.0
(5) near circle	1.6	-0.846-0.533i	-0.846+0.533i	1.0	1.0

Table 5.2: Some typical perioidic orbits

5.4.2 Characteristic equation

Since the system is Hamiltonian, the characteristic multipliers have a specific structure. The characteristic equation of the state transition matrix $\Phi(T)$ for planar orbits follows the structure

$$(\eta^2 - (k_a + 1/k_a)\eta + 1)(\eta^2 - 2k_b\eta + 1) = 0, \tag{5.71}$$

where $e^{\lambda_i T} = \eta_i$, and k_a and k_b are two real numbers. We see Equation 5.71 defines the structure of the characteristic multiplies for our system. If $e^{\lambda_1 T} = k_a$, $e^{-\lambda_1 T} = 1/k_a$, $e^{\lambda_2 T} = k_b + i\sqrt{1 - k_b^2}$, $e^{\bar{\lambda}_2 T} = k_b - i\sqrt{1 - k_b^2}$, for $-1 \leq k_a \leq 1$, $-1 \leq k_b \leq 1$. For example, a stable near circular orbit will have, $k_a = 1$, $|k_b| < 1$, and an unstable orbit may have $|k_a| < 1$, $k_b = 1$. We note that the complex conjugate of a real number is itself; and the inverse of a complex number on unit-circle is its complex conjugate.

Another way to analyze the stability of a periodic orbit is to calculate the coefficients of the characteristic equation without solving for the multipliers, and define a "stability index" which is similar to the variable $-(k_a + 1/k_a)$ or $-2k_b$ in equation 5.71. This method is discussed in [42], where it is used for the restricted three body problem with two equal mass primaries. Using this criterion, when $(k_a + 1/k_a) > 2$, $k_b = 1$ the periodic orbit is unstable, when $k_a + 1/k_a = 2$, $|k_b| < 1$, the periodic orbit is stable.

When considering the out of plane stability in planar motion, we can use Equation 5.18 to decouple the full 6 by 6 STM into a 4×4 in-plane STM Φ and a 2×2 out-of-plane STM Φ_z. If we assume

$$\Phi_z(0) = \begin{bmatrix} 1 & 0 \\ 0 & 1 \end{bmatrix}, \tag{5.72}$$

and numerically integrate

$$\dot{\Phi}_z(t) = \begin{bmatrix} 0 & 1 \\ U_{zz} & 0 \end{bmatrix} \Phi_z(t), \tag{5.73}$$

we have $\Phi_z(T)$ and its characteristic equation for a periodic orbit.

$$\eta_z^2 - 2k_c\eta_z + 1 = 0. \tag{5.74}$$

Normally, $-1 < k_c < 1$, which means that the periodic orbit is stable in the out-of-plane direction. But some retrograde periodic orbits, when their radii are close to the central body, are in-plane stable but out-of-plane unstable. This result is compatible with the secular motion analysis for a slowly rotating central body, See Equation 3.94. The variable k_c in Equation 5.74 corresponds to the "vertical stability index" in [18], where he gives a discussion of the out-of-plane stability of periodic orbits in the restricted three body problem. See Figure 5.6 for an in-plane stable and out-of-plane unstable periodic orbit for a slowly rotating asteroid.

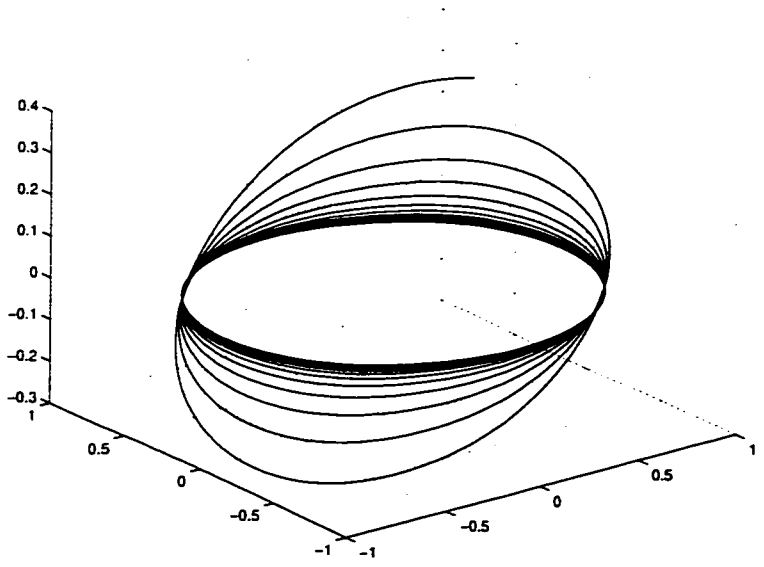

Figure 5.6: An orbit with in-plane stability and out-of-plane instability.

5.5 Families of Periodic Orbits

Figure 5.5 shows some periodic orbits, which are all direct orbits in inertial space, for asteroid 4769 Castalia. The four equilibria are located at $(\pm 0.9070, 0)$ and $(0, \pm 0.7019)$(see Section 5.2.1). We note that the minimum radius of the lobe orbits are less than the dimension of the asteroid, and are shown for theoretical interest only. For retrograde orbits there always exists stable, near-circular periodic orbits, but for direct orbits the case is different. For example in our particular case, when $x_0 = 1.3$ and $x_0 = 1.4$ it is impossible to find near circular direct periodic orbits. This corresponds to the resonant region from 1:1 to 2:1 in Figure 2.5. When the orbit radius is large enough, say $x_0 \geq 1.6$, the direct near-circular periodic orbits exist as a continuously family along the x-axis. Additionally, at some radii, for example as $x_0 = 1.1$ and $x_0 = 1.4$, by changing the energy level, we can find more than one periodic orbit. Figure 5.7 shows some examples of periodic orbits when the central body rotates slowly. When the central body rotates fast, some of these periodic orbit will disappear or change their stability.

5.5.1 Classification

The family of direct, equatorial, near circular, body-fixed periodic orbits have two branches, one near the asteroid (the small circle in Figure 5.7), the other far from the asteroid (the big circle in Figure 5.7). The near branch, where $n \gg \omega_T$, disappears when the central body rotates rapidly. The far branch, where $n \ll \omega_T$, always exists, and when the central body rotates rapidly the far branch approaches the central body. The direct periodic orbits of both the near and far branch are usually stable if they exist.

Between these two branches of direct periodic orbits are the 1:1 and 1:2 resonant

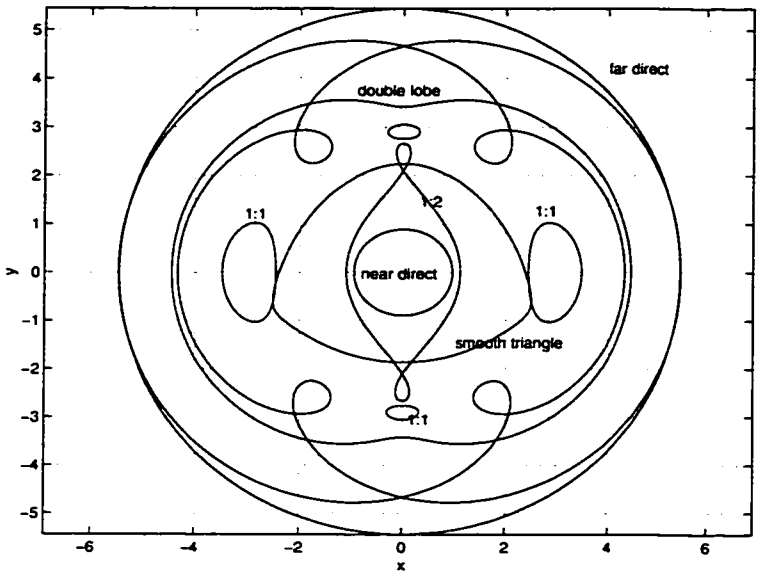

Figure 5.7: Some examples of periodic orbits when the central body rotates slowly, at 1/7th of the rotation rate of asteroid Castalia.

periodic orbits. The 1:1 resonant orbits, whose mean motion rate $n = \omega_T$ (See Figure 5.7), also have two branches. Their existence and stability have a close relationship with the equilibrium point analysis discussed in Section 5.2.1. The four equilibra here are $(\pm 2.9673, 0)$ and $(0, \pm 2.9076)$.

One branch of the 1:1 resonant periodic orbit is around the equilibra along the short equatorial axis(y-axis), which exists and is stable when

$$\omega_T \quad < \quad \frac{\mu^{1/2}}{(-C_{20} + 162C_{22})^{3/4}}. \tag{5.75}$$

(See Equation 5.36). The equilibrium at the y-axis has two center manifolds, so nearby periodic orbits exist and are stable. When the central body rotates faster, this equilibrium has one stable and one unstable spiral manifold, and thus no periodic orbits exist near this equilibrium in that case.

The other branch of the 1:1 periodic orbits is around the equilibrium along the long equatorial axis(x-axis), which always exists but is unstable. See Figure 5.5 for

the fast rotation case. Since the equilibra along the x-axis have a center and a saddle manifold, periodic orbits exist nearby the equilibrium but are always unstable.

For the Earth, C_{22} and ω_T are very small and the 1:1 resonant orbits can be either small or large, and their stability can be different upon their size. For example, in the family of 1:1 periodic orbits near the equilibrium $(x_{eq}, 0)$, the smaller ones are unstable, the larger ones which can even include three equilibra $(x_{eq},0)$,$(0,\pm y_{eq})$ are stable [26].

The near branch of the direct periodic orbits meet the 1:2 resonant periodic orbit family and disappear as its radius increases. The 1:2 resonant orbit, whose mean motion $n = 2\omega_T$, exists and is stable when the central body rotates slowly. The shape of the 1:2 resonant orbits can be seen in Figure 5.7, and will change for different Jacobi integral values. More discussions are given in Section 5.5.3. The 1:2 resonant orbits also exist along the y-axis. In Figure 5.7 we just show a 1:2 resonant orbit along the x-axis.

The retrograde, near circular periodic orbit is also in the equatorial plane but travels in the opposite sense of the asteroid rotation. Generally speaking, such retrograde orbits are stable and exist at almost all radii.

Between the above basic families of periodic orbit, there exist some special periodic orbits. For example, at the boundary between the 1:1 resonant and far direct periodic orbit there is a family of double lobe periodic orbits (See Figure 5.5 and Figure 5.7). Their stability also changes from stable to unstable as ω_T increases.

One special periodic orbit is seen in the middle of Figure 5.7 between the 1:1 and 1:2 resonant orbits, a smooth-triangle-like periodic orbit which is not symmetric about the x-axis. As the initial condition guess we used to search for it is perpendicular to the x-axis, this serves as an example how well our searching procedure

works.

5.5.2 Distribution

Figure 5.8 shows the families of the periodic orbits for the asteroid Castalia. The upper-left branch is the near-direct periodic orbit. Below and intersected with it are the 1:2 resonant orbits. The upper-right branch is the far-direct periodic orbit. The bottom line are the retrograde periodic orbits. In the middle are the 1:1 resonant, double lobe, smooth-triangle-like periodic orbits, etc. As the central body rotates faster, the entire picture will translate to the left and the left part of the picture will disappear.

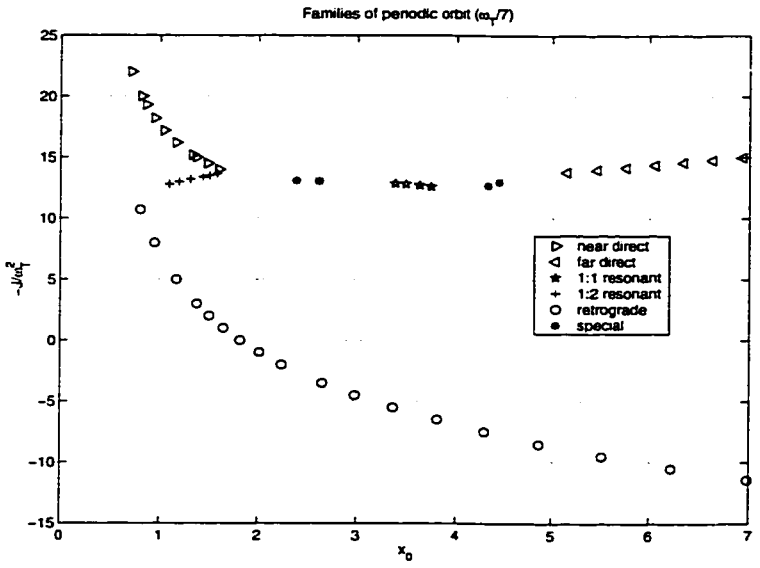

Figure 5.8: Families of periodic orbit in the slowly rotating case corresponding to Figure 5.7

Figure 5.9 is another example of periodic orbits in a slowly rotating case. We see that the direct, 1:1 and 1:2 resonant periodic orbits also exist, but the critical boundary periodic orbits are different.

Figure 2.5 shows a critical line between stable and unstable near circular quasi-

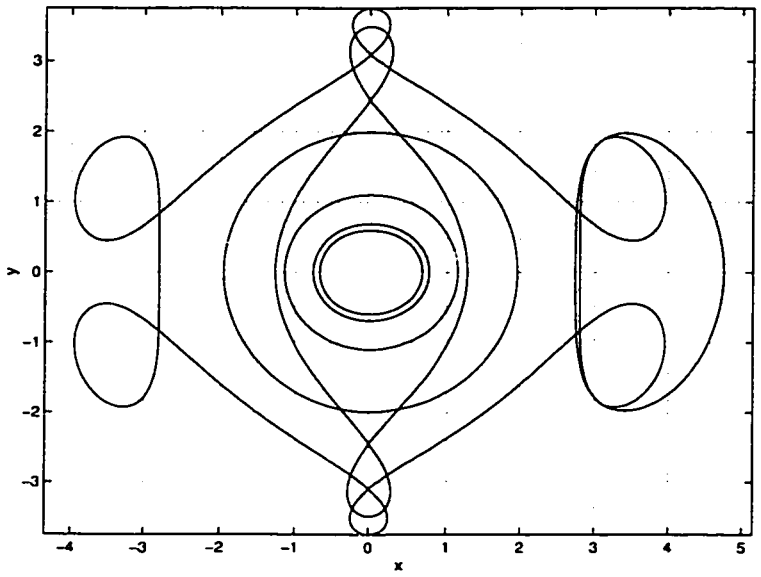

Figure 5.9: Some examples of periodic orbits at 1/10th of the rotation rate of asteroid Castalia.

periodic orbits at different ω_T in inertial space, and their relation to resonant orbits when ω_T/n is a ratio of two integers. The stable orbits defined in the plots are the orbits whose semi-major axis and eccentrity are near constant on average, which means the energy and angular momentum magnitude of the orbit do not change on average. Their orientation may change, like the well known J_2 perturbation orbits around the Earth. If there are large semi-major axis and eccentrity changes within an orbit, we regard this as unstable. We see in this picture that when the line is crossed, the system is in a region with a more strongly varying semi-major axis and ecentrity. The near direct periodic orbit exists in the lower-left region of this plot where $(n - \omega_T)/\omega_T \gg 1$, which means $n \gg 2\omega_T$. The far direct periodic orbit exists in the upper-right region of this figure when $(\omega_T - n)/n \gg 1$, which means $\omega_T \gg 2n$. The retrograde orbits exist when $\omega_T < 0$. In the middle are the resonant lines, we see that the 1:2 resonant line acts like a thin wall which prevents the near direct periodic orbit from crossing it.

For the near direct and some retrograde periodic orbits near the central body, when central body rotates slowly, $(n - \omega_T)/\omega_T \gg 1$, secular perturbations play important contribution to the periodic motion (See the out-of-plane stability analysis at Section 5.4.2).

5.5.3 The 1:2 resonant family

Here we give a more detailed discussion about the 1:2 resonant family which is a typical kind of eccentric periodic orbits. Other resonant periodic orbit families can be discussed similarly. Figure 5.10 shows some examples of the 1:2 resonant family which are also shown in Figure 5.8 (the "+" sign orbits). This family bifurcates from the near direct family at the point $x_0 \approx 1.6$ in Figure 5.8 when $k_b = 0, k_a = 1$ in Equation 5.71.

Figure 5.11 shows a 1:2 resonant orbit in both inertial coordinates(the dashed line) and in body-fixed rotating coordintates(the solid line). We see secular motion exists in inertial coordinate, i.e. the argument of periapsis is changing. The resonant condition is

$$\dot{M} - 2\omega_T + 2\dot{\Omega} + 2\dot{\omega} = 0, \tag{5.76}$$

where $\dot{\Omega} + \dot{\omega}$ is constant by Equation 3.67. See Figure 5.11, $\dot{\Omega} + \dot{\omega} > 0$, i.e, $\Omega + \omega$ ratates counter-clockwise. To satisfy the resonant condition 5.76, $\dot{M}$ should small enough, such that $\dot{M} - 2\omega_T\dot{\Omega} + \dot{\omega} < 0$. This is one reason why near circular 1:2 resonant orbit does not exist as $\dot{M} - 2\omega_T + 2\dot{\Omega} + 2\dot{\omega} > 0$ when $\dot{M}$ is larger.

Figure 5.12 shows a plot of additional variables such as the semi-major axis a, eccentricity e, radius at periapsis r_p, the longitude in body-fixed coordinate $U_r(i.e.\lambda)$ and the argument of periapsis ω for the 1:2 resonant orbit in Figure 5.11. Strictly speaking, the ω here represents the longitude of perapsis $\varpi = \Omega + \omega$.

Since this is a typical example of size-shape stable orbit, its a and e are constant on average. But its orientation, in this case ω, is changing. We also see a increases when U_r is at the quadrant II and IV, decreases when U_r is quadrant I and III, as $n_0 t \approx 2\omega_T t = 2(n_0 - \omega_T) = 2U_r$. The same scenario happens for the small eccentricity case in Section 4.1.4.

Figure 5.13 shows a numerical FFT analysis of the semi-major axis in Figure 5.12, this time we see that the dominating frequency is not unique. From the resonant condition 5.76 and Equations 4.73 and 4.74, we find

$$\begin{aligned} a(t) &= a_{00} + (a_{01} + a_{11}) \cos n_0 t + (a_{02} + a_{32}) \cos 2n_0 t \\ &\quad + (a_{03} + a_{42}) \cos 3n_0 t + \cdots . \end{aligned} \tag{5.77}$$

This is what we see in Figure 5.13, where $n_0 t - 2\omega_T t + 2\Omega + 2\omega = \pi/2$, and the coefficient a_{ij} can be found in Appendix B.1.2.

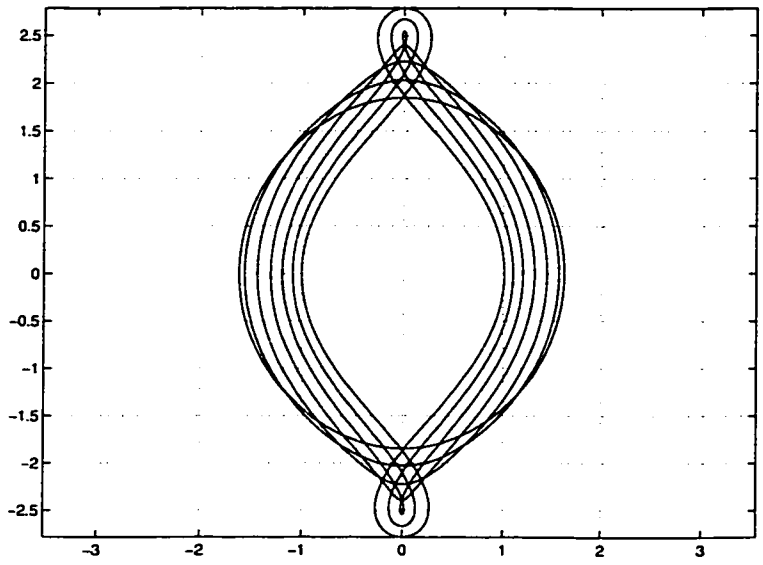

Figure 5.10: Some examples of the 1:2 resonant family for slowly rotating case

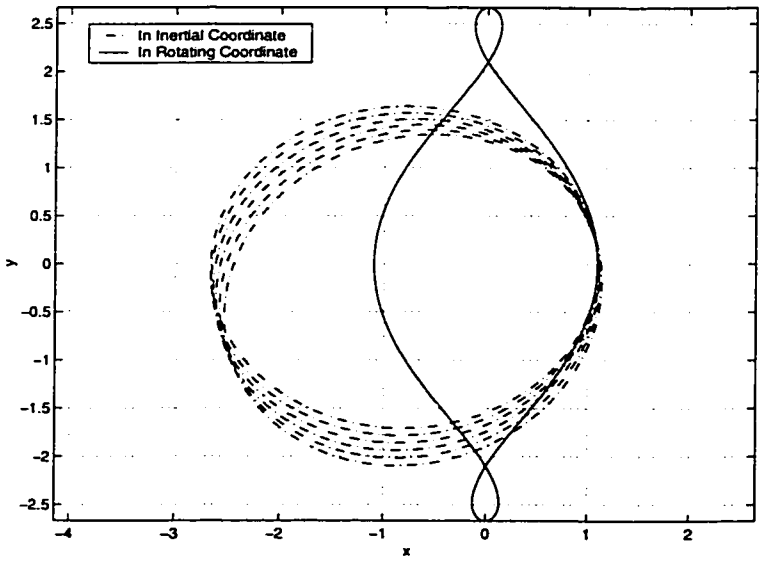

Figure 5.11: A 1:2 resonant orbit in both intertial and rotating coordinate

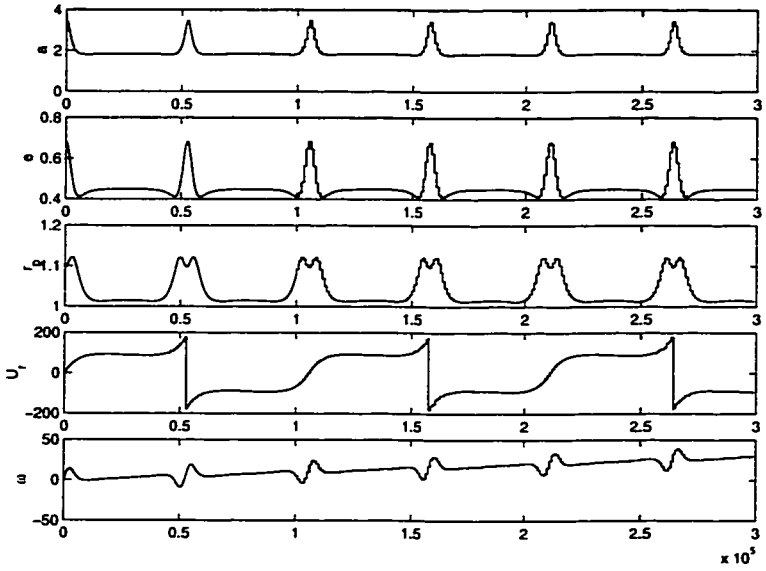

Figure 5.12: Some other variables for the 1:2 resonant orbit in Figure 5.11

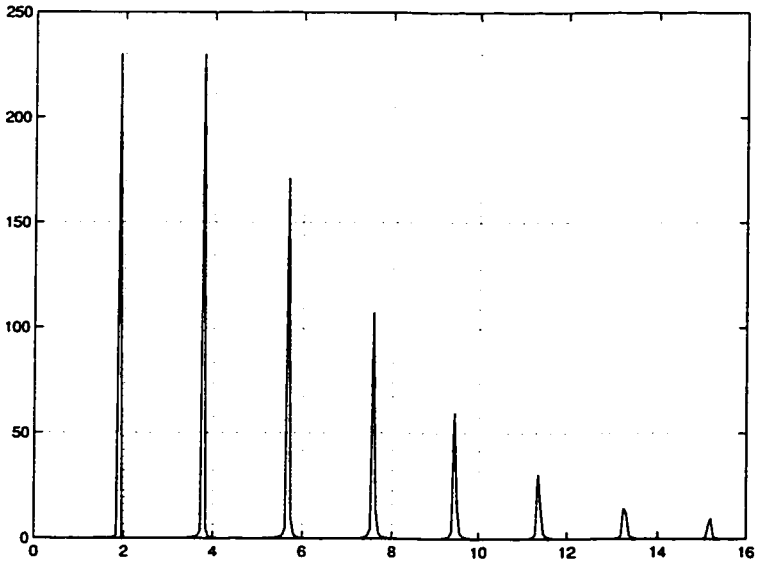

Figure 5.13: The FFT analysis for semi-major axis in Figure 5.12

5.5.4 Summary

We find some basic families of periodic orbits around a 2nd degree and order gravity field. The existence and stability of these families may change for different central body rotation rates. In Table 5.3, we give a summary of the properties of these periodic orbit families.

We note that some of the periodic orbits we discuss here have similarities to the periodic orbits of the restricted three body problem, and that all the periodic orbits discussed, except the 1:2 resonant orbits, are analyzed using first return maps. There may be other periodic orbits which are second or third return maps similar to the three body problems which are also shown in [42]. Since we focus our discussion on the size-shape stability problem in this dissertation, our discussion is limited to planar, first-return peroidic orbits. Paper [27] finds and analyzes periodic orbits with multiple returns in three dimensions.

periodic orbit	eccentricity	stability	existence
near direct	e≈0	stable	$n \gg 2\omega_T > 0$
far direct	e≈0	stable	$\omega_T \gg 2n > 0$
1:1 around y_{eq}	e≠0	stable	Equation 5.75
1:1 around x_{eq}	e≠0	unstable	always
1:2 resonant	e≠0	stable	$n \approx 2\omega_T$
retrograde	e≈0	stable	$n < 0$
special orbit	e≠0	stable/unstable	critical boundary

Table 5.3: Summary of peroidic families

5.6 A Coriolis Control

A coriolis control law which just includes the velocity state $\dot{x}, \dot{y}$ can stabilize an unstable equilibrium $(0, \pm y_{eq}, 0)$ and its nearby periodic orbits, without changing the positions of the equilibrium points, for rapidly rotating asteroids. The control law is specified as

$$\begin{bmatrix} 2K\dot{y} \\ -2K\dot{x} \end{bmatrix}, \tag{5.78}$$

where K is a positive constant. Similar to the analyses in Section 5.2.2, we can analyze the stability of the equilibrium points. The controlled system becomes

$$\ddot{x} - 2\omega_T\dot{y} = \omega_T^2 x - \frac{\mu}{r^3}x + \frac{\partial U_{20+22}}{\partial x} + 2K\dot{y}, \tag{5.79}$$

$$\ddot{y} + 2\omega_T\dot{x} = \omega_T^2 y - \frac{\mu}{r^3}y + \frac{\partial U_{20+22}}{\partial y} - 2K\dot{x}, \tag{5.80}$$

$$\ddot{z} = -\frac{\mu}{r^3}z + \frac{\partial U_{20+22}}{\partial z}. \tag{5.81}$$

Its characteristic equation is

$$\begin{vmatrix} \lambda & 0 & -1 & 0 \\ 0 & \lambda & 0 & -1 \\ -U_{xx} & -U_{xy} & \lambda & -2(\omega_T + K) \\ -U_{yx} & -U_{yy} & 2(\omega_T + K) & \lambda \end{vmatrix} = \lambda^4 + b\lambda^2 + c. \tag{5.82}$$

This time,

$$b = 4(\omega_T + K)^2 - U_{xx} - U_{yy}, \quad c = U_{xx}U_{yy}.$$

We see from Section 5.2.2 that for the equilibrim point $(0, y_{eq}, 0)$, $c > 0$ and $b^2 - 4c < 0$, the equilibrium point is unstable. After the control law is applied, and when $K > 0$ is large enough, $b^2 - 4c > 0$, and the equilibrium point becomes stable.

However for the equilibrium $(x_{eq}, 0, 0)$, $c < 0$, and the control law can't change the value of c, and so the stability can not be changed by this control law Even if a more general control law of the form

$$\begin{bmatrix} K_{xx}\dot{x} + K_{xy}\dot{y} \\ K_{yx}\dot{x} + K_{yy}\dot{y} \end{bmatrix} \tag{5.83}$$

is applied, the situation is the same.

We note the coriolis control completely modified the dynamics. Here we give some examples of periodic orbits with control or without control. First, we show some example of peroidic orbits without C_{20} and C_{22} perturbation and when $K = 0$ in Figure 5.14. For this case direct an retrograde periodic orbit coincide, and we can compared it with the perturbed case(See Figure 5.5).

Next we show some examples of a peroidc orbit when $K = 1$ in Figure 5.15. We see that some periodic orbits which do not exist in Figure 5.5 appear. For example, when $K = 0$, $x_0 = 1.3$, the direct near circular periodic orbit does not exist, But with the coriolis control, it appears. And the direct and retrograde periodic orbits no longer coincide. Through this example, we find the solutions to the controlled system are much different from the uncontrolled system.

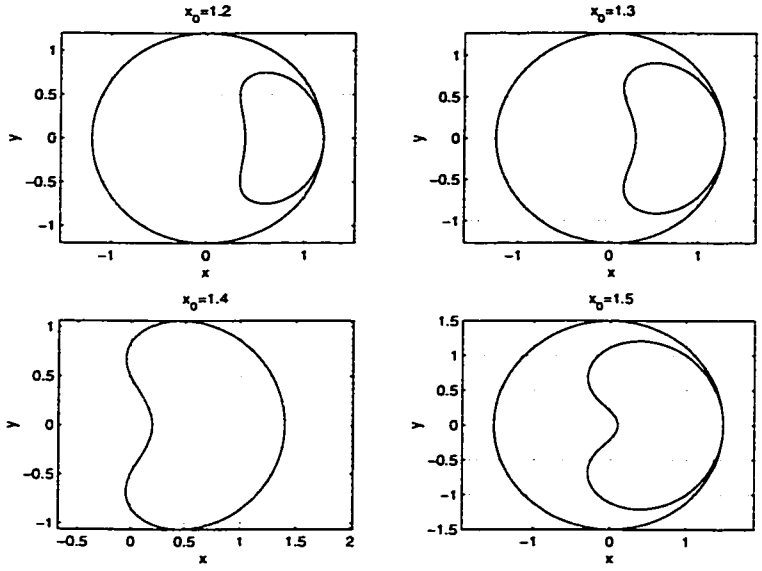

Figure 5.14: Periodic orbits when $K = 0, C_{20} = C_{22} = 0$

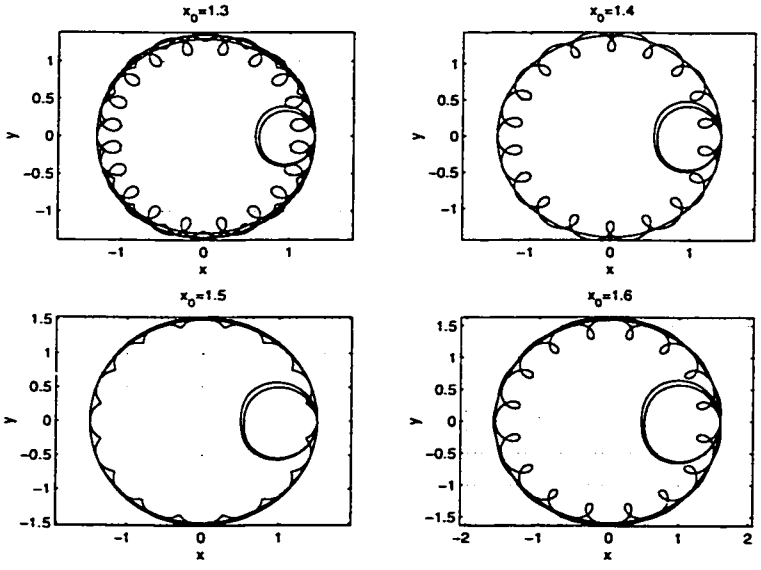

Figure 5.15: Periodic orbits when $K = 1$ for asteroid Castalia

CHAPTER VI

SUMMARY

This dissertation studies spacecraft orbital motion about rotating 2nd degree and order gravity fields, with its main application to orbital motion about an asteroid. This dynamical system is non-integrable in general. Our goal is to understand how the dynamics of this system change as a function of the central body's rotation rate and mass distribution. To carry out this analysis we use three different approaches: averaging, resonance analysis, and periodic orbit computation. By using these analyses, we can better understand the whole character of a spacecraft's motion around an asteroid, which is much different from the character of spacecraft motion around the Earth or other planets in the Solar system. We see that by using these three different methods, averaging, resonance analysis and periodic orbit computation, we reveal different aspects of the nature of our problem. We also find that they are closely related, and some results in our secular and resonant analyses can be used to discuss the existence and stability of periodic orbits

6.1 Stability of General Motions, Revisited

In Chapter II, we proposed a definition for "size-shape stability" of an orbit in a rotating second degree and order gravity field. In that definition, we assumed

that if the semi-major axis and eccentrity were constant on average, the orbit was said to be size-shape stable, which means that its energy and angular momentum magnitude are constant average. We have seen that this definition has both physical and technical significance.

Physically speaking, such stable orbits exist. In chapter III, we studied three kinds of averaged motions: when the central body does not rotate, rotates slowly, rotates rapidly. For all these three kinds of motions, the semi-major axis and eccentricity were constant on average. The only changes in these kinds of orbits were their orientation.

Technically speaking, for some near resonant orbits, this kind of size-shape stability does not exist, but we still can assume it exists but is unstable, by assuming a nominal Keplerian orbit. However, if the orbits exist, some contradictions appear. For example, large changes in semi-major axis and eccentrity over one nominal orbit may occur. These controdictions indicate that the assumed nominal orbit does not exist, or exists but is size-shape unstable. Since we assume the nominal orbit is Keplerian, there are many methods available for us to analyze the motion. This is the basic idea of fact I in Chapter I, and is used in Chapter IV.

Size-shape stability is a key assumption in this dissertation, and ties the whole dissertation together. The size-shape stability condition given in Chapter II is just the averaging condition in Chapter III. The existence but general instability assumption of a nominal orbit in Chapter II is just the condition for which elliptic expansion method can apply. This assumption is also used for near resonant orbits in Chapter IV. Some of the results in Chapter III and IV can also be used to analyze the periodic orbits in Chapter V.

6.2 Main Results in this Dissertation

This dissertation studies spacecraft orbital motion around an asteroid, an non-integrable dynamical system. First we try to understand the motion using analytical approximations for different cases of motion. One method we used is averaging. By averaging, the fast motion modes are removed and the secular, i.e., the long term, motion remains. Another method based on elliptic expansions is used to evaluate the short period variations in motion. Then, by using numerical methods, we find basic families of periodic orbits which can be analyzed using results from the above two analytical methods. With all this, we can better understand the whole character of spacecraft orbital motion around an asteroid.

Specifically, In Chapter II, we propose a definition for size-shape stability and we present two facts which are related to the orbital stability of spacecraft motion around an asteroid. These definitions are basic assumptions for the dissertation and tie it together.

In Chapter III, we study the averaged motion for three cases: when the central body does not rotate, rotates slowly, and rotates rapidly. For the slow rotation cases, we derive the averaged Lagrange planetary equations for this system and used them, in conjunction with the Jacobi integral, to give a complete description of orbital motion. We show that, under the averaging assumptions, i.e, with the size-shape stability condition, the problem is completely integrable and can be reduced to quadratures. For the case of no rotation these quadratures can be expressed in terms of elliptic functions and integrals. For the rapid rotation case, motion can be reduced to the well-known oblate body perturbation problem. One application of the secular motion analysis is to discuss the conditions for periodic orbits, for example

the 1:2 periodic family in Section 5.5.3.

In Chapter IV, we use elliptic expansions to derive the Fourier expansions of semi-major axis $a(t)$ and eccentricity $e(t)$ for nominal orbits in our system, i.e., the frequencies, amplitudes and phase angles of their Fourier expansions of $a(t), e(t)$ are estimated. With the Fourier expansions, we can explain the dynamics of the semi-major axis for near circular orbits. Additionally, by averaging along near resonant orbits, we can explain why $a(t)$ and $e(t)$ sometimes experience large changes over short time spans. Together with the resonant integrals analysis [38], we can estimate a stability index for our size-shape stability analysis, proposed in Chapter II. Also, the Fourier expansion of $a(t)$ and $e(t)$ can be used to analyze the periodic orbits in Chapter V, for example the 1:2 periodic family in Section 5.5.3. Some numerical analyses and verifications are also given.

In Chapter V, four equilibrium sulutions are analyzed in the rotating second degree and order gravity field. Two of them are always unstable, the other two can be stable or unstable, their stability determined by the central body's rotation rate ω_T, the two gravity coefficients, C_{20} and C_{22}, and the asteroid's mass. We also compute families of periodic orbits. In our search procedure, we remove the two unity eigenvalues from the state transition matrix (STM) to find a robust, non-singular Poincaré map to solve for the periodic orbits. The algorithm converges well, especially for stable periodic orbits. By calculating the STM for the periodic orbit, we find the characteristic multipliers which are the indices of stability of the periodic orbit. These are used to test the stability of the periodic orbits. Then, by using a relatively automatic searching procedure for the periodic orbits, we find five basic families of periodic orbits and discuss their existence and stability at different central body rotation rates. There are also other "special" periodic orbits which lie between

these basic periodic orbit families.

6.3 Future Work

There are many results in the dissertation that are incomplete, and could be further analyzed in the future. For example, a potential list is given bellow:

(1)More accurate models should be used to verify the results in this dissertation.

(2)Rigorous proofs to some of the conclusions may possibly be given. But this may be hard, since many orbits discussed here lie in regions of chaotic motion.

(3)When the central body does not rotate uniformly, numerical results are relatively easy to find, but simple analytical results would not exist.

(4)Since the gravity force of an asteroid is small, we need to compare the perturbation of the asteroid to other perturbations such as solar radiation, third body perturbations, etc.

APPENDICES

APPENDIX A

Elliptic Integral Solutions

A number of different elliptic functions and integrals are used in the discussion of Chapter III. Below we give the basic definitions of the functions and integrals needed for our analytical solution. See [1] for a comprehensive review and definition of elliptic functions and integrals.

A.1 Elliptic Functions

The basic elliptic functions used are the elliptic sine and cosine functions, denoted as sn and cn, respectively. These are functions of their arguments, u, and of a parameter denoted as k. In their general form we will denote them as: $\mathrm{sn}(u;k)$ and $\mathrm{cn}(u;k)$. If $k = 0$ they degenerate to the trigonometric sine and cosine functions, and if $k = 1$ they degenerate to the hyperbolic tangent and secant functions, respectively. As with the trigonometric functions, they have an amplitude constraint denoted as: $\mathrm{sn}^2(u;k) + \mathrm{cn}^2(u;k) = 1$. We will only consider these functions with real arguments of u. Then they are periodic with period $4\mathrm{K}(k)$, where K is the complete elliptic integral of the first kind. A related function is denoted as $\mathrm{dn}(u;k)$ and is defined from the relation: $\mathrm{dn}^2(u;k) + k^2\mathrm{sn}^2(u;k) = 1$. Also, tn is defined as sn/cn. The functions dn and tn have periods of 2K.

A.2 Elliptic Integrals

We require two incomplete elliptic integral definitions for our solution, that of the first and third kind. The usual definitions of these integrals are given as:

$$\mathrm{F}(\phi;k) = \int_0^{\phi} \frac{\mathrm{d}\theta}{\sqrt{1-k^2\sin^2\theta}}, \tag{A.1}$$

$$\Pi(\phi;n,k) = \int_0^{\phi} \frac{\mathrm{d}\theta}{(1+n\sin^2\theta)\sqrt{1-k^2\sin^2\theta}}. \tag{A.2}$$

With these definitions, the complete elliptic integral of the first kind is then $\mathrm{K}(k) = \mathrm{F}(\pi/2;k)$.

For the specific application we give, we use a different definition of the argument, related to argument used in the elliptic functions. To give a clearer understanding we change the integrands from trigonometric to elliptic functions using the transformation $\sin\theta = \mathrm{sn}(u)$, with the differential transformation being computed as: $\cos\theta \mathrm{d}\theta = \mathrm{cn}(u)\mathrm{dn}(u)\mathrm{d}u$, or since $\cos\theta = \mathrm{cn}(u)$, $\mathrm{d}\theta = \mathrm{dn}(u)\mathrm{d}u$. The integrals then become:

$$\mathrm{F}(u_f;k) = \int_0^{u_f} \mathrm{d}u \tag{A.3}$$

$$= \mathrm{sn}^{-1}(u_f), \tag{A.4}$$

$$\Pi(u_f;n,k) = \int_0^{u_f} \frac{\mathrm{d}u}{(1+n\mathrm{sn}^2(u;k))}. \tag{A.5}$$

We assume this particular definition in the text, as it clearly shows these integrals to be monotonically increasing functions of u_f. To transform to the usual form with argument of ϕ we can use: $\phi_f = \arcsin(\mathrm{sn}(u_f))$.

We always assume that $0 < k < 1$. Furthermore, for the evaluation of the elliptic integrals of the third kind, we note that since $0 < k^2 < n < 1$, they can be classified as the circular case of that integral.

A.3 Analytical solution for $0 < \sigma < 1$ when $\omega_T = 0$

Now the general form of the equations for $\mathrm{d}i/\mathrm{d}t$, $\mathrm{d}\Omega/\mathrm{d}t$, and C from Equations 3.15, 3.16, and 3.14 hold, respectively. Define a new variable $s = \tan\Omega$ with $1+s^2 = 1/\cos^2\Omega$ and $\mathrm{d}s/\mathrm{d}\Omega = 1 + s^2$. Rewriting the differential equation for s yields:

$$\frac{\mathrm{d}s}{\mathrm{d}t} = -(\pm)_i B\sqrt{[1 - C - \sigma + (1 - C)s^2]\,(1 - \sigma + s^2)}, \tag{A.6}$$

where the $(\pm)_i$ is defined as before.

For notational convenience we also define two constant parameters:

$$m^2 = 1 - \sigma, \tag{A.7}$$

$$\theta = \frac{1 - C - \sigma}{1 - C}, \tag{A.8}$$

where $0 < m^2 < 1$, and $-\infty < \theta < 1$ for the cases of interest.

Equation A.6 can then be separated into:

$$\frac{\mathrm{d}s}{\sqrt{(\theta + s^2)\,(m^2 + s^2)}} = \mp\sqrt{1 - C}B\mathrm{d}t. \tag{A.9}$$

The three cases $\theta < 0$, $\theta = 0$, and $\theta > 0$ will yield three different fundamental solutions, corresponding to precession about the x-axis (minimum moment of inertia), motion on the separatrix, and precession about the z-axis (maximum moment of inertia), respectively.

A.3.1 Motion along the separatrix ($\theta = 0$)

We first deal with the special case of $\theta = 0$, which is related to motion on the manifolds of the unstable equilibrium points. We noted before that at the unstable equilibrium point the energy has a value $C = 1 - \sigma$, and hence $\theta = 0$ and motion along the manifolds of this point will also have this parameter value. For this case

Equation 3.55 simplifies to:

$$\frac{\mathrm{d}s}{s\sqrt{1+s^2/m^2}} = -(\pm)_i B\sqrt{\sigma(1-\sigma)}\mathrm{d}t. \tag{A.10}$$

For an initial value of Ω we will choose $\pm 90°$ as each separatrix will pass through this value, leading to $s_o = \pm\infty$. In this subsection we denote $(\pm)_\Omega$ as positive for an initial $\Omega = 90°$ and negative for an initial $\Omega = -90°$. Integrating the equation explicitly yields:

$$\tan\Omega = \frac{(\pm)_i\sqrt{1-\sigma}}{\sinh(u_f)}, \tag{A.11}$$

$$u_f = B\sqrt{\sigma(1-\sigma)}(t-t_o). \tag{A.12}$$

At time $t = t_o$ motion commences at $\Omega = \pm 90°$. For the positive sign the node moves into quadrants I and III approaching limiting values of 0° and 180° degrees, respectively. For the negative sign the node moves into quadrants II and IV approaching limiting values of 180° and 0° degrees, respectively.

Solving for $\sin i$ and performing the quadrature for ω yields:

$$\sin i = \frac{\sqrt{\cosh^2(u_f)-\sigma}}{\cosh(u_f)}, \tag{A.13}$$

$$\begin{aligned}\omega - \omega_o = {} & -\frac{B}{2}(1-2\sigma)(t-t_o) \\ & + \arctan\frac{\cosh u_f(\cosh u_f + \sinh u_f) - \sigma}{\sqrt{\sigma(1-\sigma)}} - \arctan\sqrt{\frac{1-\sigma}{\sigma}}.\end{aligned} \tag{A.14}$$

The orbit vectors for this solution becomes:

$$\mathbf{h} = \frac{1}{\cosh u_f}\begin{bmatrix} (\pm)_\Omega\sqrt{1-\sigma} \\ -(\pm)_\Omega(\pm)_i \sinh u_f \\ (\pm)_i\sqrt{\sigma}\end{bmatrix}, \tag{A.15}$$

$$\mathbf{n} = \frac{(\pm)_\Omega}{\sqrt{\cosh^2 u_f - \sigma}}\begin{bmatrix} (\pm)_i \sinh u_f \\ \sqrt{1-\sigma} \\ 0\end{bmatrix}. \tag{A.16}$$

A.3.2 Precession about the x-axis($\theta < 0$)

When $C+\sigma > 1, \theta < 0$ and the orbit plane will precess about the x-axis (minimum moment of inertia). Defining $\nu^2 = -\theta$, we rewrite Equation 3.55 as:

$$-(\pm)_i\sqrt{1-C}B\mathrm{d}t = \frac{\mathrm{d}s}{\sqrt{(m^2+s^2)(s^2-\nu^2)}}. \tag{A.17}$$

We choose our initial value to lie at an inclination of 90°, since all librational motion will pass through this value, at which point it can be shown that $s_o = \pm\nu$. For an initial point we choose the positive root, corresponding to Ω starting in either quadrant I or III. We see then that the inclination will initially increase, giving a definite sign to our integral:

$$\sqrt{1-C}B(t-t_o) = \int_\nu^s \frac{ds}{\sqrt{(m^2+s^2)(s^2-\nu^2)}}, \tag{A.18}$$

which can be solved in terms of elliptic functions as:

$$\sqrt{(1-C)(m^2+\nu^2)}B(t-t_o) = \mathrm{cn}^{-1}(\frac{\nu}{s};\frac{m}{\sqrt{m^2+\nu^2}}). \tag{A.19}$$

Specifically solving for $\tan\Omega$, $\cos i$, and ω yields:

$$\tan\Omega = \sqrt{\frac{1-n_L}{n_L}}\frac{1}{\mathrm{cn}\,(u_f;k_L)}, \tag{A.20}$$

$$\cos i = -\sqrt{n_L-k_L^2}\frac{\mathrm{sn}\,(u_f;k_L)}{\mathrm{dn}\,(u_f;k_L)}, \tag{A.21}$$

$$\begin{aligned}\omega-\omega_o &= -\frac{B}{2}(5C-4+\sigma)(t-t_o)\\ &\quad +\sqrt{\frac{\sigma}{C}}\left[(1-n_L)\Pi(u_f;n_L,k_L)-\mathrm{F}(u_f;k_L)\right],\end{aligned} \tag{A.22}$$

$$u_f = \sqrt{\sigma C}B(t-t_o), \tag{A.23}$$

$$k_L = \sqrt{\frac{(1-\sigma)(1-C)}{\sigma C}}, \tag{A.24}$$

$$n_L = \frac{1-C}{\sigma}, \tag{A.25}$$

where F is the incomplete elliptic integral of the first kind and Π is the incomplete elliptic integral of the third kind. The orbit vectors are found to be:

$$\mathbf{h} = \frac{1}{\mathrm{dn}\,(u_f;k_L)}\begin{bmatrix} (\pm)_\Omega\sqrt{1-n_L} \\ -(\pm)_\Omega\sqrt{n_L}\mathrm{cn}\,(u_f;k_L) \\ -\sqrt{n_L-k_L^2}\mathrm{sn}\,(u_f;k_L)\end{bmatrix}, \tag{A.26}$$

$$\mathbf{n} = \frac{(\pm)_\Omega}{\sqrt{1-n_L\mathrm{sn}^2\,(u_f;k_L)}}\begin{bmatrix} \sqrt{n_L}\mathrm{cn}\,(u_f;k_L) \\ \sqrt{1-n_L} \\ 0\end{bmatrix}. \tag{A.27}$$

The period of the secular motion for the orbit normal is:

$$T_L = \frac{4}{\sqrt{\sigma CB}}\mathrm{K}(k_L), \tag{A.28}$$

where K is the complete elliptic integral of the first kind.

Note that when $\sigma \to 1$ the parameter $k_L \to 0$. In this case it can be shown that the above results reduce to the case given in Equations 3.50 and 3.51.

A.3.3 Precession about the z-axis($\theta > 0$)

When $C+\sigma < 1$, Ω will precess about the z-axis (maximum moment of inertia). In this case $0 < \theta < m^2$ and we recover Equation 3.55. Now we choose our initial value at $\Omega = 0$ as all solutions will pass through this point, yielding $s_o = 0$. Evaluating the integral yields:

$$-(\pm)_i\sqrt{1-C}B(t-t_o) = \int_0^s \frac{\mathrm{d}s}{\sqrt{(s^2+m^2)(s^2+\theta)}}, \tag{A.29}$$

which can be solved for in terms of elliptic functions as:

$$-(\pm)_i\sqrt{1-C}mB(t-t_o) = \mathrm{tn}^{-1}\left(\frac{s}{\sqrt{\theta}};\sqrt{\frac{m^2-\theta}{m^2}}\right). \tag{A.30}$$

Solving for $\tan\Omega$, $\sin i$, and ω yields:

$$\tan\Omega = -(\pm)_i\sqrt{1-n_C}\,\mathrm{tn}\,(u_f;k_C), \tag{A.31}$$

$$\sin i = \frac{k_C}{\sqrt{n_C}}\frac{\sqrt{1-n_C\mathrm{sn}^2\,(u_f;k_C)}}{\mathrm{dn}\,(u_f;k_C)}, \tag{A.32}$$

$$\begin{aligned}\omega-\omega_o &= -\frac{B}{2}(5C-4+\sigma)(t-t_o)\\ &\quad +\sqrt{\frac{1-C}{1-\sigma}}\left[(1-n_C)\Pi(u_f;n_C,k_C)-\mathrm{F}(u_f;k_C)\right],\end{aligned} \tag{A.33}$$

$$u_f = \sqrt{(1-C)(1-\sigma)}B(t-t_o), \tag{A.34}$$

$$k_C = \sqrt{\frac{\sigma C}{(1-C)(1-\sigma)}} \tag{A.35}$$

$$= \frac{1}{k_L}, \tag{A.36}$$

$$n_C = \frac{\sigma}{1-C} \tag{A.37}$$

$$= \frac{1}{n_L}. \tag{A.38}$$

The orbit vectors are expressed as:

$$\mathbf{h} = \frac{1}{\sqrt{n_C}\mathrm{dn}\,(u_f;k_C)}\begin{bmatrix} -(\pm)_i k_C\sqrt{1-n_C}\mathrm{sn}\,(u_f;k_C)\\ -k_C\mathrm{cn}\,(u_f;k_C)\\ -(\pm)_i\sqrt{n_C-k_C^2}\end{bmatrix}, \tag{A.39}$$

$$\mathbf{n} = \frac{1}{\sqrt{1-n_C\mathrm{sn}^2\,(u_f;k_C)}}\begin{bmatrix} \mathrm{cn}\,(u_f;k_C)\\ -(\pm)_i\sqrt{1-n_C}\mathrm{sn}\,(u_f;k_C)\\ 0\end{bmatrix}. \tag{A.40}$$

The period of the secular motion of the orbit normal is then:

$$T_C = \frac{4}{\sqrt{(1-C)(1-\sigma)B}}K(k_C). \tag{A.41}$$

Note that when $\sigma \to 0$ the parameters k_C and n_C go to zero. In this case it can be shown that the above results reduce to the case given in Equations 3.36 and 3.37.

APPENDIX B

Elliptic Expansions

B.1 High Order Elliptic Expansions

The expansions for radius r and true anormaly f are [43],[9]:

$$\begin{aligned}\frac{r}{a} &= 1+\frac{1}{2}e^2+\Big(-e+\frac{3}{8}e^3-\frac{5}{192}e^5+\frac{7}{9216}\Big)\cos M \\ &+\Big(-\frac{1}{2}e^2+\frac{1}{3}e^4-\frac{1}{16}e^6\Big)\cos 2M+\Big(-\frac{3}{8}e^3+\frac{45}{128}e^5-\frac{567}{5120}e^7\Big)\cos 3M \\ &+\Big(-\frac{1}{3}e^4+\frac{2}{5}e^6\Big)\cos 4M+\Big(-\frac{125}{384}e^5+\frac{4375}{9216}e^7\Big)\cos 5M \\ &-\frac{27}{80}e^6\cos 6M-\frac{16807}{46080}e^7\cos 7M+O(e^8), \end{aligned} \tag{B.1}$$

$$\begin{aligned} f &= M+\Big(2e-\frac{1}{4}e^3+\frac{5}{96}e^5+\frac{107}{4608}e^7\Big)\sin M \\ &+\Big(\frac{5}{4}e^2-\frac{11}{24}e^4+\frac{17}{192}e^6\Big)\sin 2M+\Big(\frac{13}{12}e^3-\frac{43}{64}e^5+\frac{95}{512}e^7\Big)\sin 3M \\ &+\Big(\frac{103}{96}e^4-\frac{451}{480}e^6\Big)\sin 4M+\Big(\frac{1097}{960}e^5-\frac{5957}{4608}e^7\Big)\sin 5M \\ &+\frac{1223}{960}e^6\sin 6M+\frac{47273}{32256}e^7\sin 7M+O(e^8). \end{aligned} \tag{B.2}$$

B.1.1 Expensions of potential and $\dot{a}, \dot{e}$

We use Mathematica 4.0 to expand the gravity potential to order seven:

$$U_2 = -\frac{\mu}{2a^3}\Big\{C_{20}-6C_{22}\cos(2M-2\omega_T t+2\omega)\Big\}$$

$$
\begin{aligned}
&-\frac{3\mu e}{2a^3}\Big\{3C_{20}\cos M + 3C_{22}\cos(M - 2\omega_T t + 2\omega) \\
&\quad -7C_{22}\cos(3M - 2\omega_T + 2\omega)\Big\} \\
&-\frac{3\mu e^2}{4a^3}\Big\{C_{20} + 3C_{20}\cos 2M + 10C_{22}\cos(2M - 2\omega_T t + 2\omega) \\
&\quad -34C_{22}\cos(4M - 2\omega_T t + 2\omega)\Big\} \\
&+\frac{\mu e^3}{16a^3}\Big\{ -27C_{20}\cos M - 53C_{20}\cos 3M \\
&\quad +C_{22}\cos(M + 2\omega_T t - 2\omega) + 3C_{22}\cos(M - 2\omega_T t + 2\omega) \\
&\quad -369C_{22}\cos(3M - 2\omega_T t + 2\omega) + 845C_{22}\cos(5M - 2\omega_T t + 2\omega)\Big\} \\
&-\frac{\mu e^4}{16a^3}\Big\{15C_{20} + 28C_{20}\cos 2M + 77C_{20}\cos 4M \\
&\quad -2C_{22}\cos(2M + 2\omega_T t - 2\omega) - 39C_{22}\cos(2M - 2\omega_T t + 2\omega) \\
&\quad +920C_{22}\cos(4M - 2\omega_T t + 2\omega) - 1599C_{22}\cos(6M - 2\omega_T t + 2\omega)\Big\} \\
&+\frac{\mu e^5}{1280a^3}\Big\{ -2610C_{20}\cos M - 1965C_{20}\cos 3M - 8865C_{20}\cos 5M \\
&\quad +55C_{22}\cos(M + 2\omega_T t - 2\omega) + 234C_{22}\cos(3M + 2\omega_T t - 2\omega) \\
&\quad -50C_{22}\cos(M - 2\omega_T t + 2\omega) + 14670C_{22}\cos(3M - 2\omega_T t + 2\omega) \\
&\quad -162625C_{22}\cos(5M - 2\omega_T t + 2\omega) \\
&\quad +228347C_{22}\cos(7M - 2\omega_T t + 2\omega)\Big\} \\
&-\frac{\mu e^6}{960a^3}\Big\{1050C_{20} + 2115C_{20}\cos 2M + 774C_{20}\cos 4M + 9501C_{20}\cos 6M \\
&\quad -256C_{22}\cos(4M + 2\omega_T t - 2\omega) - 84C_{22}\cos(2M + 2\omega_T t - 2\omega) \\
&\quad +350C_{22}\cos(2M - 2\omega_T t + 2\omega) - 36060C_{22}\cos(4M - 2\omega_T t + 2\omega) \\
&\quad -248886C_{22}\cos(6M - 2\omega_T t + 2\omega) \\
&\quad -293476C_{22}\cos(8M - 2\omega_T t + 2\omega)\Big\} \\
&+\frac{\mu e^7}{215040a^3}\Big\{ -500815C_{20}\cos M - 519813C_{20}\cos 3M
\end{aligned}
$$

$$
\begin{aligned}
&+174545C_{20}\cos 5M - 3024637C_{20}\cos 7M \\
&+6573C_{22}\cos(M + 2\omega_T t - 2\omega) \\
&+25515C_{22}\cos(3M + 2\omega_T t - 2\omega) \\
&+78125C_{22}\cos(5M + 2\omega_T t - 2\omega) \\
&-5005C_{22}\cos(M - 2\omega_T t + 2\omega) \\
&-555345C_{22}\cos(3M - 2\omega_T t + 2\omega) \\
&+21863625C_{22}\cos(5M - 2\omega_T t + 2\omega) \\
&-107487625C_{22}\cos(7M - 2\omega_T t + 2\omega) \\
&+109298457C_{22}\cos(9M - 2\omega_T t + 2\omega)\Big\} + O(e^8). \qquad \text{(B.3)}
\end{aligned}
$$

The Lagrange equations for a, e are

$$
\begin{aligned}
\frac{\mathrm{d}a}{\mathrm{d}t} \;=\; & -\frac{12C_{22}n}{a}\sin(2M - 2\omega_T t + 2\omega) \\
& +\frac{3ne}{a}\Big\{C_{20}\sin M + C_{22}\sin(M - 2\omega_T t + 2\omega) \\
& \quad -21C_{22}\sin(3M - 2\omega_T t + 2\omega)\Big\} \\
& +\frac{3ne^2}{a}\Big\{3C_{20}\sin 2M + 10C_{22}\sin(2M - 2\omega_T t + 2\omega) \\
& \quad -68C_{22}\sin(4M - 2\omega_T t + 2\omega)\Big\} \\
& +\frac{ne^3}{8a}\Big\{27C_{20}\sin M + 159C_{20}\sin 3M - C_{22}\sin(M + 2\omega_T t - 2\omega) \\
& \quad -3C_{22}\sin(M - 2\omega_T t + 2\omega) + 1107C_{22}\sin(3M - 2\omega_T t + 2\omega) \\
& \quad -4225C_{22}\sin(5M - 2\omega_T t + 2\omega)\Big\} \\
& +\frac{ne^4}{4a}\Big\{28C_{20}\sin 2M + 154C_{20}\sin 4M - 2C_{22}\sin(2M + 2\omega_T t - 2\omega) \\
& \quad -39C_{22}\sin(2M - 2\omega_T t + 2\omega) + 1840C_{22}\sin(4M - 2\omega_T t + 2\omega) \\
& \quad -4797C_{22}\sin(6M - 2\omega_T t + 2\omega)\Big\}
\end{aligned}
$$

$$
\begin{aligned}
&+\frac{ne^5}{640a}\Big\{2610C_{20}\sin M + 5895C_{20}\sin 3M + 44325C_{20}\sin 5M \\
&\quad -55C_{22}\sin(M + 2\omega_T t - 2\omega) + 50C_{22}\sin(M - 2\omega_T t + 2\omega) \\
&\quad -729C_{22}\sin(3M + 2\omega_T t - 2\omega) - 44010C_{22}\sin(3M - 2\omega_T t + 2\omega) \\
&\quad +813125C_{22}\sin(5M - 2\omega_T t + 2\omega) \\
&\quad -1598429C_{22}\sin(7M - 2\omega_T t + 2\omega)\Big\} \\
&+\frac{ne^6}{240a}\Big\{2115C_{20}\sin 2M + 1548C_{20}\sin 4M + 28503C_{20}\sin 6M \\
&\quad -512C_{22}\sin(4M + 2\omega_T t - 2\omega) - 84C_{22}\sin(2M + 2\omega_T t - 2\omega) \\
&\quad +350C_{22}\sin(2M - 2\omega_T t + 2\omega) - 72120C_{22}\sin(4M - 2\omega_T t + 2\omega) \\
&\quad +746658C_{22}\sin(6M - 2\omega_T t + 2\omega) \\
&\quad -1173904C_{22}\sin(8M - 2\omega_T t + 2\omega)\Big\} \\
&+\frac{ne^7}{107520a}\Big\{500815C_{20}\sin M + 1559439C_{20}\sin 3M - 872725C_{20}\sin 5M \\
&\quad +21172459C_{20}\sin 7M - 6573C_{22}\sin(M + 2\omega_T t - 2\omega) \\
&\quad -76545C_{22}\sin(3M + 2\omega_T t - 2\omega) - 390625C_{22}\sin(5M + 2\omega_T t - 2\omega) \\
&\quad +5005C_{22}\sin(M - 2\omega_T t + 2\omega) + 1666035C_{22}\sin(3M - 2\omega_T t + 2\omega) \\
&\quad -109318125C_{22}\sin(5M - 2\omega_T t + 2\omega) \\
&\quad +752413375C_{22}\sin(7M - 2\omega_T t + 2\omega) \\
&\quad -983686113C_{22}\sin(9M - 2\omega_T t + 2\omega)\Big\} + O(e^8). \qquad \text{(B.4)}
\end{aligned}
$$

$$
\begin{aligned}
\frac{\mathrm{d}e}{\mathrm{d}t} \;=\; &-\frac{3n}{2a^2}\Big\{ - C_{20}\sin M + C_{22}\sin(M - 2\omega_T t + 2\omega) \\
&\quad +7C_{22}\sin(3M - 2\omega_T t + 2\omega)\Big\} \\
&+\frac{3ne}{2a^2}\Big\{3C_{20}\sin 2M + 2C_{22}\sin(2M - 2\omega_T t + 2\omega) \\
&\quad -34C_{22}\sin(4M - 2\omega_T t + 2\omega)\Big\}
\end{aligned}
$$

$$+\frac{3ne^2}{16a^2}\Big\{C_{20}\sin M+53C_{20}\sin 3M-C_{22}\sin(M+2\omega_T t-2\omega)$$
$$+C_{22}\sin(M-2\omega_T t+2\omega)+235C_{22}\sin(3M-2\omega_T t+2\omega)$$
$$-845C_{22}\sin(5M-2\omega_T t+2\omega)\Big\}$$
$$-\frac{ne^3}{4a^2}\Big\{4C_{20}\sin 2M-77C_{20}\sin 4M+2C_{22}\sin(2M+2\omega_T t-2\omega)$$
$$+33C_{22}\sin(2M-2\omega_T t+2\omega)-766C_{22}\sin(4M-2\omega_T t+2\omega)$$
$$+1599C_{22}\sin(6M-2\omega_T t+2\omega)\Big\}$$
$$-\frac{ne^4}{256a^2}\Big\{-90C_{20}\sin M+1365C_{20}\sin 3M-8865C_{20}\sin 5M$$
$$+C_{22}\sin(M+2\omega_T t-2\omega)-86C_{22}\sin(M-2\omega_T t+2\omega)$$
$$+243C_{22}\sin(3M+2\omega_T t-2\omega)+15414C_{22}\sin(3M-2\omega_T t+2\omega)$$
$$-151655C_{22}\sin(5M-2\omega_T t+2\omega)$$
$$+228347C_{22}\sin(7M-2\omega_T t+2\omega)\Big\}$$
$$+\frac{ne^5}{160a^2}\Big\{145C_{20}\sin 2M-2564C_{20}\sin 4M+9501C_{20}\sin 6M$$
$$-256C_{22}\sin(4M+2\omega_T t-2\omega)+4C_{22}\sin(2M+2\omega_T t-2\omega)$$
$$+630C_{22}\sin(2M-2\omega_T t+2\omega)-40640C_{22}\sin(4M-2\omega_T t+2\omega)$$
$$+245874C_{22}\sin(6M-2\omega_T t+2\omega)$$
$$-293476C_{22}\sin(8M-2\omega_T t+2\omega)\Big\}$$
$$+\frac{ne^6}{30720a^2}\Big\{8905C_{20}\sin M+81297C_{20}\sin 3M-1188475C_{20}\sin 5M$$
$$+3024637C_{20}\sin 7M+303C_{22}\sin(M+2\omega_T t-2\omega)$$
$$+5103C_{22}\sin(3M+2\omega_T t-2\omega)-78125C_{22}\sin(5M+2\omega_T t-2\omega)$$
$$+3605C_{22}\sin(M-2\omega_T t+2\omega)+920295C_{22}\sin(3M-2\omega_T t-2\omega)$$
$$-25387725C_{22}\sin(5M-2\omega_T t+2\omega)$$

$$+109658843C_{22}\sin(7M-2\omega_T t+2\omega)$$
$$-109298457C_{22}\sin(9M-2\omega_T t+2\omega)\Big\}+O(e^7). \tag{B.5}$$

B.1.2 The frequencies, amplitudes and phase angles

Similar to the discuss in Section 4.1.3, we have the Fourier expansions for $a(t)$,$e(t)$ shown in Equation 4.73 and 4.74. we list them here again for convenience.

$$a(t) = \sum_{i=0,j=0}^{\infty,\infty} a_{ij}\cos(f_{ij}t+\phi_{ij}^a), \tag{B.6}$$
$$e(t) = \sum_{i=0,j=0}^{\infty,\infty} e_{ij}\cos(f_{ij}t+\phi_{ij}^e), \tag{B.7}$$

where the frequencies, amplitudes and phase angles are

$$f_{0j} = jn_0, \qquad 1\le j\le 7; \tag{B.8}$$
$$f_{ij} = in_0-j\omega_T, \qquad 1\le i\le 9, j=2; \tag{B.9}$$
$$f_{ij}^{+} = in_0+j\omega_T \qquad 1\le i\le 5, j=2. \tag{B.10}$$
$$a_{01} = \frac{C_{20}}{a_0}\Big[-3e_0-\frac{27}{8}e_0^3-\frac{261}{64}e_0^5-\frac{100163}{21504}e_0^7\Big], \tag{B.11}$$
$$a_{02} = \frac{C_{20}}{a_0}\Big[-\frac{9}{2}e_0^2-\frac{7}{2}e_0^4-\frac{141}{32}e_0^6\Big], \tag{B.12}$$
$$a_{03} = \frac{C_{20}}{a_0}\Big[-\frac{53}{8}e_0^3-\frac{393}{128}e_0^5-\frac{173271}{35840}e_0^7\Big], \tag{B.13}$$
$$a_{04} = \frac{C_{20}}{a_0}\Big[-\frac{77}{8}e_0^4-\frac{387}{240}e_0^6\Big], \tag{B.14}$$
$$a_{05} = \frac{C_{20}}{a_0}\Big[-\frac{1773}{128}e_0^5+\frac{174545}{21504}e_0^7\Big], \tag{B.15}$$
$$a_{06} = \frac{C_{20}}{a_0}\Big[-\frac{3187}{160}e_0^6\Big], \tag{B.16}$$
$$a_{07} = \frac{C_{20}}{a_0}\Big[-\frac{432091}{15360}e_0^7\Big], \tag{B.17}$$
$$a_{12} = \frac{C_{22}n_0}{a_0(n_0-2\omega_T)}\Big[-3e_0-\frac{3}{8}e_0^3-\frac{5}{64}e_0^5-\frac{1001}{21504}e_0^7\Big], \tag{B.18}$$
$$a_{22} \equiv a_{11} = \frac{C_{22}n_0}{a_0(n_0-\omega_T)}\Big[6-15e_0^2+\frac{39}{8}e_0^4-\frac{35}{48}e_0^6\Big], \tag{B.19}$$
$$a_{32} = \frac{C_{22}n_0}{a_0(3n_0-2\omega_T)}\Big[63e_0-\frac{1107}{8}e_0^3+\frac{4401}{64}e_0^5-\frac{15867}{1024}e_0^7\Big], \tag{B.20}$$

$$a_{42} \equiv a_{21} = \frac{C_{22}n_0}{a_0(2n_0-\omega_T)}\Big[102e_0^2 - 230e_0^4 + \frac{601}{4}e_0^6\Big], \tag{B.21}$$

$$a_{52} = \frac{C_{22}n_0}{a_0(5n_0-2\omega_T)}\Big[\frac{4225}{8}e_0^3 - \frac{162625}{128}e_0^5 + \frac{7287875}{7168}e_0^7\Big], \tag{B.22}$$

$$a_{62} \equiv a_{31} = \frac{C_{22}n_0}{a_0(3n_0-\omega_T)}\Big[\frac{4797}{8}e_0^4 - \frac{124443}{80}e_0^6\Big], \tag{B.23}$$

$$a_{72} = \frac{C_{22}n_0}{a_0(7n_0-2\omega_T)}\Big[\frac{1598429}{640}e_0^5 - \frac{150482675}{21504}e_0^7\Big], \tag{B.24}$$

$$a_{82} \equiv a_{41} = \frac{C_{22}n_0}{a_0(4n_0-\omega_T)}\Big[\frac{73349}{30}e_0^6\Big], \tag{B.25}$$

$$a_{92} = \frac{C_{22}n_0}{a_0(9n_0-2\omega_T)}\Big[\frac{983686113}{107520}e_0^6\Big], \tag{B.26}$$

$$a_{12}^{+} = \frac{C_{22}n_0}{a_0(n_0+2\omega_T)}\Big[\frac{1}{8}e_0^3 + \frac{11}{128}e_0^5 + \frac{2191}{35840}e_0^7\Big], \tag{B.27}$$

$$a_{22}^{+} \equiv a_{11}^{+} = \frac{C_{22}n_0}{a_0(n_0+\omega_T)}\Big[\frac{1}{4}e_0^4 + \frac{7}{40}e_0^6\Big], \tag{B.28}$$

$$a_{32}^{+} = \frac{C_{22}n_0}{a_0(3n_0+2\omega_T)}\Big[\frac{729}{640}e_0^5 + \frac{76545}{107520}e_0^7\Big], \tag{B.29}$$

$$a_{42}^{+} \equiv a_{21}^{+} = \frac{C_{22}n_0}{a_0(2n_0+\omega_T)}\Big[\frac{16}{15}e_0^6\Big], \tag{B.30}$$

$$a_{52}^{+} = \frac{C_{22}n_0}{a_0(5n_0+2\omega_T)}\Big[\frac{78125}{21504}e_0^7\Big]. \tag{B.31}$$

$$\phi_{0j}^{a} = 0, \qquad 1 \le j \le 7; \tag{B.32}$$

$$\phi_{ij}^{a} = 2\Omega + 2\omega, \qquad 1 \le i \le 9, j = 2; \tag{B.33}$$

$$\phi_{ij}^{a+} = -2\Omega - 2\omega, \qquad 1 \le i \le 5, j = 2. \tag{B.34}$$

$$e_{01} = \frac{C_{20}}{a_0^2}\Big[-\frac{3}{2} - \frac{3}{16}e_0^2 - \frac{45}{128}e_0^4 - \frac{1781}{6144}e_0^6\Big], \tag{B.35}$$

$$e_{02} = \frac{C_{22}}{a_0^2}\Big[-\frac{9}{4}e_0 + \frac{1}{2}e_0^3 - \frac{29}{64}e_0^5\Big], \tag{B.36}$$

$$e_{03} = \frac{C_{20}}{a_0^2}\Big[-\frac{53}{16}e_0^2 + \frac{455}{256}e_0^4 - \frac{9033}{10240}e_0^6\Big], \tag{B.37}$$

$$e_{04} = \frac{C_{20}}{a_0^2}\Big[-\frac{77}{16}e_0^3 + \frac{641}{169}e_0^5\Big], \tag{B.38}$$

$$e_{05} = \frac{C_{20}}{a_0^2}\Big[-\frac{1773}{256}e_0^4 + \frac{47539}{6144}e_0^6\Big], \tag{B.39}$$

$$e_{06} = \frac{C_{20}}{a_0^2}\Big[-\frac{3187}{320}e_0^5\Big], \tag{B.40}$$

$$e_{07} = \frac{C_{20}}{a_0^2}\Big[-\frac{3024637}{30720}e_0^6\Big], \tag{B.41}$$

$$e_{12} = \frac{C_{22}n_0}{a_0^2(n_0-2\omega_T)}\Big[\frac{3}{2}-\frac{3}{16}e_0^2-\frac{43}{128}e_0^4-\frac{721}{6144}e_0^6\Big], \tag{B.42}$$

$$e_{22} \equiv e_{11} = \frac{C_{22}n_0}{a_0^2(n_0-\omega_T)}\Big[-\frac{3}{2}e_0+\frac{33}{8}e_0^3-\frac{63}{32}e_0^5\Big], \tag{B.43}$$

$$e_{32} = \frac{C_{22}n_0}{a_0^2(3n_0-2\omega_T)}\Big[\frac{21}{2}-\frac{705}{16}e_0^2+\frac{7707}{128}e_0^4-\frac{61353}{2048}e_0^6\Big], \tag{B.44}$$

$$e_{42} \equiv e_{21} = \frac{C_{22}n_0}{a_0^2(2n_0-\omega_T)}\Big[\frac{51}{2}e_0-\frac{383}{4}e_0^3+127e^5\Big], \tag{B.45}$$

$$e_{52} = \frac{C_{22}n_0}{a_0^2(5n_0-2\omega_T)}\Big[\frac{2535}{16}e_0^2-\frac{151655}{256}e_0^4+\frac{5073545}{6144}e_0^6\Big], \tag{B.46}$$

$$e_{62} \equiv e_{31} = \frac{C_{22}n_0}{a_0^2(3n_0-\omega_T)}\Big[\frac{1599}{8}e_0^3-\frac{122937}{160}e_0^5\Big], \tag{B.47}$$

$$e_{72} = \frac{C_{22}n_0}{a_0^2(7n_0-2\omega_T)}\Big[\frac{228347}{256}e_0^4-\frac{109658843}{30720}e_0^6\Big], \tag{B.48}$$

$$e_{82} \equiv e_{41} = \frac{C_{22}n_0}{a_0^2(4n_0-\omega_T)}\Big[\frac{73369}{80}e_0^5\Big], \tag{B.49}$$

$$e_{92} = \frac{C_{22}n_0}{a_0^2(9n_0-2\omega_T)}\Big[\frac{109298457}{30720}e_0^6\Big], \tag{B.50}$$

$$e_{12}^+ = \frac{C_{22}n_0}{a_0^2(n_0+2\omega_T)}\Big[\frac{3}{16}e_0^2+\frac{1}{256}e_0^4-\frac{101}{10240}e_0^6\Big], \tag{B.51}$$

$$e_{22}^+ \equiv e_{11}^+ = \frac{C_{22}n_0}{a_0^2(n_0+\omega_T)}\Big[\frac{1}{4}e_0^3-\frac{1}{80}e_0^5\Big], \tag{B.52}$$

$$e_{32}^+ = \frac{C_{22}n_0}{a_0^2(3n_0+2\omega_T)}\Big[\frac{243}{256}e_0^4-\frac{5103}{30720}e_0^6\Big], \tag{B.53}$$

$$e_{42}^+ \equiv e_{21}^+ = \frac{C_{22}n_0}{a_0^2(2n_0+\omega_T)}\Big[\frac{4}{5}e_0^5\Big], \tag{B.54}$$

$$e_{52}^+ = \frac{C_{22}n_0}{a_0^2(5n_0+2\omega_T)}\Big[\frac{15625}{6144}e_0^6\Big]. \tag{B.55}$$

$$\phi_{0j}^e = 0, \qquad 1 \le j \le 7; \tag{B.56}$$

$$\phi_{ij}^e = 2\Omega+2\omega, \qquad 1 \le i \le 9, j = 2; \tag{B.57}$$

$$\phi_{ij}^{e+} = -2\Omega-2\omega, \qquad 1 \le i \le 5, j = 2. \tag{B.58}$$

B.2 Elliptic Expansion in Three Dimension

By Equation 3.6, we have the expansion in 3-D:

$$U_p = \frac{\mu}{4a^3}\Big\{-2C_{20}+12C_{22}\cos^4\frac{i}{2}\cos(2M+2\Omega+2\omega-2\omega_T t)$$

$$
\begin{aligned}
&+12C_{22}\sin^4\frac{i}{2}\cos(2M-2\Omega+2\omega-2\omega_T t)\\
&+3\sin^2 i[C_{20}+2C_{22}\cos(2\Omega-2\omega_T t)-C_{20}\cos(2M+2\omega)]\Big\}\\
&+\frac{3\mu e}{4a^3}\Big\{\cos M\Big[-2C_{20}+12C_{22}\cos^4\frac{i}{2}\cos(2M+2\Omega+2\omega-2\omega_T t)\\
&\quad+12C_{22}\sin^4\frac{i}{2}\cos(2M-2\Omega+2\omega+2\omega_T t)\\
&\quad+3\sin^2 i\Big(C_{20}+2C_{22}\cos(2\Omega-2\omega_T t)-C_{20}\cos(2M+2\omega)\Big)\Big]\\
&+4\sin M\Big[-4C_{22}\cos^4\frac{i}{2}\cos(2M+2\Omega+2\omega-2\omega_T t)\\
&\quad-4C_{22}\sin^4\frac{i}{2}\cos(2M-2\Omega+2\omega+2\omega_T t)\\
&\quad+C_{20}\sin^2 i\sin(2M+2\omega)\Big]\Big\}+O(e^2). \qquad \text{(B.59)}
\end{aligned}
$$

The time derivative of the semi-major axis is

$$
\begin{aligned}
\frac{\mathrm{d}a}{\mathrm{d}t} &= \frac{3n}{a}\Big\{C_{20}\sin^2 i\sin(2M+2\omega)-4C_{22}\cos^4\frac{i}{2}\sin(2M+2\Omega+2\omega-2\omega_T t)\\
&\quad-4C_{22}\sin^4\frac{i}{2}\sin(2M-2\Omega+2\omega+2\omega_T t)\Big\}\\
&\quad+\frac{3ne}{2a}\Big\{\sin M\Big[2C_{20}-44C_{22}\cos^4\frac{i}{2}\cos(2M+2\Omega+2\omega-2\omega_T t)\\
&\quad\quad-44C_{22}\sin^4\frac{i}{2}\cos(2M-2\Omega+2\omega+2\omega_T t)\\
&\quad\quad-3C_{20}\sin^2 i-6C_{22}\cos(2\Omega-2\omega_T t)\sin^2 i\\
&\quad\quad+11C_{20}\cos(2M+2\omega)\sin^2 i\Big]\\
&\quad+10\cos M\Big[C_{20}\sin^2 i\sin(2\Omega+2\omega)\\
&\quad\quad-4C_{22}\cos^4\frac{i}{2}\sin(2M+2\Omega+2\omega-2\omega_T t)\\
&\quad\quad-4C_{22}\sin^4\frac{i}{2}\sin(2M-2\Omega+2\omega+2\omega_T t)\Big]\Big\}+O(e^2) \qquad \text{(B.60)}\\
&= \frac{3n}{a}\Big\{C_{20}\sin^2 i\sin(2M+2\omega)-4C_{22}\cos^4\frac{i}{2}\sin(2M+2\Omega+2\omega-2\omega_T t)\\
&\quad-4C_{22}\sin^4\frac{i}{2}\sin(2M-2\Omega+2\omega+2\omega_T t)\Big\}\\
&\quad+\frac{3ne}{2a}\Big\{2C_{20}\sin M-22C_{22}\cos^4\frac{i}{2}\sin(3M+2\Omega+2\omega-2\omega_T t)
\end{aligned}
$$

$$
\begin{aligned}
&+22C_{22}\cos^4\frac{i}{2}\sin(M+2\Omega+2\omega-2\omega_T t)\\
&-22C_{22}\sin^4\frac{i}{2}\sin(3M-2\Omega+2\omega+2\omega_T t)\\
&+22C_{22}\sin^4\frac{i}{2}\sin(M-2\Omega+2\omega+2\omega_T t)\\
&-3C_{20}\sin^2 i\sin M-3C_{22}\sin(M+2\Omega-2\omega_T t)\sin^2 i\\
&+3C_{22}\sin(M-2\Omega-2\omega_T t)\sin^2 i\\
&+\frac{11}{2}C_{20}\cos(3M+2\omega)\sin^2 i-\frac{11}{2}C_{20}\cos(M+2\omega)\sin^2 i\\
&+5C_{20}\sin^2 i\sin(M+2\Omega+2\omega)-5C_{20}\sin^2 i\sin(M-2\Omega-2\omega)\\
&-20C_{22}\cos^4\frac{i}{2}\sin(3M+2\Omega+2\omega-2\omega_T t)\\
&-20C_{22}\cos^4\frac{i}{2}\sin(M+2\Omega+2\omega-2\omega_T t)\\
&-20C_{22}\sin^4\frac{i}{2}\sin(3M-2\Omega+2\omega+2\omega_T t)\\
&-20C_{22}\sin^4\frac{i}{2}\sin(M-2\Omega+2\omega+2\omega_T t)\Big\}+O(e^2). \qquad \text{(B.61)}
\end{aligned}
$$

We see that the ϕ^a_{ij}, ϕ^e_{ij} are complicated. They can be not only $2\Omega+2\omega$ (as in the planar case), but also $-2\Omega+2\omega$, 2ω, -2Ω, etc. Additionally some frequencies such as $n_0+2\omega_T$, $3n_0+2\omega_T$ appear for low order eccentricity expansions. All these change make the elliptic expansion method complicated. Thus we introduce the resonant integral analyses from paper [38] to analyze the spacecraft motion in three dimensions.

APPENDIX C

Some Definitions and Data

C.1 Six element definition

a	semi-major axis
e	eccentricity
i	inclination
Ω	longitude of ascending node
ω	argument of periapsis
f	true anomaly
u	argument of the orbit
$\mathbf{h}$	the angular momentum vector
$\mathbf{n}$	the unit vector of ascending node
$\mathbf{r}$	the position vector of spacecraft

See Figure C.1-C.2 for the geometry of the elements.

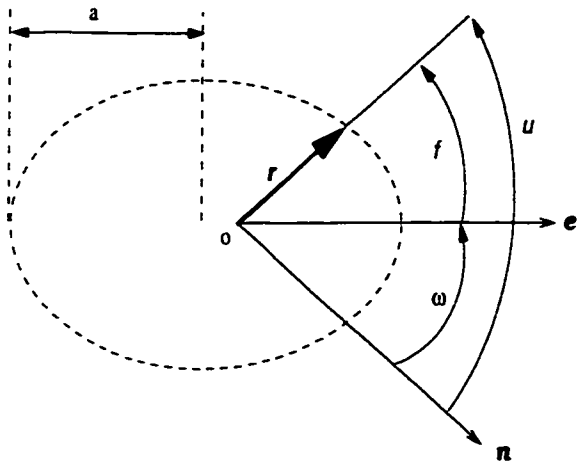

Figure C.1: The elements in orbital plane

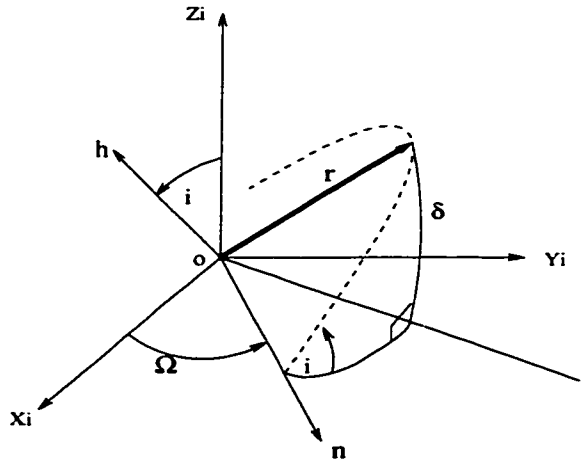

Figure C.2: The elements in three dimensions

C.2 Lagrange planetary equations

The differential equations for the orbital elements are [7],[32]

$$\frac{da}{dt} = \frac{2}{na}\frac{\partial U_p}{\partial M}, \tag{C.1}$$

$$\frac{de}{dt} = \frac{(1-e^2)}{na^2e}\frac{\partial U_p}{\partial M} - \frac{\sqrt{1-e^2}}{na^2e}\frac{\partial U_p}{\partial \omega}, \tag{C.2}$$

$$\frac{di}{dt} = \frac{\cos i}{na^2\sqrt{1-e^2}\sin i}\frac{\partial U_p}{\partial \omega} - \frac{1}{na^2\sqrt{1-e^2}\sin i}\frac{\partial U_p}{\partial \Omega}, \tag{C.3}$$

$$\frac{d\Omega}{dt} = \frac{1}{na^2\sqrt{1-e^2}\sin i}\frac{\partial U_p}{\partial i}, \tag{C.4}$$

$$\frac{d\omega}{dt} = -\frac{\cos i}{na^2\sqrt{1-e^2}\sin i}\frac{\partial U_p}{\partial i} + \frac{\sqrt{1-e^2}}{na^2e}\frac{\partial U_p}{\partial e}, \tag{C.5}$$

$$\frac{dM}{dt} = n - \frac{1-e^2}{na^2e}\frac{\partial U_p}{\partial e} - \frac{2}{na}\frac{\partial U_p}{\partial a}, \tag{C.6}$$

where U_p is a perturbation function. We note that when there is no perturbation, $U_p = 0$. This means that $C_{20} = C_{22} = 0$, $U_2 = 0$ in this disseratation. And we know that $a, e, i, \Omega, \omega, n$ are constant, and $M = nt$ at this time.

C.3 Data for Asteroid Castalia

$\mu = 9.40 \times 10^{-8}\text{Km}^3/\text{Sec}$

$C_{20} = -7.275 \times 10^{-2}\text{Km}^2$

$C_{22} = 2.984 \times 10^{-2}\text{Km}^2$

$\omega_T = 2\pi/4.07/3600 = 4.2883 \times 10^{-4}/\text{Sec}$

BIBLIOGRAPHY

BIBLIOGRAPHY

[1] Abramowitz,M. and Stegnun,I.A., *Handbook of Mathematical Functions*, Dover, 1965.

[2] Antreasian,P., Helfrich,C., Miller,J., Owen,W., Willians B., Yeomans,D., Giorgini,J., Scheeres,D., Dunham,D., Farquhar,R., McAdams J., Santo, A., Heyler,G., "Preliminary Planning for NEAR's Low-Altitude Operations at 433 Eros", *AAS/AIAA Space Flight Mechanics Meeting*, Breckenridge, CO. 1999.

[3] Arnold, V.I., *Dynamical Systems III(Encyclopaedia of Mathematical Sciences)*, Springer-Verlag, Berlin Heidelberg, 1988.

[4] Bate,R., Meuller,D. and White,J., *Fundamentals of Astrodynamics*, Dover Publications,INC., New York, 1971.

[5] Boccaletti, D. and Pucacco, G. *Theory of Orbits*, Springer, 1996(Vol.1), 1998(Vol.2).

[6] Brouwer, D., "Solution of the Problem of Artificial Satellite Theory Without Drag", *The Astronomical Journal*, Vol. 64,1959, pp. 378 - 397.

[7] Brouwer, D., and Clemence, G.M., *Methods of Celestial Mechanics*, Academic Press, 1961.

[8] Celleti,A. and Chierchia,L., "KAM Stability Estimate in Celestial Mechanics", *Planetary and Space Science*, Vol.46, No. 11/12, 1998, pp.1433-1440.

[9] Danby, J.M.A., *Fundamentals of Celestial Mechanics*, 2nd Ed., Willmann-Bell, 1992.

[10] Ely, T. A., and Howell, K. C., "Long-Term Evolution of Artificial Satellite Orbits Due to Resonant Tesseral Harmonics," *The Journal of the Astronomical Science*, Vol. 44, No. 2, 1996, pp. 167-190.

[11] Garfinkel, B., "On the Motion of a Satellite of an Oblate Planet", *The Astronomical Journal*, Vol. 63, 1958, pp. 88–96.

[12] Ferraz-Mello, S., "Slow and Fast Diffusion in Asteroid-Belt Resonances", *Celestial Mechanics and Dynamical Astronomy* Vol.73, 1999, pp. 25-37.

[13] Gedeon, G. S., "Tesseral Resonance Effects on Satellite Orbits," *Celestial Mechanics and Dynamical Astronomy*, Vol. 1, 1969, pp 167-189.

[14] Giorgini, J. D.; Miller, J. K.; Antreasian, P. G.; Williams, B. G.; Helfrich, C. E.; Owen, W. M., Jr.; Wang, T. C.; Yeomans, D. K.; Carranza, E.; Chesley, S. R., "Orbit Determination at Eros: NEAR Spacecraft Dynamics and Initial Results", *AAS/Division of Dynamical Astronomy Meeting*, American Astronomical Society, May, 2000.

[15] Greenwood, D., *Principles of Dynamics*, 2nd Ed., Prentice-Hall, 1988.

[16] Harris, A.W., "Tumbling asteroids", *Icarus*, Vol. 107, 1994, pp 209 - 211.

[17] Hechler, Martin, "ROSETTA mission design", *Advances in Space Research*, Vol. 19, Issue 1, 1997, pp 127-136.

[18] Hénon, M., "Vertical Stability of Periodic Orbits the Restricted Problem. I.Equal Masses", *Astronomy and Astrophysics*, Vol.28, 1973, pp415-426.

[19] Hénon, M., *Generating Families in the Restricted Three-Body Problem*, Springer, 1997.

[20] Hu, W. and Scheeres, D.J., "Spacecraft Motion about Slowly Rotating Asteroids", *AAS/AIAA Space Flight Mechanics Meeting*, Florida, Jan. 2000. New version to appear at AIAA Journal of Guidance, Control and Dynamics.

[21] Hu,W. and Scheeres,D.J., "Periodic Orbits in Rotating 2nd Degree and Order Gravity Fields". *9th International Space Conference of Pacific-basin Societies (ISCOPS)*, Pasadena, California, 2001.

[22] Hudson, R.S., S.J. Ostro, "Shape and non-principal axis spin state of asteroid 4179 Toutatis", *Science*, Vol. 263, 1994, pp.940 - 943.

[23] Kaula, W.M., *Theory of Satellite Geodesy*. Blaisdell, Boston, p.6, 1966.

[24] Khalil, H. *Nonlinear Systems*, Second edition, Prentice Hall, 1996.

[25] Kozai, Y., "The Motion of a Close Earth Satellite", *The Astronomical Journal*, Vol. 64, 1959, pp. 367 - 377.

[26] Lara, M., Elipe, A. "On Periodic Orbits Around Geostationary Positions", *AAS/AIAA Space Flight Mechanics Meeting*, Florida, Jan. 2000.

[27] Lara, M., Scheeres,D.J., "Stability Bounds for Three-dimensional Motion Close to Asteroids", *AAS/AIAA Space Flight Mechanics Meeting*, San Antonio, Tex, Jan. 2002.

[28] Moons, M., "Dynamical Structure of the 2/1 Commensurability with Jupiter and the Origin of the Resonant Asteroids", *Icarus*, Vol. 135, 1998, pp. 458-468.

[29] Perko, L., *Differential Equations and Dynamical Systems*, Springer-Verlag: New York, 1991.

[30] Pravec,P., and Harris,A.W., "Fast and Slowly Rotating Asteroids", *Icarus*, Vol.148, 2000, pp12-20.

[31] Riaguas,A., Elipe,A. and Lara,M., "Periodic orbits around a massive straight segment", Celestial Mechanics, Vol.73, No.1-4, 1999, pp.169-178.

[32] Roy,A.E., *Orbital Motion*, Adam Hilger. Third edition, Bristol and Philadelphia, 1988.

[33] Roy,A.E. and Steves, B.A. *From Newton to Choas*, NATO ASI Series B:Physics, Vol.336, 1995.

[34] Sansaturio,S.E., Vigo-Aguiar,I. and Ferrandiz,J.M., "Non-Integrability of the motion of a point mass around a planet of arbitrary shape", The Dynamics of Small Bodies in the Solar System, B.A. Steves and A.E. Roy, eds., 1999, pp 295–302.

[35] Scheeres,D.J., "Dynamics about Uniformly Rotating TriAxial Ellipsoids: Applications to Asteroids," *Icarus*, Vol 110, 1994, pp. 225 - 238.

[36] Scheeres,D.J., Ostro,S.J., Hudson,R.S. and Werner, R.A. "Orbits Close to Asteroid 4769 Castalia", *Icarus*, Vol.121, 1996, pp67-87.

[37] Scheeres,D.J., Ostro,S.J., Hudson,R.S., DeJong,E.M., and Suzuki,S., "Dynamics of Orbits Close to Asteroid 4179 Toutatis", *Icarus*, Vol. 132, 1998, pp 53 - 79.

[38] Scheeres,D.J., "The Effect of C_{22} on Orbit Energy and Angular Momentum", *Celestial Mechanics and Dynamical Astronomy* Vol. 73, 1999, pp 339-348.

[39] Scheeres,D.J., Williams,B.G. and Miller,J.K., "Evaluation of the Dynamic Environment of an Asteroid: Applications to 433 Eros", *Journal of Guidance, Control, and Dynamics*, Vol.23, No.3, 2000, pp466-475.

[40] Scheeres,D.J., and Hu,W., " Secular Motion in a 2nd Degree and Order Gravity Field with no Rotation", *Celestial Mechanics and Dynamical Astronomy*, Vol.79, 2001. pp183-200.

[41] Sawai,S., Kawaguchi,J., Scheeres,D., Yoshizawa,N., and Ogasawara,M., "Development of a Target Marker for Landing on Asteroids", *AAS/AIAA Space Flight Mechanics Meeting*, Florida, Jan. 2000.

[42] Szebehely,V., *Theory of Orbits*, Academic Press Inc. New York, 1967.

[43] Taff,L.G., *Celestial Mechanics: a computational guide for the practitioner*, Wiley:New York, 1985.

[44] Werner,R.A. and Scheeres,D.J. "Exterior Gravitation of a Polyhedron Derived and Compared with Harmonic and Mascon Gravitation Representation of Asteroid 4769 Castalia", *Celestial Mechanics and Dynamical Astronomy*, Vol.65, pp313-344, 1997.

[45] Wiggins,S. *Introduction to Applied Nonlinear Dynamical Systems and Chaos.* Springer-Verlag, 1990, pp526-538.

[46] Wiggins,S. *Global Bifurcations and Choas*, Springer-Verlag:New York, 1988. pp386-387.

[47] Wolfram, S., *Mathematica, A System for Doing Mathematics by Computer*, Addison-Wesley Publishing Company, Second Edition, 1993.

[48] Wytrzyszczak,I., "Stationary Orbits around the Earth and Mars", *Artificial Satellite*, Vol.33, 1998, pp11-23.